



DENSITY RATIO ESTIMATION IN VARIATIONAL BAYESIAN MACHINE LEARNING

Alexander Lam

Supervisors: Professor Scott Sisson and Doctor Edwin Bonilla

School of Mathematics and Statistics
UNSW Sydney

October 2018

SUBMITTED IN PARTIAL FULFILLMENT OF THE REQUIREMENTS OF THE DEGREE OF
BACHELOR OF SCIENCE WITH HONOURS

Plagiarism statement

I declare that this thesis is my own work, except where acknowledged, and has not been submitted for academic credit elsewhere.

I acknowledge that the assessor of this thesis may, for the purpose of assessing it:

- Reproduce it and provide a copy to another member of the University; and/or,
- Communicate a copy of it to a plagiarism checking service (which may then retain a copy of it on its database for the purpose of future plagiarism checking).

I certify that I have read and understood the University Rules in respect of Student Academic Misconduct, and am aware of any potential plagiarism penalties which may apply.

By signing this declaration I am agreeing to the statements and conditions above.

Signed: _____

Date: _____

Acknowledgements

Scott Sisson, Edwin Bonilla, Louis Tiao

Trevor Trotman

Honours Room Inhabitants, esp. Bouldering crew

Discord Group+Kong+Brian

Sunchit and Allan

누나

JC

Lammy, 11 September 2018.

Abstract

In variational Bayesian machine learning, deep neural networks can be used to efficiently model posterior distributions associated with high dimensional data or large datasets. This can be furthered to an autoencoder model which simultaneously expresses data points as a lower dimensional latent representation, and reconstructs said data given a latent variable input. Due to the implicit nature of the involved distributions, density ratio estimation techniques are used to approximate the intractable KL divergence term in the posterior network optimisation problem.

In this thesis, we generalise the estimator loss function selection to a choice of f -divergence lower bound and estimator parametrisation. We then demonstrate that, of the tested parametrisations, the class probability estimator is the optimal choice as it is feasible with large density ratios and experiences the quickest convergence. Additionally, the high accuracy yet instability of the reverse KL divergence lower bound is experimentally shown, in contrast to the stable yet inaccurate GAN divergence, implying a trade-off between estimator stability and accuracy in the choice of f -divergence.

Contents

| | | |
|-----------|---|----|
| Chapter 1 | Introduction | 1 |
| 1.1 | Aims | 1 |
| 1.2 | Problem Context | 1 |
| 1.3 | Results | 3 |
| 1.4 | Thesis Structure | 4 |
| Chapter 2 | Background on Neural Networks | 5 |
| 2.1 | Motivation | 5 |
| 2.2 | Individual Node Structure | 6 |
| 2.3 | Activation Functions | 7 |
| 2.4 | Neural Network Structure | 9 |
| 2.5 | Weight Initialisation | 11 |
| 2.6 | Optimisation | 12 |
| 2.7 | Back-Propagation | 14 |
| Chapter 3 | Variational Inference | 16 |
| 3.1 | Context | 16 |
| 3.2 | The KL Divergence | 17 |
| 3.3 | Introduction to Variational Inference | 19 |
| 3.4 | Derivation of the ELBO | 19 |
| 3.5 | Mean-Field Variational Family | 21 |
| 3.6 | Amortized Inference | 21 |
| 3.7 | Example: Variational Autoencoder | 24 |
| 3.8 | Problems with Implicit Distributions | 26 |
| 3.8.1 | Implicit Prior and/or Variational Posterior | 26 |
| 3.8.2 | Implicit Likelihood | 27 |
| Chapter 4 | Density Ratio Estimation | 30 |
| 4.1 | Class Probability Estimation | 30 |

| | | |
|-----------|--|----|
| 4.1.1 | Derivation | 30 |
| 4.1.2 | Prior-Contrastive Algorithm | 32 |
| 4.1.3 | Joint-Contrastive Algorithm | 34 |
| 4.2 | Divergence Minimisation | 36 |
| 4.2.1 | Derivation | 37 |
| 4.2.2 | Prior-Contrastive Algorithm | 38 |
| 4.2.3 | Joint-Contrastive Algorithm | 40 |
| 4.2.4 | Alternative Derivation of Class Probability Estimation | 41 |
| Chapter 5 | Algorithm Generalisation | 44 |
| 5.1 | Introduction | 44 |
| 5.2 | Algorithm Generalisation | 45 |
| 5.2.1 | Reverse KL Divergence | 45 |
| 5.2.2 | GAN Divergence | 45 |
| 5.3 | Optimization Algorithms | 46 |
| 5.3.1 | Prior-Contrastive | 46 |
| 5.3.2 | Joint-Contrastive | 47 |
| Chapter 6 | Comparing Optimal Estimators | 48 |
| 6.1 | Theory | 48 |
| 6.2 | Problem Context | 48 |
| 6.3 | Program Structure | 50 |
| 6.4 | Results | 52 |
| Chapter 7 | Comparing Undertrained Estimators | 56 |
| 7.1 | Theory | 56 |
| 7.1.1 | Estimator Bounds | 56 |
| 7.1.2 | First and Second Derivatives of Estimator Loss Functions . . | 57 |
| 7.1.3 | Displacement of Estimator Optimal Values | 60 |
| 7.2 | Experiment Outline | 61 |
| 7.3 | Results | 61 |
| Chapter 8 | Autoencoder Experiment - (MNIST Dataset) | 66 |
| 8.1 | Experiment Outline | 66 |
| 8.2 | Low Dimensional Experiment Results | 69 |
| 8.3 | High Dimensional Experiment Results | 71 |

| | |
|---|----|
| Chapter 9 Conclusion and Further Research | 75 |
| 9.1 Further Research | 75 |
| References | 77 |
| Appendix A Proofs | 81 |
| A.1 Proof of Proposition 2.6.2 | 81 |
| A.2 Proof of Lemma 3.7.1 | 82 |
| A.3 Proof of Lemma 4.1.1 | 82 |
| A.4 Proof of Lemma 4.2.2 | 83 |
| A.5 Proof of Lemma 8.3.1 | 83 |
| Appendix B Algorithms | 84 |
| B.1 Back-Propagation Algorithm | 84 |
| B.2 Coordinate Ascent Variational Inference Algorithm | 85 |
| B.3 Algorithms for “Sprinkler” Experiment | 86 |
| Appendix C Coordinate Ascent Variational Inference Derivation | 88 |
| Appendix D Mean Field Variational Inference Example | 90 |
| Appendix E Kernel Density Estimation | 94 |
| Appendix F Prior-Contrastive Optimal Estimator Experiment Plots | 95 |
| Appendix G Second Functional Derivatives of Direct Log Ratio Estimator Losses | 96 |

CHAPTER 1

Introduction

1.1 Aims

In the context of variational Bayesian machine learning, we often face an intractable optimisation problem due to the implicit nature of one or more distributions involved. By using density ratio estimation, we are able to estimate the intractable term using only samples from the implicit distributions. The primary goal of this thesis is to analyse and investigate different algorithms used to train density ratio estimators. This is accomplished by comparing the convergence of the variational posterior networks, reflective of the accuracy of the density ratio estimation. We begin by generalising the selection of a density ratio estimation algorithm to a choice of estimator parametrisation:

- Class Probability Estimator $D_\alpha(u) \simeq \frac{q(u)}{q(u)+p(u)}$,
- Direct Ratio Estimator: $r_\alpha(u) \simeq \frac{q(u)}{p(u)}$,
- Direct Log Ratio Estimator: $T_\alpha(u) \simeq \log \frac{q(u)}{p(u)}$,

and the selection of f-divergence used to formulate the estimator loss function:

- Reverse KL Divergence: $KL(q(u)||p(u))$,
- GAN Divergence: $2JS(p(u)||q(u)) - \log 4$.

We then compare all algorithm combinations in varying conditions on a basic inference problem and an autoencoder experiment to determine the optimal combination of f-divergence and estimator parametrisation.

1.2 Problem Context

In any Bayesian statistics problem, the quintessential objective is to evaluate the posterior distribution $p(z|x)$ [Gelman et al., 2004]. In cases where algebraic posterior evaluation is difficult, MCMC (Markov Chain Monte Carlo) methods have been used to estimate the posterior density, but they tend to have slow convergence when applied to high dimensional data or large datasets. Variational inference methods overcome this obstacle by optimising a different, approximate distribution $q_\phi(z)$,

dubbed the ‘variational distribution’, by minimising its reverse KL divergence with the true posterior distribution by minimising an expression equal to the negative of the evidence lower bound, $NELBO(q)$ [Blei et al., 2017]

$$\min_{\phi} \underbrace{-\mathbb{E}_{q_{\phi}(z)}[\log p(x|z)] + KL(q_{\phi}(z)||p(z))}_{=NELBO(q)}.$$

Traditionally, the variational distribution would factorise over the latent variables in ‘mean-field variational inference’. This algorithm is inefficient in large datasets, as a new variational distribution would have to be trained for each data observation. The recent increased popularity of neural networks, brought forward by improvements in computational power, has led to a new type of variational inference: amortized variational inference [Zhang et al., 2017]. This method uses the universal function approximating capability of the neural network model to condition the variational posterior on the observation, producing a flexible model that is able to generalise over large datasets. This distribution $q_{\phi}(z|x)$ is optimised with respect to the distribution of the dataset $q^*(x)$:

$$\min_{\phi} \mathbb{E}_{q^*(x)} \left[-\mathbb{E}_{q_{\phi}(z|x)}[\log p(x|z)] + KL(q_{\phi}(z|x)||p(z)) \right].$$

Typically, the variational posterior is explicitly parametrised as a multivariate Gaussian distribution with means and variances specified by the posterior network output [Kingma and Welling, 2013]. However, “Adversarial Variational Bayes” by Mescheder et al. [2017] introduces a more flexible model by adding additional random noise inputs to the posterior network, which is configured to output distribution samples. We label this posterior as ‘implicit’, as it is difficult to numerically evaluate its explicit representation. Consequently, the optimisation problem is intractable as we are unable to calculate $KL(q_{\phi}(z|x)||p(z)) = \mathbb{E}_{q_{\phi}(z|x)} \log \frac{q_{\phi}(z|x)}{p(z)}$. We therefore resort to density ratio estimation techniques, using another neural network to estimate this term. These techniques are explicitly detailed in “Density Ratio Estimation in Machine Learning” by Sugiyama et al. [2012]. There are two main methods of optimising this network: class probability estimation, which trains the network to distinguish between samples from the numerator and denominator distributions, and divergence minimisation, which minimises a loss function of a direct ratio estimator with a minimum of the reverse KL divergence $KL(q_{\phi}(z|x)||p(z))$.

Since density ratio estimation only requires samples from the distributions, we are additionally able to use this algorithm when the prior $p(z)$ is implicit. Following

the terminology in “Variational Inference using Implicit Distributions” by Huszár [2017], we refer to this as the ‘prior-contrastive’ formulation. When the likelihood distribution is additionally implicit, we use a ‘joint-contrastive’ formulation, minimizing the reverse KL divergence between the joint distributions:

$$\min_{\phi} \mathbb{E}_{q^*(x)q_{\phi}(z|x)} KL(q(z, x) || p(z, x)).$$

The uses of amortized variational inference are not limited to posterior inference; it can additionally be used to train an autoencoder, a model consisting of an encoder that represents a data point x as a lower dimensional latent variable z according to the variational posterior $q_{\phi}(z|x)$, and a decoder that reconstructs data \tilde{x} from latent z according to the likelihood $p_{\theta}(x|z)$ [Kingma and Welling, 2013]. The decoder can be used to generate new data by inputting latent z from the prior $p(z)$.

1.3 Results

After generalising the density ratio estimation algorithms, we showed that all three estimator parametrisations had similar accuracies when optimised properly, and found that the estimators were more accurate when trained with the reverse KL divergence than with the GAN divergence. We then compared the effectiveness of the estimators when under-trained, showing that the class probability estimator was the most accurate, followed by the direct ratio estimator and the direct log ratio estimator. This is likely due to the faster convergence experienced by the superior estimator. This experiment also reinforced the previous experiment’s conclusion that the estimators trained with the reverse KL divergence are more accurate, but also demonstrated initial instability. The under-trained estimators were compared again in the optimisation of an autoencoder, in both low-dimensional and high-dimensional latent spaces. Similar results were found in the low-dimensional setting, but the high-dimensional latent space led to density ratios too large to be represented by the loss functions associated with both the direct ratio estimator and the direct log ratio estimator. The class probability estimator was the only feasible estimator and is therefore superior in that regard. In the high-dimensional experiment, we also found that the estimators trained with the reverse KL divergence failed to stabilise, and therefore had inferior accuracy.

Overall, in this thesis, we have:

- generalised the derivation of a density ratio estimator loss function to a choice of f-divergence and estimator parametrisation,

- shown that the class probability estimator $D_\alpha(u) \simeq \frac{q(u)}{q(u)+p(u)}$ surpasses the direct ratio estimator $r_\alpha(u) \simeq \frac{q(u)}{p(u)}$ and the direct log ratio estimator $T_\alpha(u) \simeq \log \frac{q(u)}{p(u)}$ in both feasibility and accuracy,
- shown experimentally that estimators trained with the reverse KL divergence may be unstable, but accurately estimate the density ratio when stable,
- shown experimentally that estimators trained with the GAN divergence are much more stable, but estimate the density ratio less accurately.

1.4 Thesis Structure

The remainder of this thesis is broken up into the following chapters:

- **Chapter 2** provides a background on neural networks, the model used to represent our estimators and variational distributions.
- **Chapter 3** explains variational inference, describing the traditional mean-field variational inference and then introducing the more relevant amortized variational inference, including the problems it faces with implicit distributions.
- **Chapter 4** proposes two major algorithms used for density ratio estimation: class probability estimation and divergence minimisation.
- **Chapter 5** generalises the choice of density ratio algorithm to a selection of f -divergence used to formulate the estimator loss function, and a parametrisation of the estimator.
- **Chapter 6** introduces a basic posterior inference problem and shows that the different estimator parametrisations have similar density ratio estimation accuracies when optimally trained. This chapter also compares the choice of f -divergence used as a lower bound for the estimator loss.
- **Chapter 7** provides further experimental insights into the choice of f -divergence and differentiates between the estimator parametrisations by comparing their accuracies when under-trained.
- **Chapter 8** reinforces the conclusions of Chapter 7, again comparing the under-trained estimators in the context of data auto-encoding. The experiment was repeated for both a low dimensional and high dimensional latent space.
- **Chapter 9** summarizes the experimental results and proposes additional experiment settings, potential improvements and unanswered questions for future research.

CHAPTER 2

Background on Neural Networks

In this chapter we give a general overview of a common model used in deep learning: neural networks. We first explain the motivation and intuition behind the model, then we describe the structure of an individual node. We then expand to the overall neural network structure. After describing the network initialisation method, we conclude the chapter by demonstrating gradient descent training of neural networks and how back-propagation is used to find the required partial derivatives.

2.1 Motivation

Originally, neural networks were an attempt to create an algorithm that mimics the human brain’s method of solving problems. The first machines using a neural network structure were created in the 1950s, and they were used widely from the 1980s onwards, as computers became sufficiently powerful for network training [Goodfellow et al., 2016].

One key feature of the brain structure is the capability of the neurons to adapt to suit different purposes [Zilles, 1992]. Neuroscientists have conducted experiments on animals where they rewired the optic nerve from the eye to the auditory cortex. They found that the auditory cortex eventually adapted to process the visual signals, and the animals were able to perform tasks requiring sight. This experiment can be repeated for almost any input sensor and the neurons will adjust accordingly to process the signals in a useful manner. They deduced that each neuron has a similar structure regardless of its location in the brain. Within each neuron, electrical signal inputs are transformed and outputted to other neurons. Overall, the network of neurons was able to process an arbitrary input signal to suit a given purpose [Zilles, 1992].

Let f^* be some function from \mathbb{R} to \mathbb{R} . The primary goal of a neural network is to approximate f^* using a mapping with parameters Θ from input \mathbf{x} to output \mathbf{y} , that is, $\mathbf{y} = \mathbf{f}_\Theta(\mathbf{x})$ [Goodfellow et al., 2016]. In fact, the universal approximation theorem states that neural networks can approximate any function in a finite-dimensional space with any desired non-zero amount of error, provided they are complex enough [Cybenko, 1989; Hornik, 1991]. For example, a typical regression problem of estimating housing prices would have the network inputting the values of certain predictors such as size (continuous) and type of building (categorical), and outputting the expected price. Another example is the classification problem of recognising handwritten digits (0-9) in a black and white image [Simard et al., 2003]. There are many inputs corresponding to the value of each pixel, and the network would have 10 outputs corresponding to the probability of each digit, and the digit with the highest probability is then selected.

2.2 Individual Node Structure

Before discussing the overall structure of the neural network, we describe the structure of an individual node. A typical node takes inputs from either the external input, or the outputs from other nodes, in addition to a bias node, which has the same purpose as the intercept term in a regression problem. The nodal inputs \mathbf{x} are multiplied by weights $\boldsymbol{\theta}$ and then passed through an activation function $g(\mathbf{x})$. The individual node function is therefore

$$h_{\boldsymbol{\theta}}(\mathbf{x}) = g\left(\sum_{i=0}^n \theta_i x_i\right)$$

where n is the number of inputs excluding the bias node, which always has constant value $x_0 = 1$ [Cheng and Titterton, 1994]. An example of this is given in Figure 2.1.

The objective of the activation function is to map the network output to a given range. An example of ranges used in practice are $(0, 1)$ or \mathbb{R} . This mapping restricts the output range and determines the level of input signal required for the output to become asymptotically large [Haykin, 1998]. A list of common activation functions is given in Section 2.3.

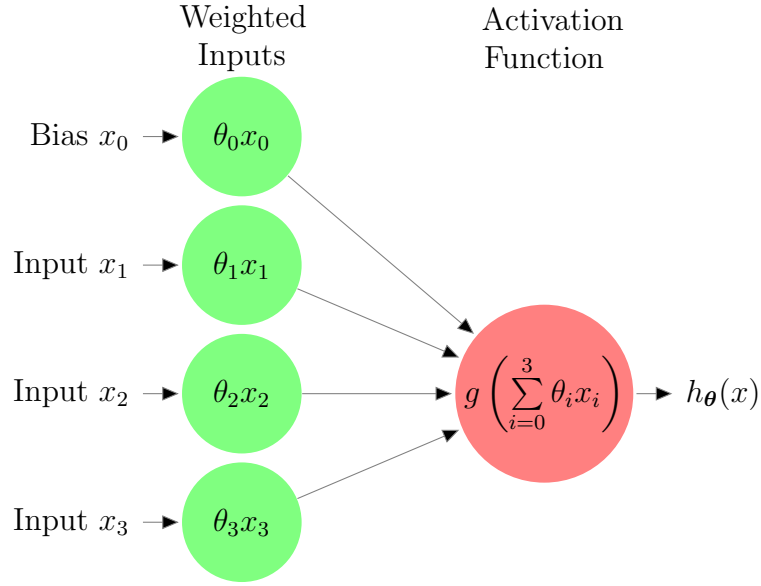


Figure 2.1: Example structure of an individual node function with 3 inputs, labelled as $\mathbf{x} = [x_0 \ x_1 \ x_2 \ x_3]^\top$, with x_0 corresponding to the bias node. The weights are denoted as $\boldsymbol{\theta} = [\theta_0 \ \theta_1 \ \theta_2 \ \theta_3]$.

2.3 Activation Functions

Some common activation functions [Goodfellow et al., 2016] are:

- The rectified linear unit or ReLU activation function output is bound in $[0, \infty)$. It has the formula $g(x) = \max\{0, x\}$ corresponding to node function $h_{\boldsymbol{\theta}}(\mathbf{x}) = \max\{0, \boldsymbol{\theta}^\top \mathbf{x}\}$.
- The sigmoid or logistic activation function outputs are restricted to $(0, 1)$, with the formula $g(x) = (1 + \exp(-x))^{-1}$ corresponding to node function $h_{\boldsymbol{\theta}}(\mathbf{x}) = (1 + \exp(-\boldsymbol{\theta}^\top \mathbf{x}))^{-1}$.
- The hyperbolic tangent function output ranges between $(-1, 1)$, denoted as $g(x) = \tanh(x)$ corresponding to $h_{\boldsymbol{\theta}}(\mathbf{x}) = \tanh(\boldsymbol{\theta}^\top \mathbf{x})$.
- The linear activation function is used to describe nodes with no activation function, as it's formula is $g(x) = x$, corresponding to $h_{\boldsymbol{\theta}}(\mathbf{x}) = \boldsymbol{\theta}^\top \mathbf{x}$.

Their plots are shown in Figure 2.2.

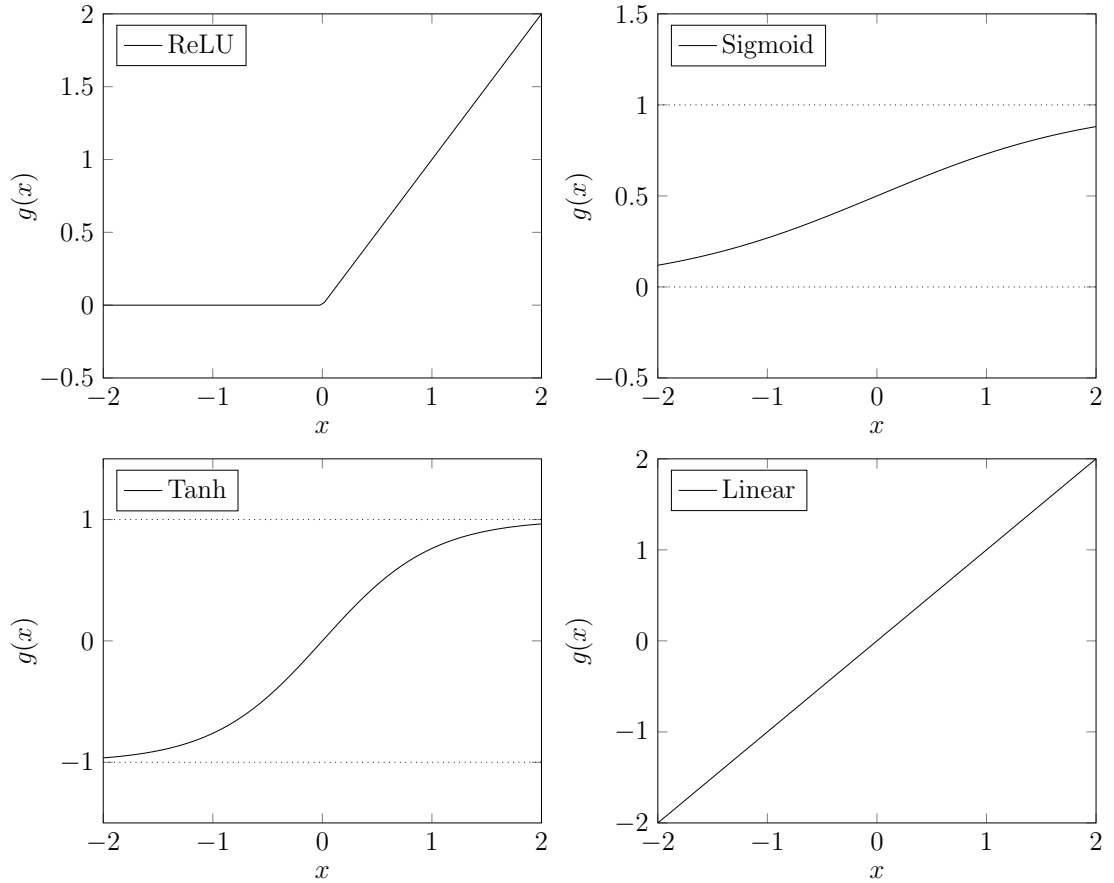


Figure 2.2: Activation Function Plots

The choice of activation function is dependent on several factors:

- The node's location in the network,
- Desired node output range,
- Continuous differentiability is ideal for gradient-based optimisation methods [Snyman, 2005],
- Monotonic activation functions ensure that the error is convex [Wu, 2009],
- In cases where the output range is restricted, the amount of input signal required for the activation function output to be asymptotically close to its limit.

For example, if the node's output is the estimate of a probability (ranging in $(0, 1)$), then the sigmoid function would be used [Cybenko, 1989]. In addition to its ideal output range, the sigmoid function is continuously differentiable and requires significant input to output a value asymptotically close to 0 or 1. This allows the probability to be estimated with greater precision than with an activation function that approaches its limits very quickly, such as the hyperbolic tangent function.

On the other hand, if the node’s output was the expectation of a non-negative quantity, such as price or time, then the ReLU activation function would be used, as it is bound by 0 and ∞ , and its linearity makes the overall node operation similar to linear regression.

We now describe the overall neural network structure, as the choice of activation function is dependent on the node’s relative location on the network.

2.4 Neural Network Structure

A typical neural network is made up of layers of interconnected nodes [Cheng and Titterton, 1994]. The first layer, called the input layer, does not have an activation function or weights, rather it simply acts as an input interface for the network. The outputs from the nodes can only be sent to other nodes in succeeding layers, with the exception of the final output layer; its result is simply the output of the network. The layers of nodes between the input and output layer are called the “hidden” layers, as their outputs are generally not interpreted by the user. Hidden layers can have an arbitrary number of nodes, whilst the nodes in the input and output layers are restricted to the number of inputs and outputs the program has. Example 2.4.1 on the next page explains the arithmetic operations within a neural network, and is illustrated in Figure 2.3.

The choice of activation function for a node in a neural network typically depends on the layer. Rectified linear units are the default choice for the hidden layers for their many advantages [Goodfellow et al., 2016]:

- Sparsity: since negative ReLU inputs result in a zero output, not all of the units are “active” (non-zero output) during the network’s runtime. Sparsity is preferred in neural networks as it reduces overfitting and makes the model more robust to insignificant input changes [Glorot et al., 2011].
- Faster computation: the $\max\{0, x\}$ function is computed much faster than the exponential or hyperbolic tangent function.
- Better gradient propagation: weight training in a neural network (discussed in Sections 2.6 and 2.7) involves ‘back-propagating’ a loss value through the network to calculate the partial derivatives of the loss function with respect to the weights. The weights receive a change proportional to their partial derivative. Back-propagation uses the chain rule, so activation functions such as sigmoid or tanh that have a low gradient near their asymptotes may experience the ‘vanishing gradient problem’, in which the calculated partial derivatives become increasingly small as the loss value propagates through the network

[Kolen and Kremer, 2001]. This causes the front layers to train very slowly. The ReLU activation function does not experience this issue as its gradient is either linear or 0.

The input layer can be described as having a linear activation function, as it has no activation function. The types of activation function used in the output layer have been explained in Section 2.3.

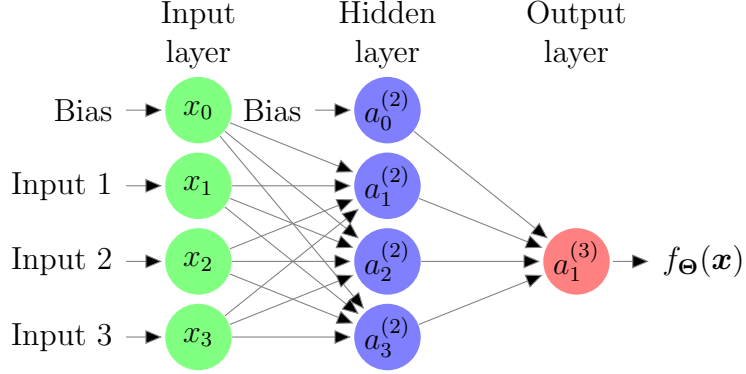


Figure 2.3: Example of a neural network structure with 3 external inputs, 1 hidden layer with 3 nodes, 1 bias node per non-output layer and 1 output node. The variable inside each node denotes its output as calculated in Section 2.2: the output of node i in layer j is denoted as $a_i^{(j)}$. Θ denotes the weights of the network.

Example 2.4.1. In this example, we follow Figure 2.3, describing a neural network with 3 inputs, 1 hidden layer with 3 nodes and 1 output node. We denote the activation function as g , the output of node i in layer j as $a_i^{(j)}$, and the matrix of weights from layer j to $j + 1$ as $\Theta^{(j)}$. The activation function may vary with each node, but typically each layer uses the same activation function for each node. We also use the subscript $\Theta_{m,n}^{(j)}$ where m is the row of the matrix corresponding to the node m in layer $j + 1$, and n is the column of the matrix relating to node n in layer j .

Denoting the weights outputting to unit i in layer $j + 1$ as $\theta_i^{(j)}$, we have the following relation between the node weights as described in Section 2.2 and these weight matrices: $\theta_i^{(j)} = \left[\Theta_{i,0}^{(j)} \quad \Theta_{i,1}^{(j)} \cdots \Theta_{i,k}^{(j)} \right]^\top$, where $k + 1$ is the number of inputs.

Individually, the outputs in the hidden nodes and the output node are:

$$x_0 = 1, \quad a_0^{(2)} = 1,$$

$$a_1^{(2)} = g \left(\Theta_{1,0}^{(1)} x_0 + \Theta_{1,1}^{(1)} x_1 + \Theta_{1,2}^{(1)} x_2 + \Theta_{1,3}^{(1)} x_3 \right) = g \left((\theta_1^{(1)})^\top \mathbf{x} \right),$$

$$a_2^{(2)} = g \left(\Theta_{2,0}^{(1)} x_0 + \Theta_{2,1}^{(1)} x_1 + \Theta_{2,2}^{(1)} x_2 + \Theta_{2,3}^{(1)} x_3 \right) = g \left((\theta_2^{(1)})^\top \mathbf{x} \right),$$

$$a_3^{(2)} = g \left(\Theta_{3,0}^{(1)}x_0 + \Theta_{3,1}^{(1)}x_1 + \Theta_{3,2}^{(1)}x_2 + \Theta_{3,3}^{(1)}x_3 \right) = g \left((\boldsymbol{\theta}_3^{(1)})^\top \mathbf{x} \right),$$

$$f_{\boldsymbol{\Theta}}(\mathbf{x}) = a_1^{(3)} = g \left(\Theta_{1,0}^{(2)}a_0^{(2)} + \Theta_{1,1}^{(2)}a_1^{(2)} + \Theta_{1,2}^{(2)}a_2^{(2)} + \Theta_{1,3}^{(2)}a_3^{(2)} \right) = g \left((\boldsymbol{\theta}_1^{(2)})^\top \mathbf{a}^{(2)} \right),$$

$$\text{where } \mathbf{a}^{(2)} = \begin{bmatrix} a_0^{(2)} & a_1^{(2)} & a_2^{(2)} & a_3^{(2)} \end{bmatrix}^\top.$$

2.5 Weight Initialisation

Proper initialisation of the weights $\boldsymbol{\Theta}$ is ideal to improve network training (discussed in Sections 2.6 and 2.7), as if the weights are too small, then the nodal outputs will continually decrease through the layers and become very small, resulting in a significant loss value which requires many iterations of training to fix. A similar scenario occurs when the initial weights are too high [Bishop, 1995]. In this section we discuss Xavier Initialization [Glorot and Bengio, 2010], a common initialisation method used in deep learning which aims to keep the signal variance constant throughout the network. To derive the initialization algorithm, first consider a single node with $n+1$ inputs, and let z denote the weighted sum of the inputs $\boldsymbol{\theta}^\top \mathbf{x}$ before it is passed through the activation function. This is written as

$$z = \theta_0 + \sum_{i=1}^n \theta_i x_i.$$

Here, θ_0 is constant with respect to the external input, so $\text{Var}(\theta_0) = 0$. Now without any prior knowledge of the inputs and weights, we assume that they are independent and have 0 mean. We can then find the variance of the other terms by using the formula for the product of independent variables [Goodman, 1960]:

$$\begin{aligned} \text{Var}(\theta_i x_i) &= \mathbb{E}[x_i]^2 \text{Var}(\theta_i) + \mathbb{E}[\theta_i]^2 \text{Var}(x_i) + \text{Var}(\theta_i) \text{Var}(x_i) \\ &= \text{Var}(\theta_i) \text{Var}(x_i). \end{aligned}$$

Assuming that the weights and inputs are also identically distributed, we have

$$\text{Var}(z) = n \text{Var}(\theta_i) \text{Var}(x_i).$$

Since we want constant variance of the signals throughout the network, we set $\text{Var}(z) = \text{Var}(x_i)$ and the result follows:

$$\text{Var}(\theta_i) = \frac{1}{n}.$$

However, this result only considers forward propagation of the signal. A variation of this result accounts for back propagation by averaging the number of input and output nodes:

$$\text{Var}(\theta_i) = \frac{2}{n_{in} + n_{out}}.$$

Thus, to enforce constant signal variance throughout the network, the ideal initialization of weights is to sample from a distribution, typically uniform or Gaussian, with 0 mean and $\frac{2}{n_{in} + n_{out}}$ variance:

$$\theta_i \sim U\left(-\sqrt{\frac{6}{n_{in} + n_{out}}}, \sqrt{\frac{6}{n_{in} + n_{out}}}\right)$$

or

$$\theta_i \sim N\left(0, \frac{2}{n_{in} + n_{out}}\right).$$

2.6 Optimisation

The goal of optimising the network is to train the weights of the network such that a loss function, which we will denote as L , is minimized. A common loss function is the squared error between the batch of network outputs and the actual results, so our objective function would be:

$$\min_{\Theta} L(\Theta) = \frac{1}{2}(\mathbf{y} - \mathbf{f}_{\Theta}(\mathbf{x}))^{\top}(\mathbf{y} - \mathbf{f}_{\Theta}(\mathbf{x})).$$

The $\frac{1}{2}$ factor is included to eliminate the factor of 2 in the derivative, simplifying the derivations. The derivative is multiplied by an arbitrary training rate during optimization so there is no significant impact of including that factor [Goodfellow et al., 2016].

Back-propagation (Section 2.7) is used to calculate the partial derivative of the loss function with respect to each individual weight. These partial derivatives are used in the gradient-based optimisation of the weights. There are many variations of neural network optimisation algorithms, but they are mostly based off gradient descent, which we will cover in this section [Ruder, 2016].

Definition 2.6.1. At point $\mathbf{x}^{(n)}$, $\mathbf{s}^{(n)}$ is a descent direction if $\nabla f(\mathbf{x}^{(n)})^{\top} \mathbf{s}^{(n)} < 0$.

Gradient descent [Boyd and Vandenberghe, 2004] is an algorithm used to find the minimizer \mathbf{x}^* of a function f by iterating on an arbitrary point $\mathbf{x}^{(n)}$, taking steps proportional to a descent direction $\mathbf{s}^{(n)}$:

$$\mathbf{x}^{(n+1)} = \mathbf{x}^{(n)} + \alpha \mathbf{s}^{(n)}, \quad \alpha > 0.$$

Proposition 2.6.2. [Beck, 2014] If $\mathbf{s}^{(n)}$ is a descent direction for $\mathbf{x}^{(n)}$, then for sufficiently small $\alpha > 0$,

$$f(\mathbf{x}^{(n)} + \alpha \mathbf{s}^{(n)}) < f(\mathbf{x}^{(n)}).$$

Proof. A proof of this proposition can be found in Appendix A.1. \square

A common choice of descent direction is the negative of the gradient, that is, $-\nabla f(\mathbf{x}^{(n)})$, leading to the method of steepest descent. It is clearly a descent direction as

$$\begin{aligned} \nabla f(\mathbf{x}^{(n)})^\top \nabla f(\mathbf{x}^{(n)}) &= -\|\nabla f(\mathbf{x}^{(n)})\|^2 \\ &< 0, \end{aligned}$$

where $\|\cdot\|$ denotes the Euclidean norm.

By nature, gradient descent is guaranteed to converge to a local minimum, which is problematic if the function has local minima which differ from the global minima. This is not an issue in this thesis, as all the loss functions we use are convex, so any local minima are also global minima. Those interested in global optimization can refer to “Deterministic Global Optimization” by Floudas [2005]. When training a neural network on a non-convex loss function there are currently no commonly used methods of guaranteeing a global minimum, but the path may escape from a local minimum if randomness is introduced to the training process. This can be accomplished by stochastic gradient descent.

Typically, the entire batch of data is used in each iteration to calculate the loss function and gradient values required for gradient descent. This method of batch gradient descent is very slow for large datasets. Stochastic gradient descent is defined by the use of only one observation per iteration, so the latent randomness associated with each observation effectively leads to noise added to each step, but the optimization is much faster. In practice, a compromise between stochastic and batch gradient descent is typically used; mini-batch gradient descent involves using several observations per iteration, leading to a reduction in the gradient variance [Li et al., 2014; Ruder, 2016]. The size of the batch depends on the size and nature of the data set. For small data sets, the batch would typically be the entire data set as this would be computationally feasible. On the other hand, online data is stochastic in nature and the data set is generally very large, so a small batch size would be used [Bengio, 2012].

Gradient descent convergence can be improved by using an adaptive learning rate, adjusting the value of α over the iterations, as a low learning rate in the process will make convergence slow, whilst a high learning rate can cause the algorithm to oscillate around the minima [Ruder, 2016].

In this thesis, we use the Adam algorithm, which incorporates these two concepts to form an effective optimization algorithm that is commonly applied to neural networks. It uses the first and second moments of the gradient decay rate to adapt the weight training rate. More details can be found in “Adam: A Method for Stochastic Optimization” by Kingma and Ba [2014].

2.7 Back-Propagation

In the back-propagation algorithm, the goal is to find the partial derivative of the loss function with respect to the individual weights

$$\frac{\partial}{\partial \Theta_{m,n}^{(j)}} L(\Theta),$$

so that gradient descent can be performed to optimize the weights [E. Rumelhart et al., 1986]. For each training sample $(\mathbf{x}^{(I)}, \mathbf{y}^{(I)})$, $I = 1, \dots, N$, the input signal is propagated forward throughout the network to calculate $\mathbf{a}^{(j)}$ for $j = 2, \dots, J$, where J is the total number of layers. The difference between the network output and the ideal result is calculated with

$$\boldsymbol{\delta}^{(J)} = \mathbf{a}^{(J)} - \mathbf{y}^{(I)},$$

and this error is propagated backwards through the network to find $\boldsymbol{\delta}^{(J-1)}, \dots, \boldsymbol{\delta}^{(2)}$ by using the formula

$$\boldsymbol{\delta}^{(j)} = \left((\Theta^{(j)})^\top \boldsymbol{\delta}^{(j+1)} \right) .* g' \left((\Theta^{(j)})^\top \mathbf{a}^{(j)} \right),$$

where $.*$ denotes element-wise multiplication and g' is the derivative of the activation function. In this case, g' takes in the sum of its weighted inputs, and as an example, the sigmoid activation function has the derivative $g' \left((\Theta^{(j)})^\top \mathbf{a}^{(j)} \right) = \mathbf{a}^{(j)} .* (1 - \mathbf{a}^{(j)})$. Note that $\boldsymbol{\delta}^{(1)}$ does not need to be calculated as the input layer is not weighted.

The errors for each layer are multiplied by each of the preceding layer’s activation outputs to form the estimated partial derivative for the training sample. This result

is added to an accumulator matrix, so that the average partial derivative from all the training samples can be computed:

$$\Delta_{m,n}^{(j)} := \Delta_{m,n}^{(j)} + a_n^{(j)} \delta_m^{(j+1)}$$

or in matrix-vector form.

$$\Delta^{(j)} := \Delta^{(j)} + \boldsymbol{\delta}^{(j+1)} (\mathbf{a}^{(j)})^\top.$$

Finally, we divide the accumulator matrix entries by the number of training samples to find the average partial derivative of the cost function with respect to the weights:

$$\frac{\partial}{\partial \Theta_{m,n}^{(j)}} L(\Theta) = \frac{1}{N} \Delta_{m,n}^{(j)}.$$

Pseudocode for back-propagation is shown in Appendix B.1.

CHAPTER 3

Variational Inference

In this chapter, we explain variational inference, a method that uses a specific functional form to approximate posterior distributions in the context of Bayesian statistics. These are denoted as ‘variational distributions’, from the use of variational calculus to derive certain expressions. We first describe the Bayesian framework and problems associated with computational intractability. We then explain, with examples, two types of variational inference: mean-field variational inference and amortized inference. Finally, the chapter concludes with a description of issues that arise when one or more of the prior or likelihood distributions are implicit, that is, samples can be readily drawn from them but the density function is difficult to numerically evaluate.

3.1 Context

A fundamental problem in Bayesian statistics is to evaluate, or estimate posterior densities to perform analysis on unknown parameters [Gelman et al., 2004]. Consider the set of latent and known variables $\mathbf{z} = (z_1, \dots, z_M) \in \mathbb{R}^M$ and $\mathbf{x} = (x_1, \dots, x_N) \in \mathbb{R}^N$, respectively, with joint density $p(\mathbf{z}, \mathbf{x})$. The posterior density $p(\mathbf{z}|\mathbf{x})$ is the distribution of the latent parameters z_1, \dots, z_M conditioned on the known variables \mathbf{x} . Applying Bayes’ theorem, it can be written as:

$$p(\mathbf{z}|\mathbf{x}) = \frac{p(\mathbf{z}, \mathbf{x})}{p(\mathbf{x})} = \frac{p(\mathbf{z})p(\mathbf{x}|\mathbf{z})}{\int_{\mathbb{R}} p(\mathbf{z}, \mathbf{x}) d\mathbf{z}},$$

where

- $p(\mathbf{z})$ is the prior distribution: the initial distribution of \mathbf{z} before the data \mathbf{x} is observed. This can be initialised to represent our subjective beliefs, or it can be an uninformative prior that implies objectivity.
- $p(\mathbf{x}|\mathbf{z})$ is the likelihood: the distribution of data \mathbf{x} conditioned on the parameters \mathbf{z} .

- $p(\mathbf{x}) = \int_{\mathbf{z}} p(\mathbf{z}, \mathbf{x}) d\mathbf{z}$ is the marginal likelihood, or the evidence: the density of the data averaged across all possible parameter values.

In simple cases, the posterior can typically be calculated algebraically by using the proportionality $p(\mathbf{z}|\mathbf{x}) \propto p(\mathbf{z})p(\mathbf{x}|\mathbf{z})$ and normalising over the constant $p(\mathbf{x})$. As the model becomes more complex, the calculations required can be extremely difficult, so traditional MCMC (Markov Chain Monte Carlo) methods overcome this obstacle by sampling from a Markov chain that converges to the stationary distribution $p(\mathbf{z}|\mathbf{x})$. However, these methods tend to have slow convergence for large datasets or high dimensional data. When faced with these issues or when desiring a faster computation, one may instead apply variational inference, an alternative approach to density estimation. Variational inference methods can be much faster than MCMC as they replace sampling with optimisation, but they are known to underestimate the true posterior variance [Blei et al., 2017].

3.2 The KL Divergence

We first define the f -divergence: a measure of how much two probability distributions differ.

Definition 3.2.1. The f -divergence of continuous probability distribution Q from P is

$$D_f(P\|Q) = \mathbb{E}_{p(x)} \left[f \left(\frac{q(x)}{p(x)} \right) \right],$$

where f is a convex function such that $f(1) = 0$.

Setting $f(x) = -\log x$ leads to the derivation of the KL (Kullback-Leibler) divergence [Kullback, 1959], a commonly used f -divergence in variational inference [Blei et al., 2017].

Definition 3.2.2. The KL divergence is the expected logarithmic difference between two distributions P and Q with respect to P :

$$KL(p(x)\|q(x)) = \int_{-\infty}^{\infty} p(x) \log \left(\frac{p(x)}{q(x)} \right) dx = \mathbb{E}_{p(x)} \left[\log \left(\frac{p(x)}{q(x)} \right) \right].$$

Remark 3.2.3. *The KL divergence is not symmetric:*

$$KL(p(x)\|q(x)) \neq KL(q(x)\|p(x)) \text{ for } p(x) \neq q(x).$$

In variational inference, $KL(p(x)\|q(x))$ is known as the forward KL divergence, whilst $KL(q(x)\|p(x))$ is the reverse KL divergence.

Lemma 3.2.4. *The reverse KL divergence is formulated when $f(u) = u \log u$ in an f -divergence.*

Proof.

$$\begin{aligned}
D_{RKL}(P\|Q) &= \mathbb{E}_{p(u)} \left[\frac{q(u)}{p(u)} \log \left(\frac{q(u)}{p(u)} \right) \right] \\
&= \int p(u) \frac{q(u)}{p(u)} \log \left(\frac{q(u)}{p(u)} \right) du \\
&= \int q(u) \log \left(\frac{q(u)}{p(u)} \right) du \\
&= \mathbb{E}_q \left[\log \left(\frac{q(u)}{p(u)} \right) \right] \\
&= KL[q(u)\|p(u)].
\end{aligned}$$

□

Note that the forward and reverse KL divergences mainly differ in the distribution that is used to take the expectation.

Lemma 3.2.5. *The KL divergence is non-negative, and it is equal to zero if and only if $p(x)$ and $q(x)$ are equivalent:*

$$KL(q(x)\|p(x)) \geq 0.$$

We prove this in the case where P and Q are continuous distributions: a similar proof holds when they are discrete.

Proof.

$$\begin{aligned}
KL(p(x)\|q(x)) &= \int_{-\infty}^{\infty} p(x) \log \left(\frac{p(x)}{q(x)} \right) dx \\
&= - \int_{-\infty}^{\infty} p(x) \log \left(\frac{q(x)}{p(x)} \right) dx \\
&\geq - \int_{-\infty}^{\infty} p(x) \left(\frac{q(x)}{p(x)} - 1 \right) dx \\
&= - \int_{-\infty}^{\infty} q(x) dx + \int_{-\infty}^{\infty} p(x) dx \\
&= 0.
\end{aligned}$$

In the third line we use $-\log x \geq -(x - 1)$ for all $x > 0$ with equality if and only if $x = 1$, therefore $KL(q(x)||p(x)) = 0$ if and only if $q(x) = p(x)$. The last line is due to $p(x)$ and $q(x)$ being probability densities. \square

3.3 Introduction to Variational Inference

Variational inference approximates the true posterior distribution $p(\mathbf{z}|\mathbf{x})$ with a different distribution $q(\mathbf{z})$, taken from a tractable family of approximate distributions \mathcal{Q} , and then minimizes the f -divergence between the two distributions in an optimization problem:

$$q^*(\mathbf{z}) = \arg \min_{q(\mathbf{z}) \in \mathcal{Q}} D_f(q(\mathbf{z})||p(\mathbf{z}|\mathbf{x})), \quad (3.3.1)$$

where D_f denotes an f -divergence [Blei et al., 2017]. This produces an analytic approximation to the posterior density. The most common f -divergence used in variational inference is the reverse KL divergence, used instead of the forward KL divergence as we are unable to sample from our true posterior $p(\mathbf{z}|\mathbf{x})$, and because it leads to an expectation maximization algorithm as opposed to an expectation propagation algorithm. Equation (3.3.1) can therefore be written as:

$$q^*(\mathbf{z}) = \arg \min_{q(\mathbf{z}) \in \mathcal{Q}} KL(q(\mathbf{z})||p(\mathbf{z}|\mathbf{x})). \quad (3.3.2)$$

From Lemma 3.2.5, it is evident that $KL(q(\mathbf{z})||p(\mathbf{z}|\mathbf{x}))$ attains a minimal value of 0 when $q(\mathbf{z}) = p(\mathbf{z}|\mathbf{x})$.

There is an issue with solving Equation (3.3.2) directly: we cannot evaluate the reverse KL divergence as $p(\mathbf{z}|\mathbf{x})$ is unknown. Instead, we rearrange the terms of Equation (3.3.1) to formulate a tractable expression that can be optimized.

3.4 Derivation of the ELBO

In this section, we formulate the evidence lower bound (ELBO) of our posterior inference problem. Maximisation of this term is equivalent to solving Equation

(3.3.1). We begin by applying Bayes' law to the problem and expanding the terms:

$$\begin{aligned}
q^*(\mathbf{z}) &= \arg \min_{q(\mathbf{z}) \in \mathcal{Q}} KL(q(\mathbf{z}) \| p(\mathbf{z} | \mathbf{x})) \\
&= \arg \min_{q(\mathbf{z}) \in \mathcal{Q}} \mathbb{E}_{q(\mathbf{z})} [\log q(\mathbf{z}) - \log p(\mathbf{z} | \mathbf{x})] \\
&= \arg \min_{q(\mathbf{z}) \in \mathcal{Q}} \mathbb{E}_{q(\mathbf{z})} \left[\log q(\mathbf{z}) - \log \frac{p(\mathbf{x} | \mathbf{z}) p(\mathbf{z})}{p(\mathbf{x})} \right] \\
&= \arg \min_{q(\mathbf{z}) \in \mathcal{Q}} (\mathbb{E}_{q(\mathbf{z})} [\log q(\mathbf{z}) - \log p(\mathbf{x} | \mathbf{z}) - \log p(\mathbf{z})] + \log p(\mathbf{x})) .
\end{aligned}$$

Note that in the last line $\mathbb{E}_{q(\mathbf{z})} [p(\mathbf{x})] = p(\mathbf{x})$ as $p(\mathbf{x})$ is independent of $q(\mathbf{z})$. Since our issues with Equation (3.3.1) result from the intractability of $p(\mathbf{x})$, we rearrange the KL divergence expression as follows:

$$\begin{aligned}
KL(q(\mathbf{z}) \| p(\mathbf{z} | \mathbf{x})) &= \mathbb{E}_{q(\mathbf{z})} [\log q(\mathbf{z}) - \log p(\mathbf{x} | \mathbf{z}) - \log p(\mathbf{z})] + \log p(\mathbf{x}) \\
\log p(\mathbf{x}) - KL(q(\mathbf{z}) \| p(\mathbf{z} | \mathbf{x})) &= -\mathbb{E}_{q(\mathbf{z})} [\log q(\mathbf{z}) - \log p(\mathbf{x} | \mathbf{z}) - \log p(\mathbf{z})] \\
&= \mathbb{E}_{q(\mathbf{z})} [\log p(\mathbf{x} | \mathbf{z})] - \mathbb{E}_{q(\mathbf{z})} [\log q(\mathbf{z}) - \log p(\mathbf{z})] \\
&= \mathbb{E}_{q(\mathbf{z})} [\log p(\mathbf{x} | \mathbf{z})] - KL(q(\mathbf{z}) \| p(\mathbf{z})) \tag{3.4.1}
\end{aligned}$$

$$\log p(\mathbf{x}) \geq \mathbb{E}_{q(\mathbf{z})} [\log p(\mathbf{x} | \mathbf{z})] - KL(q(\mathbf{z}) \| p(\mathbf{z})). \tag{3.4.2}$$

We refer to $\log p(\mathbf{x}) - KL(q(\mathbf{z}) \| p(\mathbf{z} | \mathbf{x}))$ as $ELBO(q)$, as it is equal to the marginal probability of the data subtracted by a constant ‘error term’. Now our problem of minimizing the KL divergence between $q(\mathbf{z})$ and $p(\mathbf{z} | \mathbf{x})$ is equivalent to maximizing $ELBO(q)$, which is equal to Expression (3.4.1). We can therefore rewrite our optimization problem as:

$$\begin{aligned}
q^*(\mathbf{z}) &= \arg \min_{q(\mathbf{z}) \in \mathcal{Q}} KL(q(\mathbf{z}) \| p(\mathbf{z} | \mathbf{x})) \\
&= \arg \max_{q(\mathbf{z}) \in \mathcal{Q}} ELBO(q) \\
&= \arg \max_{q(\mathbf{z}) \in \mathcal{Q}} (\mathbb{E}_{q(\mathbf{z})} [\log p(\mathbf{x} | \mathbf{z})] - KL(q(\mathbf{z}) \| p(\mathbf{z}))) . \tag{3.4.3}
\end{aligned}$$

We remark that the Expression (3.4.3) attains a maximum at the marginal likelihood of the dataset $\log p(\mathbf{x})$, hence we may use the ELBO to construct a model selection criterion [Bishop, 2006]. However, this criterion may not be reliable as it is a lower bound.

3.5 Mean-Field Variational Family

The family of variational distributions \mathcal{Q} is typically a ‘mean-field variational family’, in which the distribution $q(\mathbf{z})$ factorizes over the latent variables $\{z_i\}_{i=1}^M$, each with an individual set of parameters $\{\phi_i\}_{i=1}^M$ [Blei et al., 2017]:

$$q(\mathbf{z}) = \prod_{i=1}^M q_{\phi_i}(z_i). \quad (3.5.1)$$

The individual factors $q_{\phi_i}(z_i)$ can take any form, but they are assumed to be independent, which simplifies derivations but is less accurate when the true latent variables exhibit dependence. Fixing the forms of the individual factors, we want to choose the parameters ϕ_i so that $ELBO(q)$ is maximized. To derive an expression for the optimal factor $q_{\phi_i}^*(z_i)$, we substitute Equation (3.5.1) into the $ELBO$, factor out a specific $q_{\phi_j}(z_j)$ and equate the functional derivative of the resulting Lagrangian equation with 0. This process is detailed in Appendix C, and leads to the optimal individual factor:

$$q_{\phi_i}^*(z_i) \propto \exp \left(\mathbb{E}_{\mathbf{z}_{-i}} [\log p(z_i | \mathbf{z}_{-i}, \mathbf{x})] \right).$$

This expression can be used in an expectation-maximization algorithm, in which the $q_{\phi_i}^*(z_i)$ is evaluated and iterated from $i = 1, \dots, M$ until $ELBO(q)$ converges. We can say this occurs when there is little variation in $ELBO(q)$ over the iterations. This particular algorithm is called coordinate ascent variational inference (CAVI); pseudocode can be found in Algorithm 6 in Appendix B.2. Appendix D exemplifies mean-field variational inference, closely following the ‘Bayesian Mixture of Gaussians’ example from ‘Variational Inference: A Review for Statisticians’ by Blei et al. [2017].

3.6 Amortized Inference

Now consider the case where we have K data points, each with dimensionality N . We denote the set of data points as $\mathbf{X} = [\mathbf{x}^{(1)}, \dots, \mathbf{x}^{(K)}]^\top$, where $\mathbf{x}^{(i)} = (x_1^{(i)}, \dots, x_N^{(i)}) \in \mathbb{R}^N$, $i = 1, \dots, K$. One disadvantage of mean field variational inference is that a specific set of variational parameters needs to be derived and optimized for each of these data points. This can be computationally expensive for large datasets because the parametrisation of the posterior $p(\mathbf{z} | \mathbf{x})$ changes as the data point \mathbf{x} changes. We therefore denote our set of latent variable points as $\mathbf{Z} = (\mathbf{z}^{(1)}, \dots, \mathbf{z}^{(K)})^\top$, where $\mathbf{z}^{(i)} = (z_1^{(i)}, \dots, z_M^{(i)}) \in \mathbb{R}^M$, $i = 1, \dots, K$. In mean-field variational inference, each

latent variable $z_j^{(i)}$ has its own individual set of parameters $\phi_j^{(i)}$, so overall there are $M \times N$ sets of parameters.

Amortized inference resolves this issue by using a single, constant set of parameters for all data points, adding the data point itself as an input to the variational distribution [Zhang et al., 2017]. We denote this practice as *amortizing* the distribution. Our variational distribution therefore conditions on the observation, taking the form

$$q_\phi(\mathbf{z}|\mathbf{x}).$$

Figures 3.1 and 3.2 highlight the difference between mean-field and amortized variational inference.

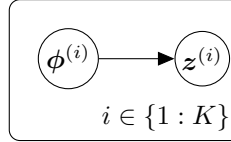


Figure 3.1: This DAG represents Mean-Field Variational Inference. For each of the K datasets, a set of parameter sets $\phi^{(i)}$ corresponding to each latent variable point $z^{(i)}$ has to be found. $\phi^{(i)}$ is M -dimensional, so there is a total of $M \times K$ sets of parameters.

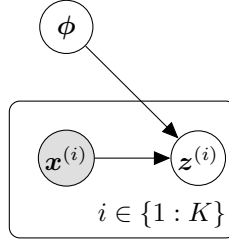


Figure 3.2: This DAG represents Amortized Variational Inference. Here, there is only one set of variational parameters ϕ , and each data point $\mathbf{x}^{(i)}$ is used as an input in the variational posterior $q_\phi(\mathbf{z}|\mathbf{x})$ to find $z^{(i)}$.

A very complex variational distribution is required to model such a structure, so it often takes the form of a neural network with \mathbf{x} as an input. This method is often used in deep learning due to the significant amount of data required to train such a network.

Now recall that $p(\mathbf{x})$ represents the marginal likelihood, or ‘true’ distribution of the data. This is typically never available, we often instead represent it with the distribution of a sample dataset. Denoting the sample dataset density function as $q^*(\mathbf{x})$, we want to optimize ϕ across the observations from our dataset, so our

objective now is to choose parameters ϕ such that the expected KL divergence with respect to $q^*(\mathbf{x})$ is minimized:

$$\begin{aligned}
\phi &= \arg \min_{\phi} \mathbb{E}_{q^*(\mathbf{x})} KL(q_{\phi}(\mathbf{z}|\mathbf{x})||p(\mathbf{z}|\mathbf{x})) \\
&= \arg \min_{\phi} \mathbb{E}_{q^*(\mathbf{x})q_{\phi}(\mathbf{z}|\mathbf{x})} [\log q_{\phi}(\mathbf{z}|\mathbf{x}) - \log p(\mathbf{z}|\mathbf{x})] \\
&= \arg \min_{\phi} \mathbb{E}_{q^*(\mathbf{x})q_{\phi}(\mathbf{z}|\mathbf{x})} \left[\log q_{\phi}(\mathbf{z}|\mathbf{x}) - \log \frac{p(\mathbf{x}|\mathbf{z})p(\mathbf{z})}{p(\mathbf{x})} \right] \\
&= \arg \min_{\phi} \left(\mathbb{E}_{q^*(\mathbf{x})q_{\phi}(\mathbf{z}|\mathbf{x})} [\log q_{\phi}(\mathbf{z}|\mathbf{x}) - \log p(\mathbf{x}|\mathbf{z}) - \log p(\mathbf{z})] + \log p(\mathbf{x}) \right).
\end{aligned}$$

Again, we cannot evaluate this expression as $\log p(\mathbf{x})$ is intractable, so we rearrange the terms to form the evidence lower bound, which we aim to maximise to minimise the KL divergence.

$$\begin{aligned}
ELBO(q) &= \mathbb{E}_{q^*(\mathbf{x})} [\log p(\mathbf{x}) - KL(q_{\phi}(\mathbf{z}|\mathbf{x})||p(\mathbf{z}|\mathbf{x}))] \\
&= -\mathbb{E}_{q^*(\mathbf{x})q_{\phi}(\mathbf{z}|\mathbf{x})} [\log q_{\phi}(\mathbf{z}|\mathbf{x}) - \log p(\mathbf{x}|\mathbf{z}) - \log p(\mathbf{z})] \\
&= \mathbb{E}_{q^*(\mathbf{x})q_{\phi}(\mathbf{z}|\mathbf{x})} [\log p(\mathbf{x}|\mathbf{z}) + \log p(\mathbf{z}) - \log q_{\phi}(\mathbf{z}|\mathbf{x})] \\
&= \mathbb{E}_{q^*(\mathbf{x})} [\mathbb{E}_{q_{\phi}(\mathbf{z}|\mathbf{x})} [\log p(\mathbf{x}|\mathbf{z})] - KL(q_{\phi}(\mathbf{z}|\mathbf{x})||p(\mathbf{z}))].
\end{aligned}$$

We take the negative to form the negative evidence lower bound $NELBO(q)$, which we aim to minimize:

$$NELBO(q) = \mathbb{E}_{q^*(\mathbf{x})} \cdot \left[-\mathbb{E}_{q_{\phi}(\mathbf{z}|\mathbf{x})} [\log p(\mathbf{x}|\mathbf{z})] + KL(q_{\phi}(\mathbf{z}|\mathbf{x})||p(\mathbf{z})) \right],$$

$$\min_{\phi} NELBO(q). \tag{3.6.1}$$

Since ϕ represents the parameters of a neural network, it is inefficient to find the specific weight values during back-propagation: we are more interested in training the network to optimality, which occurs when we minimize the objective function. Hence, it is more appropriate to write the optimization problem with min than with arg min.

In deep learning, the likelihood term $p(\mathbf{x}|\mathbf{z})$ is often represented as a neural network parametrized by θ : $p_{\theta}(\mathbf{x}|\mathbf{z})$. This network is optimized alongside the variational distribution, in a formation known as the variational autoencoder.

3.7 Example: Variational Autoencoder

A variational autoencoder (Figure 3.3) is a model consisting of two simultaneously trained neural networks: an encoder representing the posterior distribution $q_\phi(\mathbf{z}|\mathbf{x})$ that “compresses” a data point $\mathbf{x} = (x_1, \dots, x_N)$ into a lower dimensional latent representation \mathbf{z} , and a decoder representing the likelihood distribution $p_\theta(\mathbf{x}|\mathbf{z})$ that “reconstructs” the data point from the latent variable [Kingma and Welling, 2013]. It has two main purposes: lower-dimensional representation learning of data and data generation. Typically, the prior $p(\mathbf{z})$ is simply a standard multivariate normal distribution with dimensionality equal to that of the latent variable point $\mathbf{z} = (z_1, \dots, z_M): \mathcal{N}(0, I_{M \times M})$. We now reiterate our optimization problem in Equation (3.6.1), this time including the optimization of the decoder parameters θ :

$$\min_{\phi, \theta} \mathbb{E}_{q^*(\mathbf{x})} \left[-\mathbb{E}_{q_\phi(\mathbf{z}|\mathbf{x})} [\log p_\theta(\mathbf{x}|\mathbf{z})] + KL(q_\phi(\mathbf{z}|\mathbf{x}) \| p(\mathbf{z})) \right]. \quad (3.7.1)$$

The first term is the negative likelihood, which is analogous to the reconstruction error which we want to minimize. The KL divergence between the variational posterior and the true prior distribution, often a standard multivariate normal distribution acts as a regularizer term. Without it, the encoder would learn to segregate distinct data types in separate regions of the Euclidean plane, which runs contrary to the randomness of a probability distribution. Due to this regularizer term, we can generate new data \mathbf{x} by sampling $\mathbf{z} \sim p(\mathbf{z})$ and feeding it through the decoder [Doersch, 2016]. This is illustrated in Figure 3.4.

In our current formulation, we are trying to represent the variational posterior distribution with a deterministic neural network, so for any given data point \mathbf{x} , the encoder will always output the same \mathbf{z} . The solution is to add a noise distribution to the model to make it probabilistic. Instead of the encoder outputting the posterior sample \mathbf{z} directly, we configure it to output a mean vector $\boldsymbol{\mu} = (\mu_1, \mu_2, \dots, \mu_M)^\top$ and variance vector $\boldsymbol{\sigma}^2 = (\sigma_1^2, \sigma_2^2, \dots, \sigma_M^2)^\top$, each with dimensions equal to that of latent variable \mathbf{z} . We then define \mathbf{z} as an output from a multivariate normal distribution with means and variances as specified by the encoder output:

$$q_\phi(\mathbf{z}|\mathbf{x}) \sim \mathcal{N}(\boldsymbol{\mu}, \boldsymbol{\sigma}^2 I_{M \times M}).$$

Often in practice, this is achieved by sampling random standard normal noise ϵ , multiplying it by the variance and adding the result to the mean:

$$\epsilon \sim \mathcal{N}(0, I_{M \times M}), \quad \mathbf{z} = \boldsymbol{\mu} + \epsilon \cdot \boldsymbol{\sigma}^2.$$

A similar process of adding random noise is used for the decoder network representing the likelihood distribution $p_\theta(\mathbf{x}|\mathbf{z})$, but the parametrisation of the distribution is chosen depending on the nature of the data. For example, for most continuous data, we can use a multivariate normal parametrisation similar to our variational posterior. For binary data, a sigmoid output layer is specified in the neural network and the likelihood distribution is expressed as a Bernoulli distribution with probabilities given by the network output.

Lemma 3.7.1. *Using the explicit form of the multivariate normal $q_\phi(\mathbf{z}|\mathbf{x})$ and $p(\mathbf{z})$ densities, the KL divergence term can be calculated through the equation:*

$$KL(q_\phi(\mathbf{z}|\mathbf{x})||p(\mathbf{z})) = \frac{1}{2} \sum_{i=1}^M (\sigma_i^2 + \mu_i^2 - \log(\sigma_i^2) - 1).$$

Proof. Proof of this lemma can be found in Appendix A.2. □

We can now evaluate and minimise the *NELBO* in Equation (3.7.1) as we have an explicit parametrisation of all of the terms.

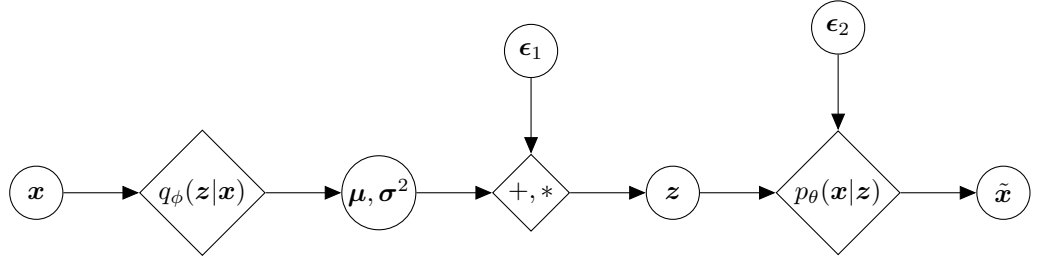


Figure 3.3: A simple DAG representing a Variational Autoencoder. An arbitrary data point \mathbf{x} is passed through the encoder $q_\phi(\mathbf{z}|\mathbf{x})$ to produce a mean vector $\boldsymbol{\mu}$ and a variance vector $\boldsymbol{\sigma}^2$. Random noise $\boldsymbol{\epsilon}_1$ is sampled from $\mathcal{N}(0, I_{M \times M})$ and transformed to generate \mathbf{z} : $\mathbf{z} = \boldsymbol{\mu} + \boldsymbol{\epsilon} \cdot \boldsymbol{\sigma}^2$. This latent variable \mathbf{z} is passed through the decoder $p_\theta(\mathbf{x}|\mathbf{z})$ to reconstruct the data point as $\tilde{\mathbf{x}}$.

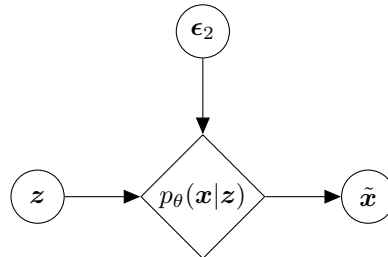


Figure 3.4: To generate new data $\tilde{\mathbf{x}}$ similar to existing data \mathbf{x} , we sample latent variable \mathbf{z} from the prior distribution $p(\mathbf{z})$ and pass it through the decoder $p_\theta(\mathbf{x}|\mathbf{z})$.

3.8 Problems with Implicit Distributions

The above sections assume that the prior $p(\mathbf{z})$, likelihood ($p(\mathbf{x}|\mathbf{z})$ or $p_\theta(\mathbf{x}|\mathbf{z})$) and variational posterior $q_\phi(\mathbf{z}|\mathbf{x})$ have an explicit form. However, there are two main scenarios in which at least one of these distributions is implicit, that is, the parametrisation of their density is difficult to numerically evaluate but we are able to easily generate samples from them. This poses problems with optimization as the objective function becomes difficult to compute.

3.8.1 Implicit Prior and/or Variational Posterior

In the first scenario, at least one of the prior $p(\mathbf{z})$ or variational posterior $q_\phi(\mathbf{z}|\mathbf{x})$ distributions is implicit, but the likelihood is known. An implicit prior is rare but may occur in posterior inference. The implicit variational posterior is more common (in both posterior inference and data generation), detailed in “Adversarial Variational Bayes” by Mescheder et al. [2017].

Typically in amortized inference and variational autoencoders, the variational posterior sample \mathbf{z} is sampled from a multivariate normal distribution with mean and variance defined by the variational network. The problem with this representation is the lack of dependencies between the latent variables and the inability to model multi-modal or flexible densities. In his paper, Mescheder adds random noise $\epsilon \sim \pi(\epsilon)$ as additional inputs to the variational network, training the network to directly output \mathbf{z} . $\pi(\epsilon)$ is a typical noise distribution, such as $\mathcal{N}(0, I_{p \times p})$ where p is the desired number of noise inputs. This added noise allows the probabilistic nature of a random distribution to be represented by a deterministic neural network. However, note that the neural network does not output the probability density $q_\phi(\mathbf{z}|\mathbf{x})$, rather it outputs the distribution sample $\mathbf{z} \sim q_\phi(\mathbf{z}|\mathbf{x})$. Retaining the network parameters ϕ , we denote the generator of posterior samples as $\mathcal{G}_\phi(\epsilon; \mathbf{x})$. A diagram illustrating this is shown in Figure 3.5.

Due to the complex nature of the neural network, it is difficult to numerically compute the explicit form of $q_\phi(\mathbf{z}|\mathbf{x})$ in this representation, but we are able to easily generate samples by feeding data and noise through the network, hence its implicit nature.

Now again recall our optimization problem from Equation (3.7.1):

$$\min_{\phi, \theta} \mathbb{E}_{q^*(\mathbf{x})} \left[-\mathbb{E}_{q_\phi(\mathbf{z}|\mathbf{x})} [\log p_\theta(\mathbf{x}|\mathbf{z})] + KL(q_\phi(\mathbf{z}|\mathbf{x}) \| p(\mathbf{z})) \right].$$

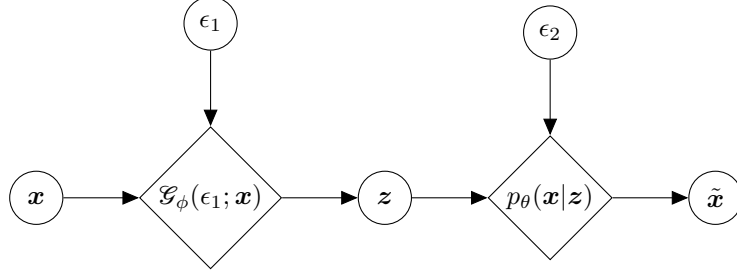


Figure 3.5: This diagram depicts the “Adversarial Variational Bayes” formulation of the variational autoencoder. Rather than transforming random noise ϵ_1 according to the mean vector $\boldsymbol{\mu}$ and variance vector $\boldsymbol{\sigma}$ output of the variational posterior $q_\phi(\mathbf{z}|\mathbf{x})$, we add the noise to the encoder network $\mathcal{G}_\phi(\epsilon_1; \mathbf{x})$ directly as an additional input. The likelihood distribution $p_\theta(\mathbf{x}|\mathbf{z})$ has the same explicit representation as in Figures 3.3 and 3.4.

When either the prior or variational posterior is implicit, this expression is difficult to evaluate as we are unable to calculate the KL divergence

$$KL(q_\phi(\mathbf{z}|\mathbf{x})\|p(\mathbf{z})) = \mathbb{E}_{q_\phi(\mathbf{z}|\mathbf{x})} \left[\log \frac{q_\phi(\mathbf{z}|\mathbf{x})}{p(\mathbf{z})} \right].$$

We therefore resort to density ratio estimation techniques (Chapter 4) to approximate $\frac{q_\phi(\mathbf{z}|\mathbf{x})}{p(\mathbf{z})}$, using only samples from the two densities.

3.8.2 Implicit Likelihood

When we apply amortized variational inference to an implicit likelihood distribution, the optimization problem is intractable even with density ratio estimation, as it is difficult to evaluate the term $-\mathbb{E}_{q_\phi(\mathbf{z}|\mathbf{x})}[\log p_\theta(\mathbf{x}|\mathbf{z})]$. This can occur in posterior inference or in some autoencoder variations where an implicit generative function $G_\theta(\epsilon; \mathbf{x})$ is used to represent the likelihood distribution $p_\theta(\mathbf{x}|\mathbf{z})$ [Dumoulin et al., 2016]. An example of the latter case is illustrated in Figure 3.6.

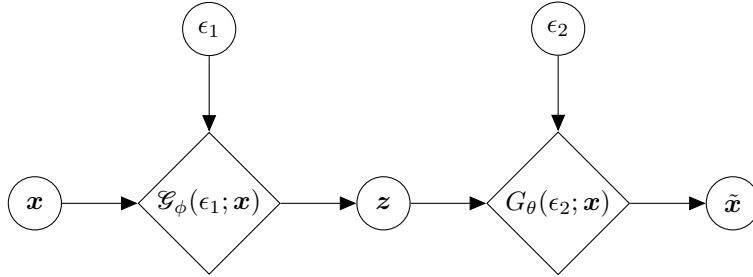


Figure 3.6: This diagram depicts a variation of “Adversarial Variational Bayes”, in which noise is additionally added to the input of the generator of likelihood distribution samples $G_\theta(\epsilon_2; \mathbf{x})$. The likelihood distribution $p_\theta(\mathbf{x}|\mathbf{z})$ is therefore implicit and consequently, its corresponding term in the optimisation problem cannot be evaluated.

We rephrase the optimisation problem, instead minimising the reverse KL divergence between the two joint distributions: $KL(q(\mathbf{z}, \mathbf{x}) \| p(\mathbf{z}, \mathbf{x})) = \mathbb{E}_{q(\mathbf{z}, \mathbf{x})} \left[\log \frac{q(\mathbf{z}, \mathbf{x})}{p(\mathbf{z}, \mathbf{x})} \right]$ [Tran et al., 2017]. We begin deriving this by restating the reverse KL divergence between the true and variational posterior distributions, but this time applying Bayes’ theorem to formulate the joint densities:

$$\begin{aligned} \mathbb{E}_{q^*(\mathbf{x})} [KL(q_\phi(\mathbf{z}|\mathbf{x}) \| p_\theta(\mathbf{z}|\mathbf{x}))] &= \mathbb{E}_{q^*(\mathbf{x})q(\mathbf{z}|\mathbf{x})} \left[\log \frac{q(\mathbf{z}|\mathbf{x})p(\mathbf{x})}{p(\mathbf{x}|\mathbf{z})p(\mathbf{z})} \right] \\ &= \mathbb{E}_{q^*(\mathbf{x})q(\mathbf{z}|\mathbf{x})} \left[\log \frac{q(\mathbf{z}|\mathbf{x})q^*(\mathbf{x})}{p(\mathbf{x}|\mathbf{z})p(\mathbf{z})} \right] + \mathbb{E}_{q^*(\mathbf{x})} \left[\log \frac{p(\mathbf{x})}{q^*(\mathbf{x})} \right] \\ &= \mathbb{E}_{q^*(\mathbf{x})q(\mathbf{z}|\mathbf{x})} \left[\log \frac{q(\mathbf{z}, \mathbf{x})}{p(\mathbf{z}, \mathbf{x})} \right] - KL(q^*(\mathbf{x}) \| p(\mathbf{x})). \end{aligned}$$

Recall that $p(\mathbf{x})$ is typically unavailable, so we are unable to evaluate $KL(q^*(\mathbf{x}) \| p(\mathbf{x}))$ even with density ratio estimation techniques. Since it is constant, we add it to both sides of the equation, leading to the following expression for $NELBO(q)$:

$$\begin{aligned} NELBO(q) &= KL(q^*(\mathbf{x}) \| p(\mathbf{x})) + \mathbb{E}_{q^*(\mathbf{x})} KL(q_\phi(\mathbf{z}|\mathbf{x}) \| p_\theta(\mathbf{z}|\mathbf{x})) \\ &= \mathbb{E}_{q^*(\mathbf{x})q_\phi(\mathbf{z}|\mathbf{x})} \left[\log \frac{q(\mathbf{z}, \mathbf{x})}{p(\mathbf{z}, \mathbf{x})} \right]. \end{aligned}$$

This expression attains a minimum at $KL(q^*(\mathbf{x}) \| p(\mathbf{x}))$ when

$$\mathbb{E}_{q^*(\mathbf{x})} [KL(q_\phi(\mathbf{z}|\mathbf{x}) \| p_\theta(\mathbf{z}|\mathbf{x}))] = 0,$$

that is, the true and variational posteriors are equivalent with respect to the distribution of the data set. We therefore have the following lower bound:

$$\mathbb{E}_{q^*(\mathbf{x})q_\phi(\mathbf{z}|\mathbf{x})} \left[\log \frac{q(\mathbf{z}, \mathbf{x})}{p(\mathbf{z}, \mathbf{x})} \right] \geq KL(q^*(\mathbf{x}) \| p(\mathbf{x})).$$

Our objective now is to minimize this $NELBO$ with respect to our variational parameters ϕ , which can be approximated with density ratio estimation techniques:

$$\min_{\phi} \mathbb{E}_{q^*(\mathbf{x})q_\phi(\mathbf{z}|\mathbf{x})} \left[\log \frac{q(\mathbf{z}, \mathbf{x})}{p(\mathbf{z}, \mathbf{x})} \right]. \quad (3.8.1)$$

For consistency, we have retained the notation of our variational posterior loss function as $NELBO(q)$. Note that the likelihood parameters no longer appear in the objective function, hence this expression on its own is only sufficient for posterior inference. The objective problem no longer has an explicit likelihood term, so

it can be used with an implicit likelihood. In fact, since density ratio estimation only requires samples from the two distributions, both the prior and variational posterior densities can also be implicit, hence the “Adversarial Variational Bayes” representation (Figure 3.5) of the variational network can be used.

In the autoencoder representation (Figure 3.6), we would additionally have to minimize the forward KL divergence with respect to the likelihood parameters [Tiao et al., 2018]:

$$\min_{\theta} \mathbb{E}_{p(\mathbf{z})p_{\theta}(\mathbf{x}|\mathbf{z})} \left[\log \frac{p(\mathbf{z}, \mathbf{x})}{q(\mathbf{z}, \mathbf{x})} \right]. \quad (3.8.2)$$

In this scenario, separate density ratio estimators would be used for Equations (3.8.1) and (3.8.2), as we have taken the expectation of the density ratios with respect to different distributions.

CHAPTER 4

Density Ratio Estimation

In this chapter, we derive two common methods of density ratio estimation used with implicit models [Mohamed and Lakshminarayanan, 2016; Sugiyama et al., 2012]: class probability estimation and divergence minimisation, applying them to both the implicit prior/posterior and implicit likelihood objective functions to formulate bi-level optimization problems. In this thesis, we use Huszar’s terminology, referring to the implicit prior/posterior objective as “prior-contrastive” and the implicit likelihood objective as “joint-contrastive” [Huszar, 2017].

4.1 Class Probability Estimation

4.1.1 Derivation

First, consider the probability density functions $p(u)$ and $q(u)$ defined on $U \subseteq \mathbb{R}^S$. We aim to estimate the density ratio $\frac{q(u)}{p(u)}$, given only samples from the two densities. In this thesis, we assume that for all $u \in U$, $p(u) > 0$ and $q(u) > 0$, avoiding the division of zero in density ratio estimation.

We take m samples from $p(u)$: $U_p = \{u_1^{(p)}, \dots, u_m^{(p)}\}$ and label them with $y = 0$, then we take n samples from $q(u)$: $U_q = \{u_1^{(q)}, \dots, u_n^{(q)}\}$ and label them with $y = 1$. Therefore, $p(u) = P(u|y = 0)$ and $q(u) = P(u|y = 1)$. By applying Bayes’ theorem, we derive an expression for the density ratio:

$$\begin{aligned} \frac{q(u)}{p(u)} &= \frac{P(u|y = 1)}{P(u|y = 0)} \\ &= \frac{P(y = 1|u)P(u)}{P(y = 0|u)P(u)} \bigg/ \frac{P(y = 0|u)P(u)}{P(y = 1|u)P(u)} \\ &= \frac{P(y = 1|u)}{P(y = 0|u)} \times \frac{P(y = 0)}{P(y = 1)} \\ &= \frac{P(y = 1|u)}{P(y = 0|u)} \times \frac{n}{m}. \end{aligned}$$

Often in practice, $m = n$, simplifying the density ratio to:

$$\frac{q(u)}{p(u)} = \frac{P(y = 1|u)}{P(y = 0|u)}$$

which is the ratio of the probability that an arbitrary sample u was taken from the distribution $q(u)$ to the probability that it was taken from $p(u)$. If we define a *discriminator* function $D(u) \simeq P(y = 1|u)$ that estimates these probabilities, then our density ratio can be expressed in terms of this discriminator function:

$$\frac{q(u)}{p(u)} \simeq \frac{D(u)}{1 - D(u)}.$$

At optimality, the discriminator provides an exact estimate of the probability that the sample was taken from $q(u)$, so we have $D^*(u) = P(y = 1|u)$ and therefore,

$$\frac{q(u)}{p(u)} = \frac{D^*(u)}{1 - D^*(u)}.$$

The discriminator function typically takes the form of a neural network with parameters α trained with Bernoulli loss (the negative log-likelihood of the Bernoulli distribution), which we denote as L_D [Sugiyama et al., 2012]:

$$L_D := -\mathbb{E}_{q(u)}[\log D_\alpha(u)] - \mathbb{E}_{p(u)}[\log(1 - D_\alpha(u))].$$

Lemma 4.1.1. *The discriminator reaches optimality at $D_\alpha^*(u) = \frac{q(u)}{q(u)+p(u)}$, minimizing its Bernoulli loss [Goodfellow et al., 2014].*

Proof. Proof of this lemma can be found in Appendix A.3. □

Remark 4.1.2. $D_\alpha^*(u)$ is bound in $(0, 1)$, so typically a sigmoid activation function is used for its output layer. Note that $D_\alpha^*(u) \neq 0$ and $D_\alpha^*(u) \neq 1$ as we have assumed $p(u) > 0$ and $q(u) > 0$ for all $u \in U$.

Remark 4.1.3. When $q(u)$ and $p(u)$ are equivalent, that is, $q(u) = p(u)$, the discriminator cannot distinguish between samples from the two distributions, outputting a probability of $\frac{1}{2}$: $D_\alpha^*(u) = \frac{1}{2}$. Substituting this value into the Bernoulli loss function, we obtain its minimal value when the two distributions are equivalent and the discriminator is at its optimal parametrisation: $L_{D^*} = \log 4$.

In the context of amortized variational inference, the optimal discriminative loss can be used to check posterior convergence, that is, when the variational distribution $q_\phi(z|x)$ is equivalent to the true posterior distribution $p(z|x)$.

4.1.2 Prior-Contrastive Algorithm

We now turn to the prior-contrastive problem in Expression (3.6.1) of minimizing the *NELBO*:

$$\begin{aligned} \min_{\phi} NELBO(q) &= \min_{\phi} \mathbb{E}_{q^*(x)} [-\mathbb{E}_{q_{\phi}(z|x)} [\log p(x|z)] + KL(q_{\phi}(z|x) || p(z))] \\ &= \min_{\phi} -\mathbb{E}_{q^*(x)q_{\phi}(z|x)} [\log p(x|z)] + \mathbb{E}_{q^*(x)q_{\phi}(z|x)} \left[\log \frac{q_{\phi}(z|x)}{p(z)} \right], \end{aligned} \quad (4.1.1)$$

which requires us to find the density ratio between $q_{\phi}(z|x)$ and $p_{\theta}(z)$.

Again, if we label samples from $q_{\phi}(z|x)$ with $y = 1$ and samples from $p(z)$ with $y = 0$, we have the density ratio expression:

$$\frac{q_{\phi}(z|x)}{p(z)} = \frac{P(y = 1|z)}{P(y = 0|z)}.$$

We now define a discriminator function with parameters α that calculates the probability that an arbitrary sample z belongs to the variational posterior $q_{\phi}(z|x)$. Since the posterior changes depending on the observation x , we also amortize the discriminator by taking an additional input from the dataset x , as opposed to training multiple discriminators for each observation x :

$$D_{\alpha}(z, x) \simeq P(y = 1|z).$$

As a binary classifier, this function can be trained by inputting an equal number of samples from both distributions and minimizing its Bernoulli loss:

$$\min_{\alpha} -\mathbb{E}_{q^*(x)q_{\phi}(z|x)} [\log D_{\alpha}(z, x)] - \mathbb{E}_{q^*(x)p_{\theta}(z)} [\log(1 - D_{\alpha}(z, x))]. \quad (4.1.2)$$

We can now express the expected log ratio in terms of the probability that a posterior sample is correctly classified by the discriminator:

$$\begin{aligned} \mathbb{E}_{q^*(x)q_{\phi}(z|x)} \left[\log \frac{q_{\phi}(z|x)}{p(z)} \right] &= \mathbb{E}_{q^*(x)q_{\phi}(z|x)} \left[\log \frac{P(y = 1|z)}{P(y = 0|z)} \right] \\ &\simeq \mathbb{E}_{q^*(x)q_{\phi}(z|x)} \left[\log \frac{D_{\alpha}(z, x)}{1 - D_{\alpha}(z, x)} \right]. \end{aligned}$$

Our *NELBO* optimization objective in Expression (4.1.1) can now be written as:

$$\min_{\phi} -\mathbb{E}_{q^*(x)q_{\phi}(z|x)}[\log p(x|z)] + \mathbb{E}_{q^*(x)q_{\phi}(z|x)} \left[\log \frac{D_{\alpha}(z, x)}{1 - D_{\alpha}(z, x)} \right]. \quad (4.1.3)$$

Recall from Remark 4.1.2 that a sigmoid activation function is typically used for the discriminator’s output layer, so theoretically, the discriminator should never output its asymptotic limits of 0 or 1. However, numbers arbitrarily close to these limits may underflow or overflow to them when computationally stored as a floating point representation. Thus, when implementing this algorithm, we introduce a small constant $c > 0$ to the numerator and denominator of the estimated density ratio:

$$\min_{\phi} -\mathbb{E}_{q^*(x)q_{\phi}(z|x)}[\log p(x|z)] + \mathbb{E}_{q^*(x)q_{\phi}(z|x)} \left[\log \frac{D_{\alpha}(z, x) + c}{1 - D_{\alpha}(z, x) - c} \right].$$

Since our variational posterior distribution is represented as a generative neural network function, our optimization objectives in Expressions (4.1.2) and (4.1.3) become:

$$\min_{\alpha} -\mathbb{E}_{q^*(x)\pi(\epsilon)}[\log D_{\alpha}(\mathcal{G}_{\phi}(\epsilon; x), x) - \mathbb{E}_{p_{\theta}(z)q^*(x)}[\log(1 - D_{\alpha}(z, x))]], \quad (4.1.4)$$

$$\min_{\phi} -\mathbb{E}_{q^*(x)\pi(\epsilon)}[\log p(x|\mathcal{G}_{\phi}(\epsilon; x))] + \mathbb{E}_{q^*(x)\pi(\epsilon)} \left[\log \frac{D_{\alpha}(\mathcal{G}_{\phi}(\epsilon; x), x)}{1 - D_{\alpha}(\mathcal{G}_{\phi}(\epsilon; x), x)} \right]. \quad (4.1.5)$$

In practice, the algorithm cycles between taking multiple gradient descent steps of the discriminative loss in Expression (4.1.4) with respect to α (with the generator parameters fixed) and taking one gradient descent step of the *NELBO*, as stated in Expression (4.1.5) (with the discriminator parameters fixed). If we apply this algorithm to an autoencoder, we would additionally parametrize the likelihood with θ and optimize the *NELBO* with respect to those parameters. Also note that from Equation (3.4.1) that the *NELBO* has a lower bound of $-p(x)$, which is unknown. It is therefore inadequate to assess convergence using the value of the *NELBO*, we would additionally check that the discriminative loss is arbitrarily close to $\log 4$, using Remark 4.1.3.

Pseudocode for this algorithm is shown in Algorithm 1.

Data: Dataset distribution $q^*(x)$, (implicit) prior $p(z)$, likelihood $p(x|z)$,
noise distribution $\pi(\epsilon)$

Result: Optimized posterior generator $\mathcal{G}_\phi(\epsilon; x)$

```

for  $j = 1$  to  $J$  do
  for  $k = 1$  to  $K$  do
    Sample  $\{\epsilon^{(i,k)}\}_{i=1}^B \sim \pi(\epsilon)$ ;
    Sample  $\{x^{(i,k)}\}_{i=1}^B \sim q^*(x)$ ;
    foreach  $\epsilon^{(i,k)}, x^{(i,k)}$  do
      | Sample  $z_q^{(i,k)} = \mathcal{G}(\epsilon^{(i,k)}; x^{(i,k)})$ ;
    end
    Sample  $\{z_p^{(i,k)}\}_{i=1}^B \sim p(z)$ ;
    update  $\alpha$  by optimization step on
       $\min_{\alpha} \frac{1}{B} \sum_{i=1}^B \left[ -\log D_{\alpha} \left( z_q^{(i,k)}, x^{(i,k)} \right) - \log \left( 1 - D_{\alpha} \left( z_p^{(i,k)}, x^{(i,k)} \right) \right) \right]$ 
    end
    Sample  $\{\epsilon^{(i)}\}_{i=1}^B \sim \pi(\epsilon)$ ;
    Sample  $\{x^{(i)}\}_{i=1}^B \sim q^*(x)$ ;
    foreach  $\epsilon^{(i)}, x^{(i)}$  do
      | Sample  $z_q^{(i)} = \mathcal{G}(\epsilon^{(i)}; x^{(i)})$ ;
    end
    update  $\phi$  by optimization step on
       $\min_{\phi} \frac{1}{B} \sum_{i=1}^B \left[ -\log p \left( x^{(i)} | z_q^{(i)} \right) + \log \frac{D_{\alpha}(z_q^{(i)}, x^{(i)})}{1 - D_{\alpha}(z_q^{(i)}, x^{(i)})} \right];$ 
  end

```

Algorithm 1: Prior-Contrastive Class Probability Estimation

4.1.3 Joint-Contrastive Algorithm

We now restate from Expression (3.8.1) our optimization objective when the likelihood distribution is implicit:

$$\min_{\phi} \mathbb{E}_{q^*(x)q_{\phi}(z|x)} \log \frac{q(z, x)}{p(z, x)},$$

or

$$\min_{\phi} \mathbb{E}_{q^*(x)q_{\phi}(z|x)} \log \frac{q_{\phi}(z|x)q^*(x)}{p(x|z)p(z)}.$$

Similar to the prior-contrastive case, we can label samples from $q(z, x)$ with $y = 1$ and samples from $p(z, x)$ with $y = 0$, leading to the density ratio expression:

$$\frac{q(z, x)}{p(z, x)} = \frac{P(y = 1|z, x)}{P(y = 0|z, x)}.$$

Again, we use a discriminator neural network $D_\alpha(z, x) = P(y = 1|z, x)$ to estimate the probability that samples (z, x) came from the joint variational distribution $q(z, x)$. Using this discriminator function, our density ratio expression becomes:

$$\frac{q(z, x)}{p(z, x)} \simeq \frac{D_\alpha(z, x)}{1 - D_\alpha(z, x)}.$$

The class probability algorithm again cycles between Bernoulli loss minimisation of the discriminator:

$$\min_{\alpha} -\mathbb{E}_{q^*(x)q_\phi(z|x)}[\log D_\alpha(z, x)] - \mathbb{E}_{p(z)p(x|z)}[\log(1 - D_\alpha(z, x))] \quad (4.1.6)$$

and optimization of the variational posterior:

$$\min_{\phi} \mathbb{E}_{q^*(x)q_\phi(z|x)} \log \frac{D_\alpha(z, x)}{1 - D_\alpha(z, x)}. \quad (4.1.7)$$

Using the posterior generator parametrization $\mathcal{G}_\phi(\epsilon; x)$, the optimization objectives in Expressions (4.1.6) and (4.1.7) become:

$$\min_{\alpha} -\mathbb{E}_{q^*(x)\pi(\epsilon)}[\log D_\alpha(\mathcal{G}_\phi(\epsilon; x), x)] - \mathbb{E}_{p(z)p(x|z)}[\log(1 - D_\alpha(z, x))]$$

$$\min_{\phi} \mathbb{E}_{q^*(x)\pi(\epsilon)} \log \frac{D_\alpha(\mathcal{G}_\phi(\epsilon; x), x)}{1 - D_\alpha(\mathcal{G}_\phi(\epsilon; x), x)}.$$

Using Remark 4.1.3, it can be seen that when $q(z, x) = p(z, x)$, the optimal generative loss is $\log \frac{1/2}{1-1/2} = 0$. Pseudocode for the joint-contrastive class probability estimation algorithm is shown in Algorithm 2.

Data: Dataset distribution $q^*(x)$, (implicit) prior $p(z)$, (implicit) likelihood $p(x|z)$, noise distribution $\pi(\epsilon)$

Result: Optimized posterior generator $\mathcal{G}_\phi(\epsilon; x)$

```

for  $j = 1$  to  $J$  do
  for  $k = 1$  to  $K$  do
    Sample  $\{\epsilon^{(i,k)}\}_{i=1}^B \sim \pi(\epsilon)$ ;
    Sample  $\{x_q^{(i,k)}\}_{i=1}^B \sim q^*(x)$ ;
    foreach  $\epsilon^{(i,k)}, x^{(i,k)}$  do
      | Sample  $z_q^{(i,k)} = \mathcal{G}(\epsilon^{(i,k)}; x_q^{(i,k)})$ ;
    end
    Sample  $\{z_p^{(i,k)}\}_{i=1}^B \sim p(z)$ ;
    foreach  $z_p^{(i,k)}$  do
      | Sample  $x_p^{(i,k)} \sim p(x|z_p^{(i,k)})$ ;
    end
    update  $\alpha$  by optimization step on
       $\min_{\alpha} \frac{1}{B} \sum_{i=1}^B \left[ -\log D_{\alpha} \left( z_q^{(i,k)}, x_q^{(i,k)} \right) - \log \left( 1 - D_{\alpha} \left( z_p^{(i,k)}, x_p^{(i,k)} \right) \right) \right]$ 
    end
    Sample  $\{\epsilon^{(i)}\}_{i=1}^B \sim \pi(\epsilon)$ ;
    Sample  $\{x_q^{(i)}\}_{i=1}^B \sim q^*(x)$ ;
    foreach  $\epsilon^{(i)}, x^{(i)}$  do
      | Sample  $z_q^{(i)} = \mathcal{G}(\epsilon^{(i)}; x_q^{(i)})$ ;
    end
    update  $\phi$  by optimization step on
       $\min_{\phi} \frac{1}{B} \sum_{i=1}^B \left[ \log \frac{D_{\alpha}(z_q^{(i)}, x_q^{(i)})}{1 - D_{\alpha}(z_q^{(i)}, x_q^{(i)})} \right];$ 
  end

```

Algorithm 2: Joint-Contrastive Class Probability Estimation

4.2 Divergence Minimisation

In this section, we derive the divergence minimisation density ratio estimation algorithm and apply it to our prior-contrastive and joint-contrastive optimisation problems.

4.2.1 Derivation

Recall from Definition 3.2.1 that an f -divergence is defined by a convex function f such that $f(1) = 0$. A lower bound for the f -divergence in terms of a direct ratio estimator $r(u) \simeq \frac{q(u)}{p(u)}$ can be found using the following theorem.

Theorem 4.2.1. [Nguyen et al., 2010] *If f is a convex function with derivative f' and convex conjugate f^* , and \mathcal{R} is a class of functions with codomains equal to the domain of f' , then we have the lower bound for the f -divergence between distributions $p(u)$ and $q(u)$ in terms of a density ratio estimator $r(u) \in \mathcal{R}$:*

$$D_f[p(u)||q(u)] \geq \sup_{r \in \mathcal{R}} \{\mathbb{E}_{q(u)}[f'(r(u))] - \mathbb{E}_{p(u)}[f^*(f'(r(u)))]\},$$

with equality when $r(u) = q(u)/p(u)$.

We omit the proof of this theorem as it is beyond the scope of this thesis. Details of the proof can be found in “Estimating divergence functionals and the likelihood ratio by convex risk minimization” by Nguyen et al. [2010].

The derivative and convex conjugate of $f(u) = u \log u$ are

$$f'(u) = 1 + \log u, \quad f^*(u) = \exp(u - 1),$$

so the convex conjugate of the derivative is simply $f^*(f'(u)) = u$.

Using Theorem 4.2.1, we derive the following reverse KL divergence lower bound:

$$\begin{aligned} D_{RKL}(P||Q) &:= KL[q(u)||p(u)] \\ &\geq \sup_{r \in \mathcal{R}} \{\mathbb{E}_{q(u)}[1 + \log r(u)] - \mathbb{E}_{p(u)}[r(u)]\}. \end{aligned} \quad (4.2.1)$$

Fixing the variational density $q(u)$, $KL(q(u)||p(u))$ is constant, so recalling that the bound reaches equality when $r(u) = q(u)/p(u)$, we can represent the direct ratio estimator as a neural network parametrised by α and minimize the negative of Expression (4.2.1), which we define as L_r , with respect to α :

$$L_r := -\mathbb{E}_{q(u)}[\log r_\alpha(u)] + \mathbb{E}_{p(u)}[r_\alpha(u)]. \quad (4.2.2)$$

Note we have removed the $+1$ term as it is independent of α .

Lemma 4.2.2. *The direct ratio estimator reaches optimality at $r_\alpha^*(u) = q(u)/p(u)$, minimizing its ratio loss.*

Proof. A proof using the first and second functional derivatives of the ratio loss can be found in Appendix A.4. This lemma can be alternatively intuited by using Theorem 4.2.1. \square

Remark 4.2.3. $r_\alpha^*(u)$ is bound in $(0, \infty)$. Note that $r_\alpha^*(u) \neq 0$ as we have assumed that $p(u) > 0$ and $q(u) > 0$ for all $u \in U$.

Remark 4.2.4. When the probability densities are equivalent, that is, $q(u) = p(u)$, the ratio estimator has a constant output of 1: $r_\alpha^*(u) = 1$. This corresponds to a ratio estimator loss of $L_{r^*} = 1$.

Using Remark 4.2.4, we can check for posterior convergence by observing when the ratio estimator loss becomes arbitrarily close to 1.

4.2.2 Prior-Contrastive Algorithm

We begin by restating the optimization objective from Expression (4.1.1):

$$\min_{\phi} -\mathbb{E}_{q^*(x)q_{\phi}(z|x)}[\log p(x|z)] + \mathbb{E}_{q^*(x)q_{\phi}(z|x)} \left[\log \frac{q_{\phi}(z|x)}{p(z)} \right].$$

Applying Theorem 4.2.1, we have the lower bound for the reverse KL divergence:

$$KL[q_{\phi}(z|x)||p(z)] \geq \sup_{\hat{r} \in \mathcal{R}} \{ \mathbb{E}_{q_{\phi}(z|x)}[1 + \log r(z)] - \mathbb{E}_{p(z)}[r(z)] \}.$$

Now we let our direct ratio estimator be a neural network parametrized by α , and since $q_{\phi}(z|x)$ is dependent on the input $x \sim q^*(x)$, we add x as an input and amortize the KL divergence across $q^*(x)$:

$$\mathbb{E}_{q^*(x)} KL[q_{\phi}(z|x)||p(z)] \geq \sup_{\alpha} \{ \mathbb{E}_{q^*(x)q_{\phi}(z|x)}[1 + \log r_{\alpha}(z, x)] - \mathbb{E}_{q^*(x)p(z)}[r_{\alpha}(z, x)] \}.$$

By taking the negative of this lower bound, we formulate the minimisation problem for the direct ratio estimator:

$$\min_{\alpha} -\mathbb{E}_{q^*(x)q_{\phi}(z|x)}[\log r_{\alpha}(z, x)] + \mathbb{E}_{q^*(x)p(z)}[r_{\alpha}(z, x)]. \quad (4.2.3)$$

Since $r_{\alpha}(z, x) \simeq \frac{q_{\phi}(z|x)}{p(z)}$, we write our *NELBO* optimization problem in terms of the direct ratio estimator:

$$\min_{\phi} -\mathbb{E}_{q^*(x)q_{\phi}(z|x)}[\log p(x|z)] + \mathbb{E}_{q^*(x)q_{\phi}(z|x)}[\log r_{\alpha}(z, x)]. \quad (4.2.4)$$

Substituting the generator form of the posterior into Expressions (4.2.3) and (4.2.4), we have the simultaneous optimization problem:

$$\begin{aligned} & \min_{\alpha} -\mathbb{E}_{q^*(x)\pi(\epsilon)}[\log r_{\alpha}(\mathcal{G}_{\phi}(\epsilon; x), x)] + \mathbb{E}_{q^*(x)p(z)}[r_{\alpha}(z, x)] \\ & \min_{\phi} -\mathbb{E}_{q^*(x)\pi(\epsilon)}[\log p(x|\mathcal{G}_{\phi}(\epsilon; x))] + E_{q^*(x)\pi(\epsilon)}[\log r_{\alpha}(\mathcal{G}_{\phi}(\epsilon; x), x)]. \end{aligned}$$

Similar to class probability estimation, the algorithm involves cycling between multiple ratio estimator optimisation steps and a single step of *NELBO* minimisation, as shown in Algorithm 3.

Data: Dataset distribution $q^*(x)$, (implicit) prior $p(z)$, likelihood $p(x|z)$, noise distribution $\pi(\epsilon)$

Result: Optimized posterior generator $\mathcal{G}_{\phi}(\epsilon; x)$

```

for  $j = 1$  to  $J$  do
  for  $k = 1$  to  $K$  do
    Sample  $\{\epsilon^{(i,k)}\}_{i=1}^B \sim \pi(\epsilon)$ ;
    Sample  $\{x^{(i,k)}\}_{i=1}^B \sim q^*(x)$ ;
    foreach  $\epsilon^{(i,k)}, x^{(i,k)}$  do
      | Sample  $z_q^{(i,k)} = \mathcal{G}(\epsilon^{(i,k)}; x^{(i,k)})$ ;
    end
    Sample  $\{z_p^{(i,k)}\}_{i=1}^B \sim p(z)$ ;
    update  $\alpha$  by optimization step on
       $\min_{\alpha} \frac{1}{B} \sum_{i=1}^B \left[ -\log \left( r_{\alpha} \left( z_q^{(i,k)}, x^{(i,k)} \right) \right) + r_{\alpha} \left( z_p^{(i,k)}, x^{(i,k)} \right) \right]$ ;
    end
    Sample  $\{\epsilon^{(i)}\}_{i=1}^B \sim \pi(\epsilon)$ ;
    Sample  $\{x^{(i)}\}_{i=1}^B \sim q^*(x)$ ;
    foreach  $\epsilon^{(i)}, x^{(i)}$  do
      | Sample  $z_q^{(i)} = \mathcal{G}(\epsilon^{(i)}; x^{(i)})$ ;
    end
    update  $\phi$  by optimization step on
       $\min_{\phi} \frac{1}{B} \sum_{i=1}^B \left[ -\log p \left( x^{(i)} | z_q^{(i)} \right) + \log r_{\alpha} \left( z_q^{(i)}, x^{(i)} \right) \right]$ ;
  end
end

```

Algorithm 3: Prior-Contrastive Divergence Minimisation

4.2.3 Joint-Contrastive Algorithm

First, we restate the problem from Expression (3.8.1) of minimizing the reverse KL divergence between the joint distributions:

$$\min_{\phi} \mathbb{E}_{q^*(x)q_{\phi}(z|x)} \log \frac{q(z, x)}{p(z, x)}.$$

Applying Theorem 4.2.1, a lower bound for our KL divergence is

$$KL[q(z, x)||p(z, x)] \geq \sup_{r \in \mathcal{R}} \{\mathbb{E}_{q(z, x)}[1 + \log r(z, x)] - \mathbb{E}_{p(z, x)}[r(z, x)]\}.$$

Note here we do not have to amortize our ratio estimator as the joint probability distribution already includes the dataset. Again we set our ratio estimator to take the form of a neural network parametrized by α :

$$r_{\alpha}(z, x) \simeq \frac{q(z, x)}{p(z, x)}$$

so that the lower bound becomes

$$KL[q(z, x)||p(z, x)] \geq \sup_{\alpha} \{\mathbb{E}_{q(z, x)}[1 + \log r_{\alpha}(z, x)] - \mathbb{E}_{p(z, x)}[r_{\alpha}(z, x)]\}.$$

Again taking the negative of this lower bound, we formulate the following minimization problem for the direct ratio estimator:

$$\min_{\alpha} -\mathbb{E}_{q^*(x)q_{\phi}(z|x)}[\log r_{\alpha}(z, x)] + \mathbb{E}_{p(z)p(x|z)}[r_{\alpha}(z, x)]. \quad (4.2.5)$$

The *NELBO* minimization problem in terms of the direct ratio estimator is:

$$\min_{\phi} \mathbb{E}_{q^*(x)q_{\phi}(z|x)}[\log r_{\alpha}(z, x)]. \quad (4.2.6)$$

Finally, we derive the simultaneous optimization problem by writing the variational posterior term in Expressions (4.2.5) and (4.2.6) in terms of their generator form:

$$\min_{\alpha} -\mathbb{E}_{q^*(x)\pi(\epsilon)}[\log r_{\alpha}(\mathcal{G}(\epsilon; x), x)] + \mathbb{E}_{p(z)p(x|z)}[r_{\alpha}(z, x)]$$

$$\min_{\phi} \mathbb{E}_{q^*(x)\pi(\epsilon)}[\log r_{\alpha}(\mathcal{G}(\epsilon; x), x)].$$

Again this process, shown in Algorithm 4, involves cycling between multiple steps of optimizing the ratio estimator and taking a single optimization step of the *NELBO*.

Data: Dataset distribution $q^*(x)$, (implicit) prior $p(z)$, (implicit) likelihood $p(x|z)$, noise distribution $\pi(\epsilon)$

Result: Optimized posterior generator $\mathcal{G}_\phi(\epsilon; x)$

```

for  $j = 1$  to  $J$  do
  for  $k = 1$  to  $K$  do
    Sample  $\{\epsilon^{(i,k)}\}_{i=1}^B \sim \pi(\epsilon)$ ;
    Sample  $\{x_q^{(i,k)}\}_{i=1}^B \sim q^*(x)$ ;
    foreach  $\epsilon^{(i,k)}, x_q^{(i,k)}$  do
      | Sample  $z_q^{(i,k)} = \mathcal{G}(\epsilon^{(i,k)}; x_q^{(i,k)})$ ;
    end
    Sample  $\{z_p^{(i,k)}\}_{i=1}^B \sim p(z)$ ;
    foreach  $z_p^{(i,k)}$  do
      | Sample  $x_p^{(i,k)} \sim p(x|z_p^{(i,k)})$ ;
    end
    update  $\alpha$  by optimization step on
       $\min_\alpha \frac{1}{B} \sum_{i=1}^B \left[ -\log \left( r_\alpha \left( z_q^{(i,k)}, x_q^{(i,k)} \right) \right) + r_\alpha \left( z_p^{(i,k)}, x_p^{(i,k)} \right) \right];$ 
    end
    Sample  $\{\epsilon^{(i)}\}_{i=1}^B \sim \pi(\epsilon)$ ;
    Sample  $\{x_q^{(i)}\}_{i=1}^B \sim q^*(x)$ ;
    foreach  $\epsilon^{(i)}, x_q^{(i)}$  do
      | Sample  $z_q^{(i)} = \mathcal{G}(\epsilon^{(i)}; x_q^{(i)})$ ;
    end
    update  $\phi$  by optimization step on
       $\min_\phi \frac{1}{B} \sum_{i=1}^B \left[ \log r_\alpha \left( z_q^{(i)}, x_q^{(i)} \right) \right];$ 
  end
end

```

Algorithm 4: Joint-Contrastive Divergence Minimisation

4.2.4 Alternative Derivation of Class Probability Estimation

If we apply Theorem 4.2.1 with the function $f(u) = u \log u - (u + 1) \log(u + 1)$, the resulting bi-level optimization problem is equivalent to that of class probability estimation [Tiao et al., 2018]. Before deriving the corresponding f -divergence, we define the Jensen-Shannon divergence which will be used in the expression.

Definition 4.2.5. The Jensen-Shannon divergence is a symmetric metric used to measure the discrepancy between two probability distributions [Fuglede and Topsøe,

2004]:

$$JS[p(u)\|q(u)] = \frac{1}{2}KL(p(u)\|m(u)) + \frac{1}{2}KL(q(u)\|m(u))$$

where $m(u) = \frac{q(u)+p(u)}{2}$.

We denote this f -divergence as D_{GAN} after the generative adversarial networks which typically use the class probability estimation optimisation problem [Goodfellow et al., 2014].

$$\begin{aligned} D_{GAN}(p\|q) &= \mathbb{E}_p \left[\frac{q(u)}{p(u)} \log \left(\frac{q(u)}{p(u)} \right) - \left(\frac{q(u)}{p(u)} + 1 \right) \log \left(\frac{q(u)}{p(u)} + 1 \right) \right] \\ &= \int q(u) \log \left(\frac{q(u)}{p(u)} \right) - (q(u) + p(u)) \log \left(\frac{q(u) + p(u)}{p(u)} \right) du \\ &= \int q(u) (\log(q(u)) - \log(p(u))) - (q(u) + p(u)) \log(q(u) + p(u)) \\ &\quad + (q(u) + p(u)) \log p(u) du \\ &= \int q(u) \log \left(\frac{q(u)}{q(u) + p(u)} \right) + p(u) \log \left(\frac{p(u)}{q(u) + p(u)} \right) du \\ &= \int p(u) \log \left(\frac{2p(u)}{q(u) + p(u)} \right) - p(u) \log 2 + q(u) \log \left(\frac{2q(u)}{q(u) + p(u)} \right) \\ &\quad - q(u) \log 2 du \\ &= \int p(u) \log \left(\frac{p(u)}{m(u)} - \log 2 \right) + q(u) \log \left(\frac{q(u)}{m(u)} - \log 2 \right) du \\ &\text{where } m(u) = \frac{q(u) + p(u)}{2} \\ &= \mathbb{E}_p \left[\log \frac{p(u)}{m(u)} - \log 2 \right] + \mathbb{E}_q \left[\log \frac{q(u)}{m(u)} - \log 2 \right] \\ &= KL(p(u)\|m(u)) + KL(q(u)\|m(u)) - \log 4 \\ &= 2JS[p(u)\|q(u)] - \log 4. \end{aligned}$$

Recall one of the conditions of f to form an f -divergence is $f(1) = 0$, but in this case, $f(1) = -\log 4$, hence the constant term in our GAN divergence.

The derivative and convex conjugate of $f(u) = u \log u - (u + 1) \log(u + 1)$ are

$$f'(u) = \log \frac{u}{u+1}, \quad f^*(u) = -\log(1 - \exp u)$$

so the convex conjugate of the derivative is

$$f^*(f'(u)) = \log(u + 1).$$

Using Theorem 4.2.1, we derive the following lower bound for the Jensen-Shannon divergence:

$$\begin{aligned}
D_{GAN}(p\|q) &:= 2JS[p(u)\|q(u)] - \log 4 \\
&\geq \sup_{r \in \mathcal{R}} \{ \mathbb{E}_{q(u)} \left[\log \frac{r(u)}{r(u) + 1} \right] - \mathbb{E}_{p(u)} [\log(r(u) + 1)] \} \\
&= \sup_D \{ \mathbb{E}_{q(u)} [\log D(u)] + \mathbb{E}_{p(u)} [\log(1 - D(u))] \},
\end{aligned}$$

where $D(u) = \frac{r(u)}{r(u)+1}$. Maximisation of the lower bound, equivalent to minimising its negative, follows the optimization problem:

$$\min_{\alpha} -\mathbb{E}_{q(u)} [\log D(u)] - \mathbb{E}_{p(u)} [\log(1 - D(u))],$$

which is the discriminative loss of the class probability estimation approach. Equality of the bound is accomplished at the optimal function of

$$\begin{aligned}
D^*(u) &= \frac{\frac{q(u)}{p(u)}}{\frac{q(u)}{p(u)} + 1} \\
&= \frac{q(u)}{q(u) + p(u)},
\end{aligned}$$

which is the optimal discriminator of class probability estimation. Thus, the density ratio in terms of this discriminator function is

$$\frac{q(u)}{p(u)} \simeq \frac{D(u)}{1 - D(u)},$$

and therefore our previous formulation of class probability estimation by minimizing the Bernoulli loss of a discriminator function is equivalent to maximizing the lower bound of the “GAN” divergence between the two distributions.

CHAPTER 5

Algorithm Generalisation

In this chapter, we present the two density ratio estimation techniques in a comparable form, that is, in terms of the relevant f -divergence's lower bound as derived in Section 4.2 using Theorem 4.2.1. From this, we generalise the density ratio algorithms to a selection of f -divergence to formulate the lower bound, and a parametrisation of the density ratio estimator. We also suggest a third estimator parametrisation: the direct log density ratio estimator $T_\alpha(u)$. The formal generalisation of density ratio estimation algorithms is the first contribution of this thesis.

5.1 Introduction

First, recall that within each of the prior-contrastive and joint-contrastive formulations, both class probability estimation and divergence minimisation methods use the same loss function to optimise the posterior weights. It is therefore evident that the only differences between the two density ratio estimation techniques are the lower bound of the loss function and the parametrization of the estimator. We demonstrate this by restating the f -divergence lower bounds used to formulate these loss functions, as derived in Section 4.2. For divergence minimisation, the lower bound is achieved using the reverse KL divergence $D_{RKL}(p||q) = KL(q(u)||p(u))$:

$$D_{RKL}(p||q) \geq \sup_{\alpha} \{ \mathbb{E}_{q(u)}[1 + \log r_{\alpha}(u)] - \mathbb{E}_{p(u)}[r_{\alpha}(u)] \},$$

and class probability estimation follows the GAN divergence $D_{GAN}(p||q) = 2D_{JS}(p||q) - \log 4$:

$$D_{GAN}(p||q) \geq \sup_{\alpha} \{ \mathbb{E}_{q(u)} \left[\log \frac{r_{\alpha}(u)}{r_{\alpha}(u) + 1} \right] - \mathbb{E}_{p(u)}[\log(r_{\alpha}(u) + 1)] \},$$

with equality at $r_{\alpha}(u) = \frac{q(u)}{p(u)}$.

To convert the latter equation to class probability estimation loss function, we have used the estimator transformation $r_{\alpha}(u) = \frac{D_{\alpha}(u)}{1 - D_{\alpha}(u)} \iff D_{\alpha}(u) = \frac{r_{\alpha}(u)}{r_{\alpha}(u) + 1}$. Since

this mapping is bijective and monotonically increasing, the equality of the bound is retained at equivalent points. We can therefore also use this transformation on the lower bound of the reverse KL divergence, deriving its respective loss function as a function of $D_\alpha \simeq \frac{q(u)}{q(u)+p(u)}$ instead of $r_\alpha \simeq \frac{q(u)}{p(u)}$.

We also propose a third estimator parametrisation, the direct log density ratio estimator

$$T_\alpha(u) \simeq \log \frac{q(u)}{p(u)}.$$

This is derived by simply using the transformation $T_\alpha(u) = \log r_\alpha(u)$.

5.2 Algorithm Generalisation

For each f -divergence, we can derive a loss function for each of our three estimator parametrisations.

5.2.1 Reverse KL Divergence

Direct Ratio Estimator $r_\alpha(u)$:

$$\min_{\alpha} -\mathbb{E}_{q(u)}[\log r_\alpha(u)] + \mathbb{E}_{p(u)}[r_\alpha(u)]$$

Class Probability Estimator/Discriminator $D_\alpha(u)$:

$$\min_{\alpha} \mathbb{E}_{q(u)} \left[\log \frac{1 - D_\alpha(u)}{D_\alpha(u)} \right] + \mathbb{E}_{p(u)} \left[\frac{D_\alpha(u)}{1 - D_\alpha(u)} \right]$$

Direct Log Ratio Estimator $T_\alpha(u)$:

$$\min_{\alpha} -\mathbb{E}_{q(u)}[T_\alpha(u)] + \mathbb{E}_{p(u)}[e^{T_\alpha(u)}]$$

5.2.2 GAN Divergence

Direct Ratio Estimator $r_\alpha(u)$:

$$\min_{\alpha} \mathbb{E}_{q(u)} \left[\log \frac{r_\alpha(u) + 1}{r_\alpha(u)} \right] + \mathbb{E}_{p(u)}[\log(r_\alpha(u) + 1)]$$

Class Probability Estimator/Discriminator $D_\alpha(u)$:

$$\min_{\alpha} -\mathbb{E}_{q(u)}[\log D_\alpha(u)] - \mathbb{E}_{p(u)}[\log(1 - D_\alpha(u))]$$

Direct Log Ratio Estimator $T_\alpha(u)$:

$$\min_{\alpha} \mathbb{E}_{q(u)} \left[\log \frac{e^{T_\alpha(u)} + 1}{e^{T_\alpha(u)}} \right] + \mathbb{E}_{p(u)} [\log(e^{T_\alpha(u)} + 1)]$$

We have therefore generalised the choice of algorithm for training density ratio estimators to a choice of f -divergence:

- Reverse KL Divergence: $D_{KL}(p||q) = \mathbb{E}_{q(u)} [1 + \log \frac{q(u)}{p(u)}] - \mathbb{E}_{p(u)} \left[\frac{q(u)}{p(u)} \right]$,
- GAN Divergence: $D_{GAN}(p||q) = \mathbb{E}_{q(u)} \left[\log \frac{q(u)}{q(u)+p(u)} \right] + \mathbb{E}_{p(u)} \left[\log \frac{p(u)}{q(u)+p(u)} \right]$,

and a choice of estimator parametrization:

- Direct ratio estimator: $r_\alpha(u) \simeq \frac{q(u)}{p(u)}$,
- “Class probability” estimator/Discriminator: $D_\alpha(u) \simeq \frac{q(u)}{q(u)+p(u)}$,
- Direct log ratio estimator: $T_\alpha(u) \simeq \log \frac{q(u)}{p(u)}$.

The original “KL divergence minimization approach” simply chooses the reverse KL Divergence and the direct ratio estimator, and “class probability estimation” uses the GAN Divergence and the “Class probability” estimator. These are just two variations of the six available algorithms.

5.3 Optimization Algorithms

The ratio estimator in the posterior loss functions also has to be transformed accordingly. In the following sections we give the specific prior-contrastive and joint-contrastive *NELBOs* as functions of each estimator parametrisation. For completeness, we also list the two different estimator loss functions for each case, corresponding to the two f -divergences that we have discussed.

5.3.1 Prior-Contrastive

Direct Ratio Estimator $r_\alpha(u)$:

$$\text{Reverse KL: } \min_{\alpha} -\mathbb{E}_{q^*(x)\pi(\epsilon)} [\log r_\alpha(\mathcal{G}(\epsilon; x), x)] + \mathbb{E}_{p(z)q^*(x)} [r_\alpha(z, x)]$$

$$\text{GAN: } \min_{\alpha} \mathbb{E}_{q^*(x)\pi(\epsilon)} \left[\log \frac{r_\alpha(\mathcal{G}(\epsilon; x), x) + 1}{r_\alpha(\mathcal{G}(\epsilon; x), x)} \right] + \mathbb{E}_{p(z)q^*(x)} [\log(r_\alpha(z, x) + 1)]$$

$$\min_{\phi} -\mathbb{E}_{q^*(x)\pi(\epsilon)} [\log p(x|\mathcal{G}_\phi(\epsilon; x))] + \mathbb{E}_{q^*(x)\pi(\epsilon)} [\log r_\alpha(\mathcal{G}(\epsilon; x), x)]$$

Class Probability Estimator/Discriminator $D_\alpha(u)$:

$$\text{Reverse KL: } \min_{\alpha} \mathbb{E}_{q^*(x)\pi(\epsilon)} \left[\log \frac{1 - D_\alpha(\mathcal{G}(\epsilon; x), x)}{D_\alpha(\mathcal{G}(\epsilon; x), x)} \right] + \mathbb{E}_{p(z)q^*(x)} \left[\frac{D_\alpha(\mathcal{G}(\epsilon; x), x)}{1 - D_\alpha(\mathcal{G}(\epsilon; x), x)} \right]$$

$$\text{GAN: } \min_{\alpha} -\mathbb{E}_{q^*(x)\pi(\epsilon)}[\log D_{\alpha}(\mathcal{G}(\epsilon; x), x)] - \mathbb{E}_{p(z)q^*(x)}[\log(1 - D_{\alpha}(z, x))]$$

$$\min_{\phi} -\mathbb{E}_{q^*(x)\pi(\epsilon)}[\log p(x|\mathcal{G}_{\phi}(\epsilon; x))] + \mathbb{E}_{q^*(x)\pi(\epsilon)} \left[\log \frac{D_{\alpha}(\mathcal{G}(\epsilon; x), x)}{1 - D_{\alpha}(\mathcal{G}(\epsilon; x), x)} \right]$$

Direct Log Ratio Estimator $T_{\alpha}(u)$:

$$\text{Reverse KL: } \min_{\alpha} -\mathbb{E}_{q^*(x)\pi(\epsilon)}[T_{\alpha}(\mathcal{G}(\epsilon; x), x)] + \mathbb{E}_{p(z)q^*(x)}[\exp(T_{\alpha}(z, x))]$$

$$\text{GAN: } \min_{\alpha} \mathbb{E}_{q^*(x)\pi(\epsilon)} \left[\log \frac{e^{T_{\alpha}(\mathcal{G}(\epsilon; x), x)} + 1}{e^{T_{\alpha}(\mathcal{G}(\epsilon; x), x)}} \right] + \mathbb{E}_{p(z)q^*(x)}[\log(e^{T_{\alpha}(z, x)} + 1)]$$

$$\min_{\phi} -\mathbb{E}_{q^*(x)\pi(\epsilon)}[\log p(x|\mathcal{G}_{\phi}(\epsilon; x))] + \mathbb{E}_{q^*(x)\pi(\epsilon)}[T_{\alpha}(\mathcal{G}(\epsilon; x), x)]$$

5.3.2 Joint-Contrastive

Direct Ratio Estimator $r_{\alpha}(u)$:

$$\text{Reverse KL: } \min_{\alpha} -\mathbb{E}_{q^*(x)\pi(\epsilon)}[\log r_{\alpha}(\mathcal{G}(\epsilon; x), x)] + \mathbb{E}_{p(z)p(x|z)}[r_{\alpha}(z, x)]$$

$$\text{GAN: } \min_{\alpha} \mathbb{E}_{q^*(x)\pi(\epsilon)} \left[\log \frac{r_{\alpha}(\mathcal{G}(\epsilon; x), x) + 1}{r_{\alpha}(\mathcal{G}(\epsilon; x), x)} \right] + \mathbb{E}_{p(z)p(x|z)}[\log(r_{\alpha}(z, x) + 1)]$$

$$\min_{\phi} \mathbb{E}_{q^*(x)\pi(\epsilon)} \log r_{\alpha}(\mathcal{G}_{\phi}(\epsilon; x), x)$$

Class Probability Estimator/Discriminator $D_{\alpha}(u)$:

$$\text{Reverse KL: } \min_{\alpha} \mathbb{E}_{q^*(x)\pi(\epsilon)} \left[\log \frac{1 - D_{\alpha}(\mathcal{G}(\epsilon; x), x)}{D_{\alpha}(\mathcal{G}(\epsilon; x), x)} \right] + \mathbb{E}_{p(z)p(x|z)} \left[\log \frac{D_{\alpha}(\mathcal{G}(\epsilon; x), x)}{1 - D_{\alpha}(\mathcal{G}(\epsilon; x), x)} \right]$$

$$\text{GAN: } \min_{\alpha} -\mathbb{E}_{q^*(x)\pi(\epsilon)}[\log D_{\alpha}(\mathcal{G}(\epsilon; x), x)] - \mathbb{E}_{p(z)p(x|z)}[\log(1 - D_{\alpha}(z, x))]$$

$$\min_{\phi} \mathbb{E}_{q^*(x)\pi(\epsilon)} \log \frac{D_{\alpha}(\mathcal{G}_{\phi}(\epsilon; x), x)}{1 - D_{\alpha}(\mathcal{G}_{\phi}(\epsilon; x), x)}$$

Direct Log Ratio Estimator $T_{\alpha}(u)$:

$$\text{Reverse KL: } \min_{\alpha} -\mathbb{E}_{q^*(x)\pi(\epsilon)}[T_{\alpha}(\mathcal{G}(\epsilon; x), x)] + \mathbb{E}_{p(z)p(x|z)}[\exp(T_{\alpha}(z, x))]$$

$$\text{GAN: } \min_{\alpha} \mathbb{E}_{q^*(x)\pi(\epsilon)} \left[\log \frac{e^{T_{\alpha}(\mathcal{G}(\epsilon; x), x)} + 1}{e^{T_{\alpha}(\mathcal{G}(\epsilon; x), x)}} \right] + \mathbb{E}_{p(z)p(x|z)}[\log(e^{T_{\alpha}(z, x)} + 1)]$$

$$\min_{\phi} \mathbb{E}_{q^*(x)\pi(\epsilon)} T_{\alpha}(\mathcal{G}_{\phi}(\epsilon; x), x)$$

CHAPTER 6

Comparing Optimal Estimators

In this chapter, we verify that for a fixed f -divergence, each estimator parametrisation leads to similar levels of convergence when optimally trained. In this experiment, we also determine whether the f -divergence used to derive the estimator loss function has any effect on posterior convergence.

6.1 Theory

Recall from Section 5.1 that the estimator transformation preserves the equality of the bound. There should be no significant difference in posterior convergence when the estimators are optimized sufficiently between each posterior iteration step, as they reach equality of the f -divergence lower bound, therefore optimally estimating the *NELBO*.

Theorem 4.2.1 states that equality of the bound is attained at $r_\alpha^*(u) = \frac{q(u)}{p(u)}$ regardless of the f -divergence used, so we also expect similar levels of convergence between the f -divergences. However, “f-GAN: Training Generative Neural Samplers using Variational Divergence Minimization” by Nowozin et al. [2016] shows experimentally that the fastest posterior convergence is attained when the f -divergence used to optimize the variational posterior is also used to derive the lower bound. Since we train our posterior network by minimising its reverse KL divergence with the true posterior, this paper implies the estimator loss functions corresponding to the reverse KL divergence would correspond to superior posterior convergence.

6.2 Problem Context

We use the basic “Continuous Sprinkler” posterior inference experiment as described in “Variational Inference using Implicit Distributions” by Huszár [2017]. This experiment involves the hypothetical scenario of grass wetness as a result of two independent sources: rainfall and a sprinkler. The problem exhibits “explaining away” [P. Wellman and Henrion, 1993], a pattern of reasoning in which the confirmation of one cause of an effect reduces the need to discuss alternative causes. In

this example, despite the two possible sources of wetness being independent, when we condition on the observation of wet grass, the causes become dependent, as it is correlated with the significance of either water source.

The latent variables $\mathbf{z} = (z_1, z_2)$ represent the sprinkler and the rain respectively, and the observation x represents the wetness of the grass:

$$p(z_1, z_2) \sim \mathcal{N}(0, \sigma^2 I_{2 \times 2}),$$

$$p(x|\mathbf{z}) \sim \text{Exp}(3 + \max\{0, z_1\}^3 + \max\{0, z_2\}^3).$$

The prior-contrastive algorithm requires the likelihood function of the likelihood distribution:

$$p(x|\mathbf{z}) = -\log(3 + \max\{0, z_1\}^3 + \max\{0, z_2\}^3) - \frac{x}{3 + \max\{0, z_1\}^3 + \max\{0, z_2\}^3}.$$

This likelihood function is not required for the joint-contrastive algorithms as it is assumed to be implicit.

The unnormalised true posterior is derived as shown below. The lack of normalisation does not affect the variational distribution as the true posterior is assumed to be unknown, and the algorithm only uses samples from the prior and likelihood distributions.

Posterior Calculation:

$$\begin{aligned} p(z_1, z_2|x) &= \exp(\log p(z_1, z_2) + \log p(x|z_1, z_2)) \\ &\propto \exp \left(\frac{1}{2} \mathbf{z}^T (\sigma^{-2} I_{2 \times 2}) \mathbf{z} - \log(3 + \max\{0, z_1\}^3 + \max\{0, z_2\}^3) \right. \\ &\quad \left. - \frac{x}{3 + \max\{0, z_1\}^3 + \max\{0, z_2\}^3} \right) \\ &\propto \exp \left(\frac{1}{2\sigma^2} (z_1^2 + z_2^2) - \log(3 + \max\{0, z_1\}^3 + \max\{0, z_2\}^3) \right. \\ &\quad \left. - \frac{x}{3 + \max\{0, z_1\}^3 + \max\{0, z_2\}^3} \right). \end{aligned} \tag{6.2.1}$$

In the experiment, we let $\sigma^2 = 2$, and consider observations $x = 0, 5, 8, 12, 50$. Our data distribution is therefore:

$$q^*(x) \sim \text{Categorical} \left(0, 5, 8, 12, 50; \frac{1}{5}, \dots, \frac{1}{5} \right).$$

In Figure 6.1, we plot the true (unnormalised) posterior $p(\mathbf{z}|x)$ over a range of equally spaced points from $(z_1, z_2) = [(-5, -5), \dots, (5, 5)]$. We are not concerned with the lack of normalisation as the purpose of the plots is to depict the shape and relative density of the posterior distribution.



Figure 6.1: This figure depicts the true (unnormalised) posterior plots for the “Continuous Sprinkler” experiment. As x increases, the posteriors become increasingly multimodal and unusually shaped. Clearly a flexible model for the posterior distribution is required, as a typical multivariate Gaussian model would fail to capture these features.

6.3 Program Structure

Recall from Subsection 3.8.1 that our generator $\mathcal{G}_\phi(x, \epsilon)$ is a neural network that takes in noise $\epsilon \sim \pi(\epsilon)$ along with data sample $x \sim q^*(x)$ to output a sample from the variational posterior distribution $\mathbf{z} \sim q_\phi(\mathbf{z}|x)$. In this experiment, the generator has 3 noise inputs $\epsilon = (\epsilon_1, \epsilon_2, \epsilon_3)^\top \sim \mathcal{N}(0, I_{3 \times 3})$ along with 1 data input x , and 2 posterior outputs z_1, z_2 . The structure of this network is as depicted in Figure 6.2:

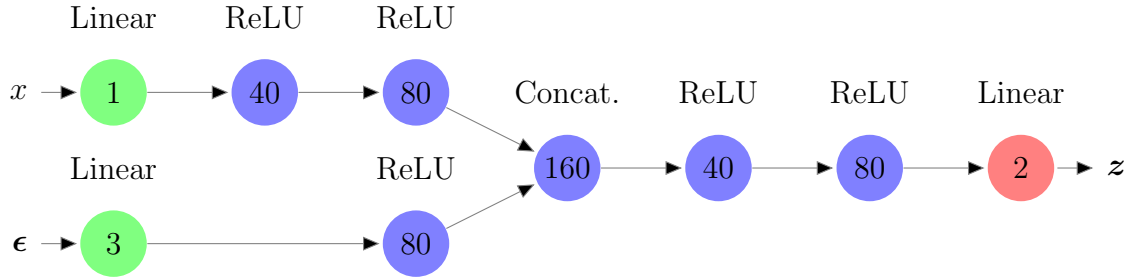


Figure 6.2: This figure illustrates the structure of the generator network $\mathcal{G}(x, \epsilon)$ used in the “Continuous Sprinkler” experiment. The number inside the node indicates how many nodes the layer has, and the text above the node describes the activation function. Recall that the input layer does not have an activation function, and Rectified Linear Units (ReLU) are used for most of the hidden layers due to their many advantages. In the Concat. layer, the two input vectors are concatenated and there is no activation function. We do not use an activation function for the output layer as $q_\phi(\mathbf{z}|x) \in \mathbb{R}$.

The structure of the estimator (discriminator $D_\alpha(\mathbf{z}, x) \simeq \frac{q(\cdot)}{q(\cdot) + p(\cdot)}$, direct ratio estimator $r_\alpha(\mathbf{z}, x) \simeq \frac{q(\cdot)}{p(\cdot)}$ or direct log ratio estimator $T_\alpha(\mathbf{z}, x) \simeq \log \frac{q(\cdot)}{p(\cdot)}$) is similar

to that of the generator, with an additional hidden layer associated with the z input and a different activation function for the output layer, corresponding to the estimator’s identity. Note that the only differences between the two estimators are the activation function of the their output layers and the loss functions being minimised. The estimator structure is shown in Figure 6.3:

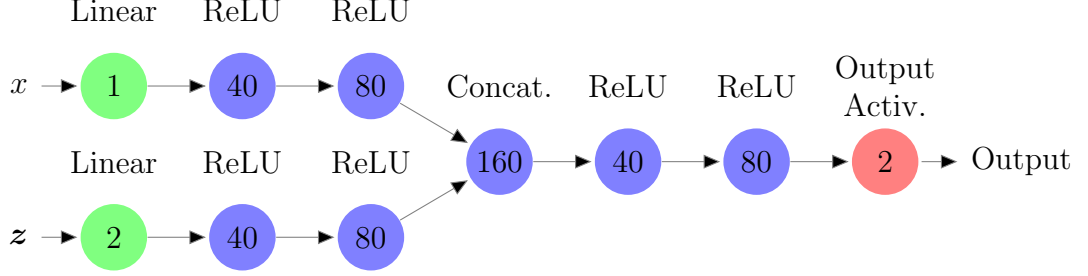


Figure 6.3: This figure depicts the structure of the estimator network for the “Continuous Sprinkler Experiment”. The notation is the same as in Figure 6.2. When the estimator takes the parametrisation of a discriminator $D_\alpha(z, x)$, a sigmoid output layer is used [Goodfellow et al., 2014]. An exponential activation is used for the output layer when the estimator output is the direct density ratio $r_\alpha(z, x)$, and a linear output is used for the direct log density ratio estimator $T_\alpha(z, x)$ [Nowozin et al., 2016].

The network weights are initialized with Xavier initialization, and trained using the Adam optimizer with learning rate 0.0001 for the prior-contrastive setting and 0.00001 for joint-contrastive. Recall that we only train the network on data values $x = 0, 5, 8, 12, 50$. In each training iteration, 200 samples are taken for each x -value, corresponding to a batch size of 1000. This large batch size makes training more consistent, as the samples are probabilistic in nature. Due to the similar network structure in both algorithms, they have near-identical runtime, as the majority of the training time is spent in back-propagation [Goodfellow et al., 2016].

To prevent taking $\log 0$ in the loss functions, we add a small constant $c = 10^{-18}$ to the log function’s input. The estimator is pre-trained for 5000 iterations to ensure that optimization of the variational network begins with an optimal estimator; an inaccurate ratio estimation leads to incorrect optimization of the posterior network. The variance of the results is also reduced as the initial parametrisation of the estimator is similar for each fixed generator initialization. Afterwards, the generator is optimized for 10000 iterations for the prior-contrastive experiment, and 40000 iterations in the joint-contrastive formulation. The algorithm alternates between 100 training steps of the estimator and 1 training step of the generator. The processes for

class probability estimation and divergence minimisation, based off the algorithms derived in Chapter 4, are shown in Algorithms 7 and 8 in Appendix B.3.

We evaluate the techniques by comparing the average KL divergence between the true and variational posteriors at the end of the program’s runtime:

$$\mathbb{E}_{q^*(x)} [KL(q_\phi(\mathbf{z}|x)||p(\mathbf{z}|x))].$$

To do so, we estimate the probability density function of the variational posterior output for each of the 5 data points using a Gaussian kernel density estimator $\hat{q}(\mathbf{z}|x)$. We then calculate its expected KL divergence with the unnormalised true posterior as derived in Equation (6.2.1). The normalisation constant $p(x)$ is independent of the variational posterior $q_\phi(\mathbf{z}|x)$ that we compare it with, so its omission has no impact on our comparison of the algorithms. This density estimation technique is suitable for our low dimensional problem, and the accuracy is independent of the algorithm used. An explanation of kernel density estimation can be found in Appendix E. Due to the stochastic nature of the optimisation, it is desirable to have a large number of experiment repetitions for reliable results. However, due to limited computational time, each algorithm was only run 30 times. At the end of each posterior optimisation step, the estimator loss and *NELBO* estimation was stored. Additionally, the ‘true’ KL divergence was estimated every 100 iterations.

6.4 Results

Tables 6.1 and 6.2 compare the final posterior convergence between the 30 iterations. Figure 6.4 compares variational posterior output plots corresponding to different ‘true’ KL divergences. There is no significant difference in posterior convergence for the algorithms in the prior-contrastive context, and the variation in the results is very low. However, Figure 6.4 suggests that the variational posterior reaches optimality at the ‘true’ KL divergence of around 1.326. This was verified by running a prior-contrastive algorithm for twice as long (20000 posterior iterations) and observing that the KL divergence did not decrease any further. In the prior-contrastive experiment, all of the programs reached optimality, so we cannot draw any conclusions from those results. Plots corresponding to the prior-contrastive optimal estimator experiment can be found in Appendix F.

Figures 6.5-6.7 correspond to the average KL divergence, estimator loss and estimated *NELBO* over the runtime of the program for the joint-contrastive cases.

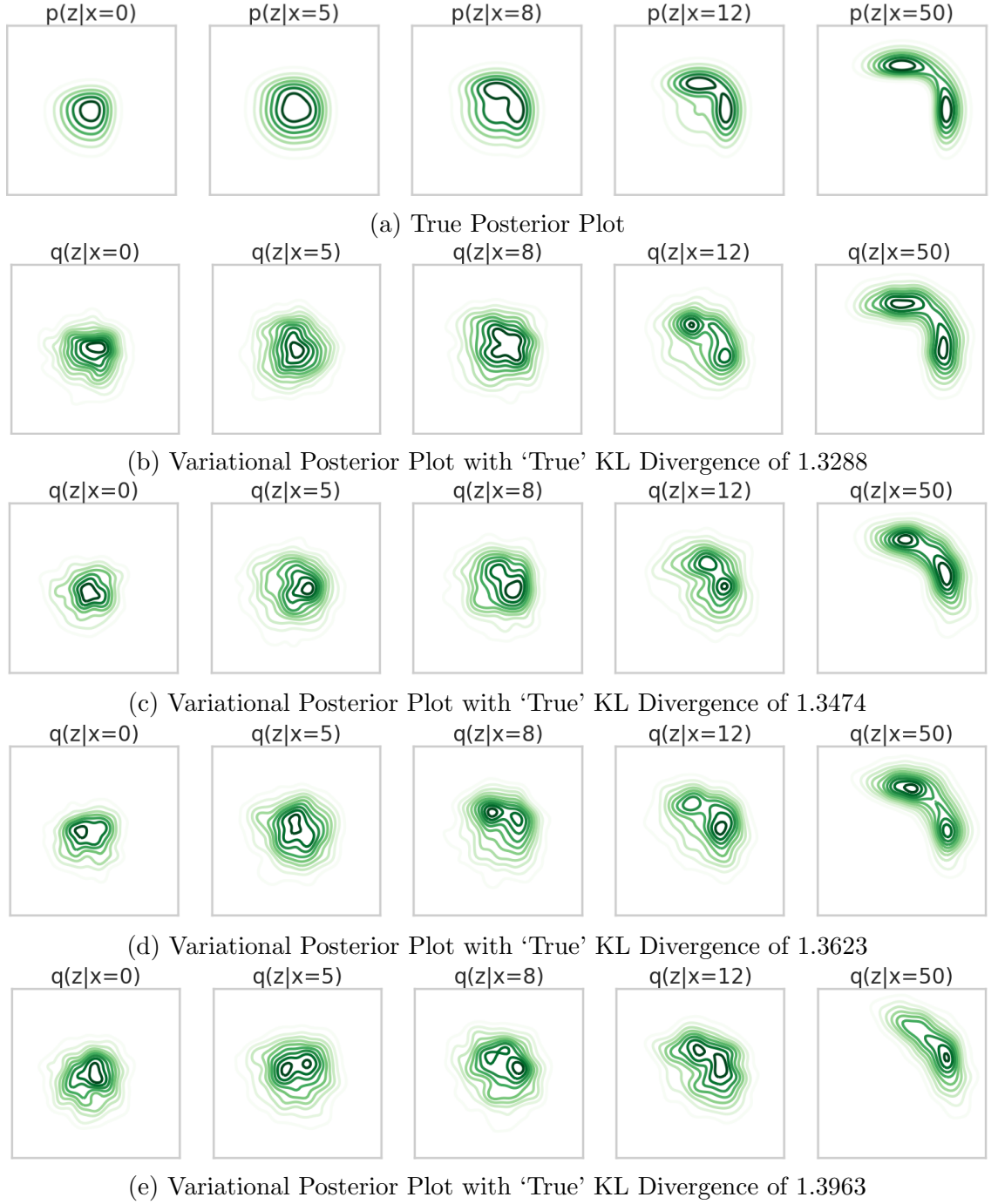


Figure 6.4: Above we compare the true (unnormalised) posterior as plotted in Figure 6.1 against variational posterior outputs corresponding to varying KL divergences. Sub-figures (b)-(3) were created by fitting a Gaussian kernel density estimation over 1000 posterior samples. Note that the variational posterior is relatively optimal at a 'true' KL divergence of 1.3288, and that the output appears less flexible as the divergence increases. In sub-figure (e), the variational posterior fails to capture the bimodality of the true posterior.

| Algorithm | Mean KL Divergence | Standard Deviation |
|---|--------------------|--------------------|
| PC Reverse KL - $D_\alpha(\mathbf{z}, x)$ | 1.3271 | 0.0041 |
| PC Reverse KL - $r_\alpha(\mathbf{z}, x)$ | 1.3265 | 0.0045 |
| PC Reverse KL - $T_\alpha(\mathbf{z}, x)$ | 1.3262 | 0.0041 |
| PC GAN - $D_\alpha(\mathbf{z}, x)$ | 1.3267 | 0.0041 |
| PC GAN - $r_\alpha(\mathbf{z}, x)$ | 1.3263 | 0.0035 |
| PC GAN - $T_\alpha(\mathbf{z}, x)$ | 1.3258 | 0.0039 |

Table 6.1: This table presents the results from the prior-contrastive experiment. Since the programs reached optimality in this case, it is uncertain from those results whether the choice of f -divergence or estimator parametrisation impacts posterior convergence.

| Algorithm | Mean KL Divergence | Standard Deviation |
|---|--------------------|--------------------|
| JC Reverse KL - $D_\alpha(\mathbf{z}, x)$ | 1.3416 | 0.0068 |
| JC Reverse KL - $r_\alpha(\mathbf{z}, x)$ | 1.3397 | 0.0066 |
| JC Reverse KL - $T_\alpha(\mathbf{z}, x)$ | 1.3446 | 0.0108 |
| JC GAN - $D_\alpha(\mathbf{z}, x)$ | 1.3648 | 0.0242 |
| JC GAN - $r_\alpha(\mathbf{z}, x)$ | 1.3657 | 0.0302 |
| JC GAN - $T_\alpha(\mathbf{z}, x)$ | 1.3670 | 0.0387 |

Table 6.2: From these joint-contrastive results, it is evident that for each f -divergence, similar posterior convergence is associated with the different estimator parametrisations. As Nowozin’s paper suggests, the GAN divergence demonstrates slower and more inconsistent results than the reverse KL divergence.

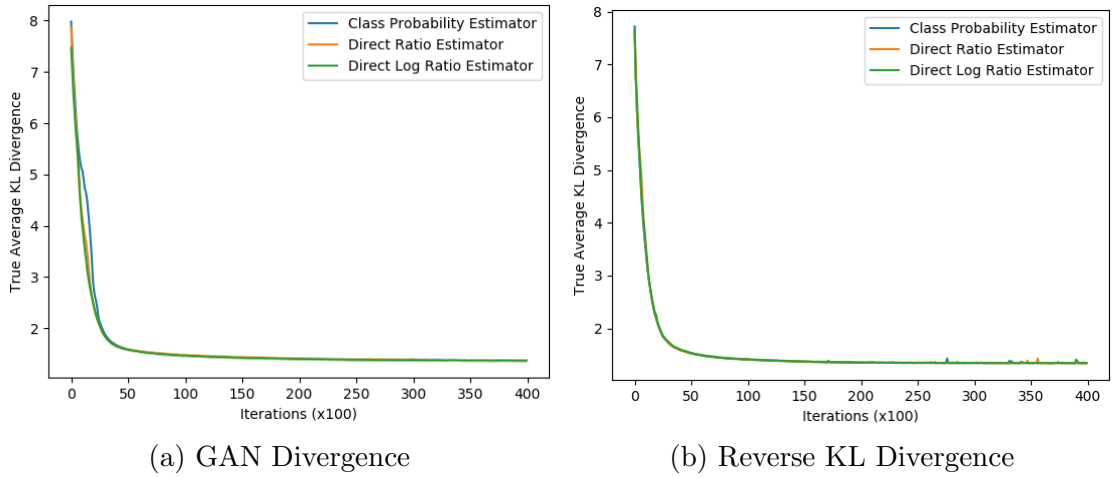


Figure 6.5: These plots of the true KL divergence in the joint-contrastive context show near identical convergence for all estimators.

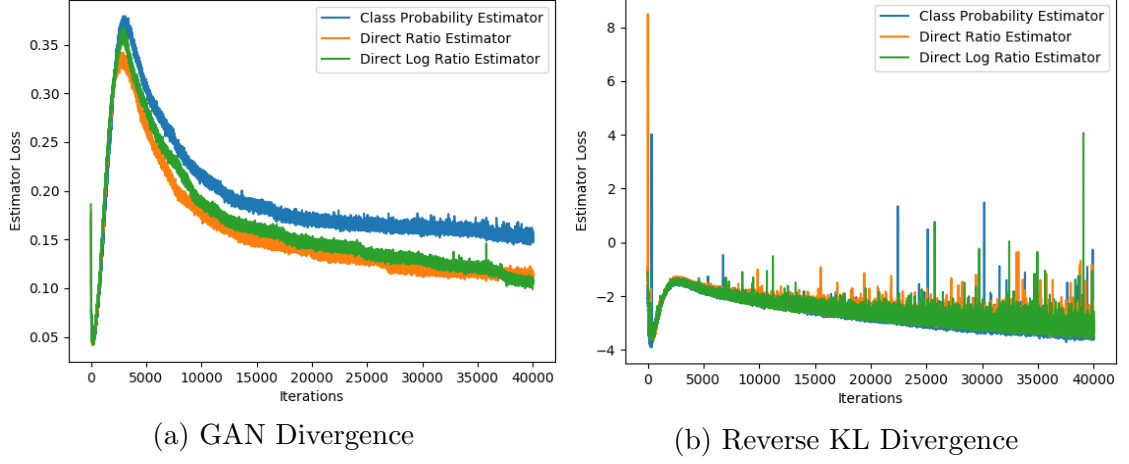


Figure 6.6: In sub-figure (a), the estimators have similar levels of stability, but the class probability estimator loss appears to be higher than the other two estimator parametrisations. All three estimators in sub-figure (b) have similar, increasingly unstable losses.

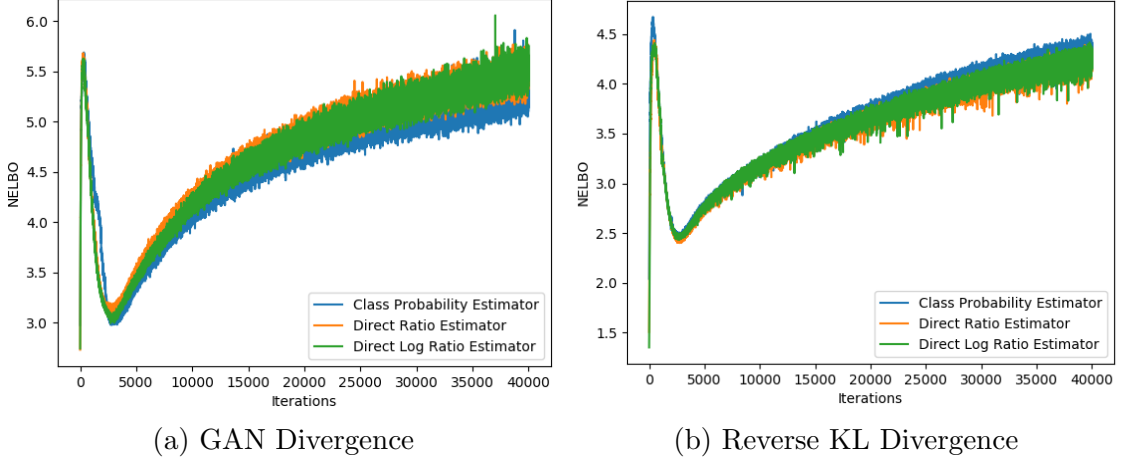


Figure 6.7: These joint-contrastive *NELBO* plots generally mirror the estimator loss trends depicted in Figure 6.6. Lower and more stable *NELBO* estimations are associated with the reverse KL divergence, correlating with its superior posterior convergence. It is unclear why the *NELBO* increases over the iterations when its minimisation theoretically leads to posterior convergence.

CHAPTER 7

Comparing Undertrained Estimators

Since all three estimator parametrisations have similar accuracies at optimality, it does not matter which one is chosen in that context. However, insufficient estimator training iterations can lead to an inaccurate estimation of the *NELBO*, reducing the speed at which the variational posterior converges. In this chapter, we first theoretically compare the rates of estimator convergence between the three parametrisations by analysing the bounds of the estimator outputs, the second functional derivatives of their loss functions and the displacement in the optimal estimator output with each posterior optimisation step. We then compare the performance of undertrained estimators with different parametrisations and f -divergence lower bounds.

7.1 Theory

7.1.1 Estimator Bounds

Consider the bounds on the estimator outputs. The class probability estimator $D_\alpha(u) \simeq \frac{q(u)}{q(u)+p(u)}$ is bound in $(0, 1)$, so from any arbitrary starting point in the same space, very few optimization steps are required to reach the global minimum. On the other hand, the direct ratio estimator $r_\alpha(u) \simeq \frac{q(u)}{p(u)}$ is bound in $\mathbb{R}^+ \setminus \{0\}$, and the direct log ratio estimator $T_\alpha(u) \simeq \log \frac{q(u)}{p(u)}$ can take any value in \mathbb{R} , so optimization can take many iterations if the difference between the estimator's initial and optimal values is too large. This can be problematic if there are insufficient iterations of optimizing the estimator, particularly in the initialization stage: the estimator may not properly converge and the posterior will be trained with an inaccurate density ratio estimation. Essentially, the gradient descent convergence can be improved by using an appropriate transformation [LeCun et al., 2012].

By converting the loss functions to integral form, we are able to visualise the bounds on the loss function output by fixing $q(u)$ and $p(u)$ as arbitrary values in

$(0, 1)$, and plotting the functional inside the integral. Figure 7.1 depicts plots of estimator outputs against the loss functional where $q(u) = p(u) = 0.5$.

Example 7.1.1. In this example we formulate the loss functional plotted in Figure 7.1 (a): the class probability estimator $D_\alpha(u)$ derived from the GAN divergence. The relevant estimator loss function is:

$$\begin{aligned} -\mathbb{E}_{q(u)}[\log D_\alpha(u)] - \mathbb{E}_{p(u)}[\log(1 - D_\alpha(u))] &= \int -q(u) \log D_\alpha(u) \\ &\quad - p(u) \log(1 - D_\alpha(u)) du \\ &= \int -\frac{\log D_\alpha(u) + \log(1 - D_\alpha(u))}{2} du. \end{aligned}$$

In the derivation above we have set $q(u) = p(u) = 0.5$. Note we plot the functional inside the integral:

$$f(u) = -\frac{\log D_\alpha(u) + \log(1 - D_\alpha(u))}{2}.$$

7.1.2 First and Second Derivatives of Estimator Loss Functions

Recall that both divergences attain the same global minimum, which is a parametrization of the estimator, and that these estimators are optimized via stochastic gradient descent. Thus, for a fixed estimator parametrization, the divergences will have varying rates of convergence, which can be analyzed by observing the second derivative. The convergence rate of a gradient descent method is proportional to the size of its second derivative [LeCun et al., 2012]. Below we formulate the second functional derivatives of the estimator losses with respect to the estimator function. It can be shown that the conditions to take the first and second functional derivative using the Euler-Legendre equation are met. Due to the exponential term in the direct log ratio estimator loss functions, it is difficult to compare their second derivatives, hence we omit them in this section. Their derivations can be found in Appendix G.

Reverse KL Divergence Bound:

Class Probability Estimator:

$$\begin{aligned} f_{RKL}(u) &:= -\mathbb{E}_{q(u)} \left[\log \frac{D(u)}{1 - D(u)} \right] + \mathbb{E}_{p(u)} \left[\frac{D(u)}{1 - D(u)} \right] \\ &= - \int q(u) \left(\log \frac{D(u)}{1 - D(u)} \right) du + \int p(u) \left(\frac{D(u)}{1 - D(u)} \right) du \\ \frac{df_{RKL}(u)}{dD(u)} &= -\frac{q(u)}{D(u)} - \frac{q(u)}{1 - D(u)} + \frac{p(u)}{1 - D(u)} + \frac{p(u)D(u)}{(1 - D(u))^2} \end{aligned}$$

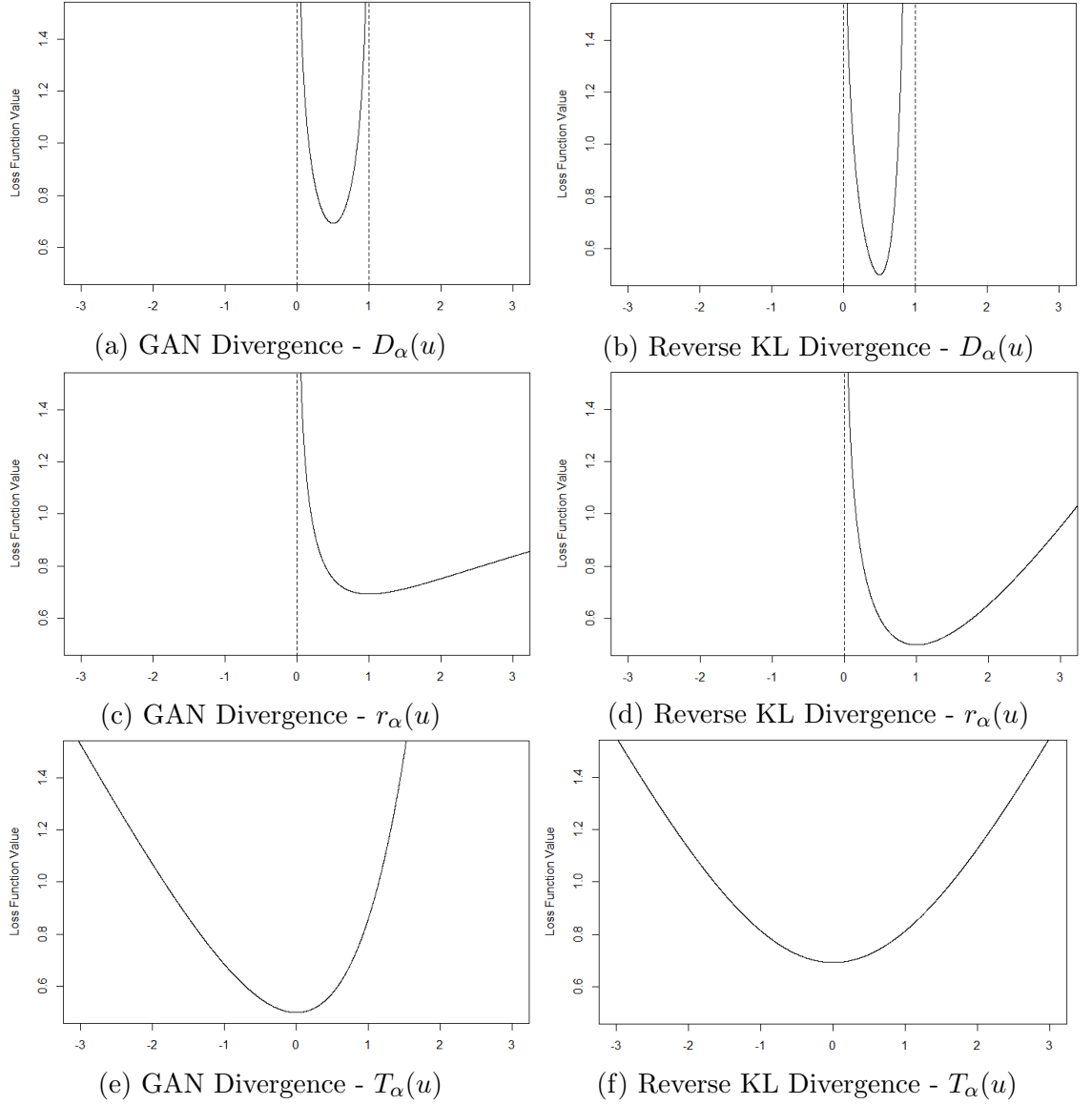


Figure 7.1: Above we have plotted the estimator output against its loss functional. The same x and y-axis scales are used for all plots. Due to the bounds, it is evident that the loss functionals using the class probability estimator $D_\alpha(u)$ are associated with the highest gradient values and therefore the fastest convergence. It is difficult to compare the direct ratio estimator $r_\alpha(u)$ and the direct log ratio estimator $T_\alpha(u)$, as the former estimator appears to have higher gradients when $q(u) < p(u)$, but slower convergence when $q(u) > p(u)$. Since the relative gradients of the graph can vary with the choice of $p(u)$ and $q(u)$, we cannot compare the f -divergences.

$$\begin{aligned}
&= -\frac{q(u)}{D(u)} - \frac{q(u)}{1-D(u)} + \frac{p(u)}{(1-D(u))^2} \\
\frac{d^2 f_{RKL}(u)}{dD^2(u)} &= \frac{q(u)}{D^2(u)} - \frac{q(u)}{(1-D(u))^2} + \frac{2p(u)}{(1-D(u))^3}.
\end{aligned}$$

Direct Ratio Estimator:

$$\begin{aligned}
f_{RKL}(u) &:= -\mathbb{E}_{q(u)}[\log r(u)] + \mathbb{E}_{p(u)}[r(u)] \\
&= -\int q(u) \log r(u) du + \int p(u) r(u) du \\
\frac{df_{RKL}(u)}{dr(u)} &= -\frac{q(u)}{r(u)} + p(u) \\
\frac{d^2 f_{RKL}(u)}{dr^2(u)} &= \frac{q(u)}{r^2(u)}.
\end{aligned}$$

GAN Divergence Bound:

Class Probability Estimator:

$$\begin{aligned}
f_{GAN}(u) &:= -\mathbb{E}_{q(u)}[\log D(u)] - \mathbb{E}_{p(u)}[\log(1 - D(u))] \\
&= -\int q(u) \log D(u) du - \int p(u) \log(1 - D) du \\
\frac{df}{dD(u)} &= -\frac{q(u)}{D(u)} + \frac{p(u)}{1 - D(u)} \\
\frac{d^2 f}{dD^2(u)} &= \frac{q(u)}{D^2(u)} + \frac{p(u)}{(1 - D(u))^2}.
\end{aligned}$$

Direct Ratio Estimator:

$$\begin{aligned}
f_{GAN}(u) &:= -\mathbb{E}_{q(u)} \left[\log \frac{r(u)}{r(u) + 1} \right] + \mathbb{E}_{p(u)} [\log(r(u) + 1)] \\
&= -\int q(u) \left[\log \frac{r(u)}{r(u) + 1} \right] du + \int p(u) [\log(r(u) + 1)] du \\
\frac{df_{GAN}(u)}{dr(u)} &= -\frac{q(u)}{r(u)} + \frac{q(u)}{r(u) + 1} + \frac{p(u)}{r(u) + 1} \\
\frac{d^2 f_{GAN}(u)}{dr^2(u)} &= \frac{q(u)}{r^2(u)} - \frac{q(u)}{(r(u) + 1)^2} - \frac{p(u)}{(r(u) + 1)^2}.
\end{aligned}$$

It can be seen that within the GAN divergence, the second derivative of the class probability estimator is strictly superior to that of the direct ratio estimator. Also, the direct ratio estimator has a strictly greater second derivative when its loss function is bounded by the reverse KL divergence than with the GAN divergence. As previously stated, the effectiveness of different f -divergence upper bounds has been tested in Nowozin et al. [2016]. They found that the ideal f -divergence used for the estimator's loss function is the same f -divergence that is being minimized in the variational posterior training: in our case, it is the reverse KL divergence.

7.1.3 Displacement of Estimator Optimal Values

Furthermore, we can also consider the effect of the posterior density displacement from each training step: every time $q(u)$ changes, the optimal value of the estimator also changes. Consequently, the estimator must take optimization steps to ‘catch up’, but again, if the displacement is too significant, then the estimator may not converge in time.

Lemma 7.1.2. *For a fixed displacement of the variational distribution $q(u)$, the class probability estimator’s global minimum displaces less than the direct ratio estimator, that is, $|D_{n+1}^* - D_n^*| < |r_{n+1}^* - r_n^*|$:*

Proof. Letting $\varepsilon \neq 0$ be the change in $q(u)$ with an optimization step, and noting that $|\varepsilon| < q(u)$, we have

$$\begin{aligned}
|D_{n+1}^* - D_n^*| &= \left| \frac{q(u) + \varepsilon}{q(u) + \varepsilon + p(u)} - \frac{q(u)}{q(u) + p(u)} \right| \\
&= \left| \frac{q^2(u) + q(u)p(u) + \varepsilon q(u) + \varepsilon p(u)}{(q(u) + \varepsilon + p(u))(q(u) + p(u))} - \frac{q^2(u) + \varepsilon q(u) + q(u)p(u)}{(q(u) + \varepsilon + p(u))(q(u) + p(u))} \right| \\
&= \left| \frac{\varepsilon p(u)}{(q(u) + \varepsilon + p(u))(q(u) + p(u))} \right| \\
&= \left| \frac{\varepsilon}{(q(u) + \varepsilon + p(u)) \left(\frac{q(u)}{p(u)} + 1 \right)} \right|, \\
|r_{n+1}^* - r_n^*| &= \left| \frac{q(u) + \varepsilon}{p(u)} - \frac{q(u)}{p(u)} \right| \\
&= \left| \frac{\varepsilon}{p(u)} \right|.
\end{aligned}$$

If $\varepsilon > 0$, then

$$|D_{n+1}^* - D_n^*| < |r_{n+1}^* - r_n^*| \text{ as } (q(u) + \varepsilon + p(u)) \left(\frac{q(u)}{p(u)} + 1 \right) > p(u).$$

If $\varepsilon < 0$, then recalling that $|\varepsilon| < q(u) < q(u) + p(u)$,

$$\begin{aligned}
(q(u) + \varepsilon + p(u)) \left(\frac{q(u)}{p(u)} + 1 \right) &= \frac{q^2(u)}{p(u)} + 2q(u) + p(u) + \varepsilon \left(\frac{q(u)}{p(u)} + 1 \right) \\
&= (q(u) + \varepsilon) \left(\frac{q(u)}{p(u)} + 1 \right) + q(u) + p(u) \\
&> p(u).
\end{aligned}$$

□

Remark 7.1.3. *The class probability estimator $D_\alpha(u)$ has more accurate density ratio estimation than the direct ratio estimator $r_\alpha(u)$ when the estimators are undertrained.*

For the direct log ratio estimator, we have

$$\begin{aligned} |T_{n+1}^* - T_n^*| &= \left| \log \frac{q(u) + \varepsilon}{p(u)} - \log \frac{q(u)}{p(u)} \right| \\ &= \left| \log \frac{q(u) + \varepsilon}{q(u)} \right|. \end{aligned}$$

It is difficult to make a direct comparison with the other displacement expressions.

7.2 Experiment Outline

In this experiment, we aim to confirm our theory that the estimator parametrisations have differing density ratio estimation accuracies when improperly trained, also determining which undertrained estimator is the most accurate by observing the convergence of the variational posterior.

The same ‘‘Continuous Sprinkler’’ experimental setup is used, but with several changes to the training parameters. We significantly reduce the amount of estimator training, lowering the estimator training rate to 0.00004 and the estimator steps before each posterior iteration to 11 for both contrastive settings. We also increase the posterior training rate to 0.0002 and to account for this change, the number of optimization steps of the variational distribution is reduced to 2000 for the prior-contrastive context and 4000 in the joint-contrastive algorithms.

7.3 Results

For each contrastive context and f -divergence lower bound, the class probability estimator $D_\alpha(\mathbf{z}, x)$ consistently demonstrates the lowest mean KL divergence, followed by the direct ratio estimator $r_\alpha(\mathbf{z}, x)$ and the direct log ratio estimator $T_\alpha(\mathbf{z}, x)$. The standard deviation of the results also generally increases with this trend: a lower standard deviation implies more consistent results. These results support the theory presented in Section 7.1, but their significance varies depending on the comparison.

The differences between the prior-contrastive estimators are relatively insignificant. This is likely because a likelihood term $-\mathbb{E}_{q^*(x)\pi(\varepsilon)}[\log p(x|\mathcal{G}_\phi(\varepsilon; x))]$ is additionally used to optimise the posterior weights ϕ , so convergence is less dependent on an accurate density ratio estimation.

| Algorithm | Mean KL Divergence | Standard Deviation |
|---|--------------------|--------------------|
| PC Reverse KL - $D_\alpha(\mathbf{z}, x)$ | 1.3572 | 0.0136 |
| PC Reverse KL - $r_\alpha(\mathbf{z}, x)$ | 1.3607 | 0.0199 |
| PC Reverse KL - $T_\alpha(\mathbf{z}, x)$ | 1.3641 | 0.0141 |
| PC GAN - $D_\alpha(\mathbf{z}, x)$ | 1.3788 | 0.0258 |
| PC GAN - $r_\alpha(\mathbf{z}, x)$ | 1.3811 | 0.0365 |
| PC GAN - $T_\alpha(\mathbf{z}, x)$ | 1.3849 | 0.0450 |

Table 7.1: In these prior-contrastive results, it is evident that using the reverse KL divergence to derive the lower bound for the estimator loss function leads to significantly higher posterior convergence, supporting our experimental results in Chapter 6.

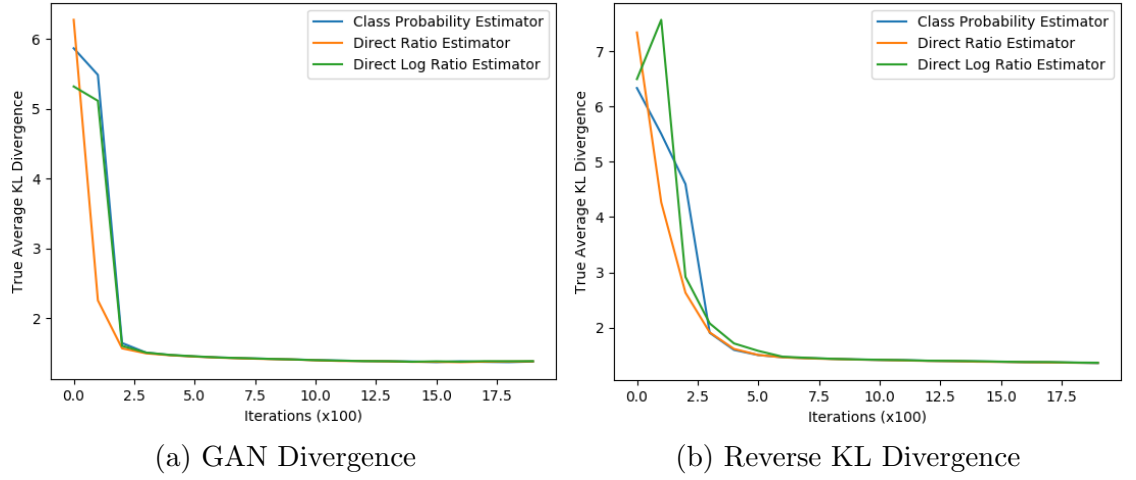


Figure 7.2: This figure illustrates the reduction in the true average KL divergence over the prior contrastive experiments' runtime. Although the direct ratio estimator plots initially experience a faster reduction, all three estimator plots meet at approximately the same KL divergence. It can be seen that the GAN divergence is associated with a faster initial drop than the reverse KL divergence, yet experiences lower overall posterior convergence.

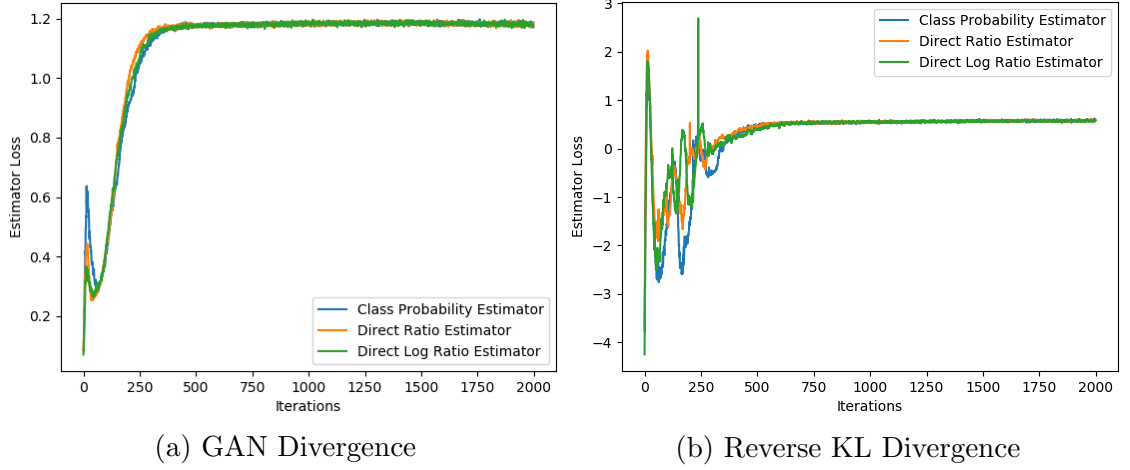


Figure 7.3: In these prior-contrastive estimator loss plots, it is evident that the estimators bound by the reverse KL divergence experience initial fluctuations which eventually stabilise, whilst the GAN divergence is associated with higher stability. This is consistent with the observations made in Figure 7.2, and implies a trade-off between estimator stability and accuracy in the choice of f -divergence.

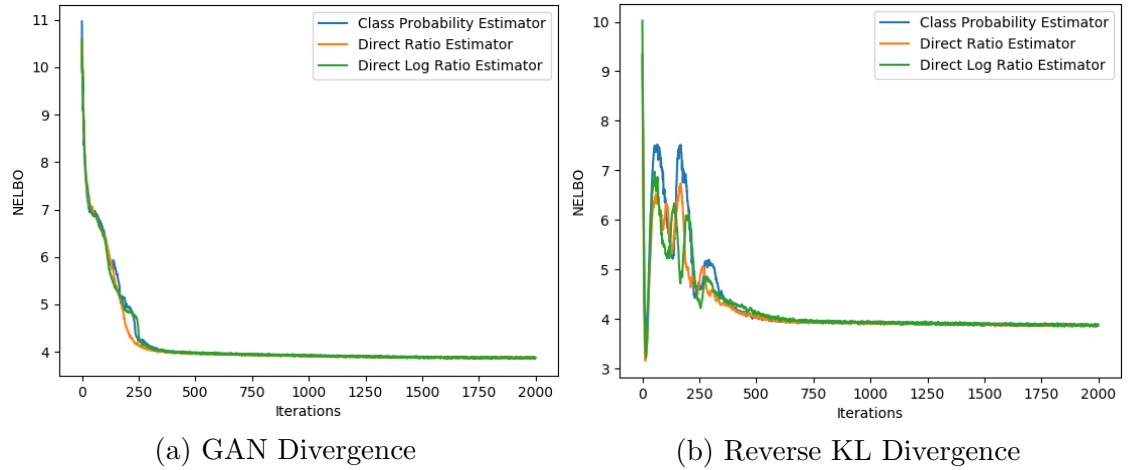


Figure 7.4: The trends shown in the *NELBO* plots above are generally consistent with the corresponding estimator loss plots. All of the estimators converge at approximately the same estimated *NELBO*, indicating that the effects of under-training the estimator are mostly experienced in the early program iterations.

More significant results are found in the joint-contrastive experiments, tabulated in 7.2. This is likely because the entirety of the joint-contrastive *NELBO* is a density ratio:

$$NELBO(q) = \mathbb{E}_{q^*(x)q_\phi(z|x)} \left[\frac{q(z, x)}{p(z, x)} \right],$$

so posterior optimisation is more dependent on an accurate density ratio estimation.

| Algorithm | Mean KL Divergence | Standard Deviation |
|----------------------------------|--------------------|--------------------|
| JC Reverse KL - $D_\alpha(z, x)$ | 1.3786 | 0.0286 |
| JC Reverse KL - $r_\alpha(z, x)$ | 1.3934 | 0.0410 |
| JC Reverse KL - $T_\alpha(z, x)$ | 1.4133 | 0.0597 |
| JC GAN - $D_\alpha(z, x)$ | 1.4017 | 0.0286 |
| JC GAN - $r_\alpha(z, x)$ | 1.4086 | 0.0555 |
| JC GAN - $T_\alpha(z, x)$ | 1.4214 | 0.0518 |

Table 7.2: In these joint-contrastive results, there is a significant difference between the three estimators when the reverse KL bound is used. However, when the GAN divergence is used to formulate the estimator loss function, only the direct log ratio estimator demonstrates significantly worse posterior convergence than the other two estimators.

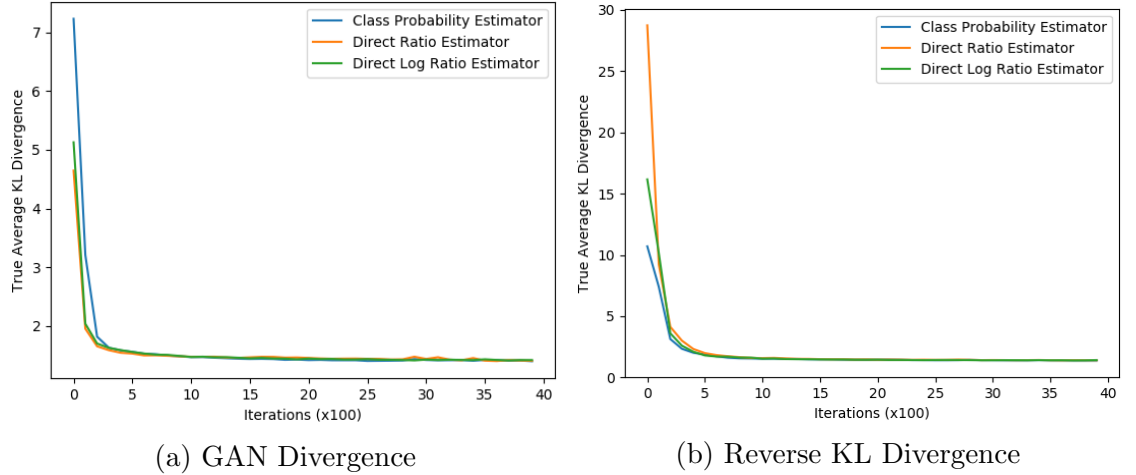


Figure 7.5: Similar to the true KL divergence plots in Figure 7.2, these joint-contrastive plots show that the estimators formulated with the GAN divergence experience faster initial convergence. However, this is unreliable as the reverse KL divergence experiments appear to initialise at a much higher true KL divergence.

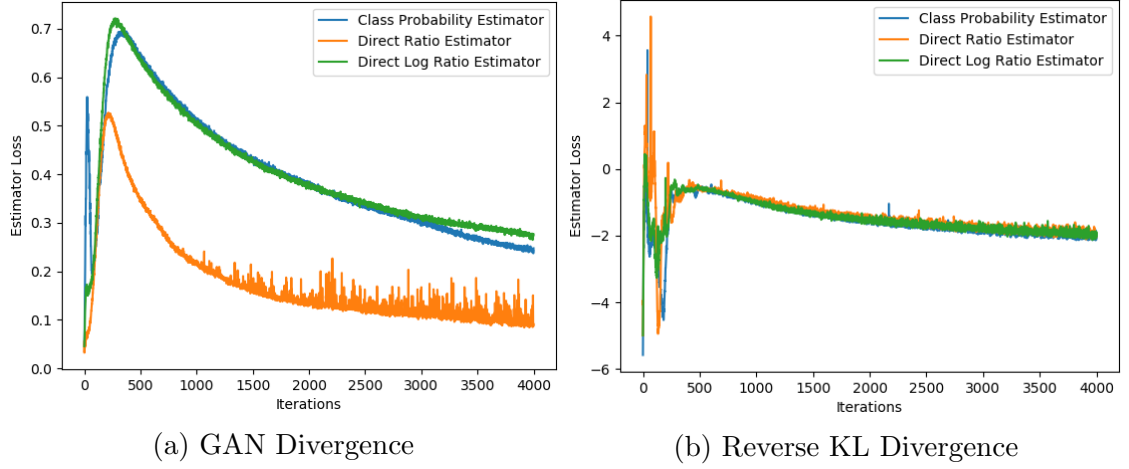


Figure 7.6: In these estimator loss plots, we again see that the reverse KL divergence plot demonstrates initial estimator instability. This is in stark contrast to the relatively stable GAN divergence plot. From sub-figure (a), we note that the direct ratio estimator is more unstable and has a lower loss value than the other two estimators. This may be the result of an outlier experiment, as the direct ratio estimator results have the highest standard deviation of the GAN divergence experiments, yet it has similar posterior convergence to the more consistent class probability estimator.

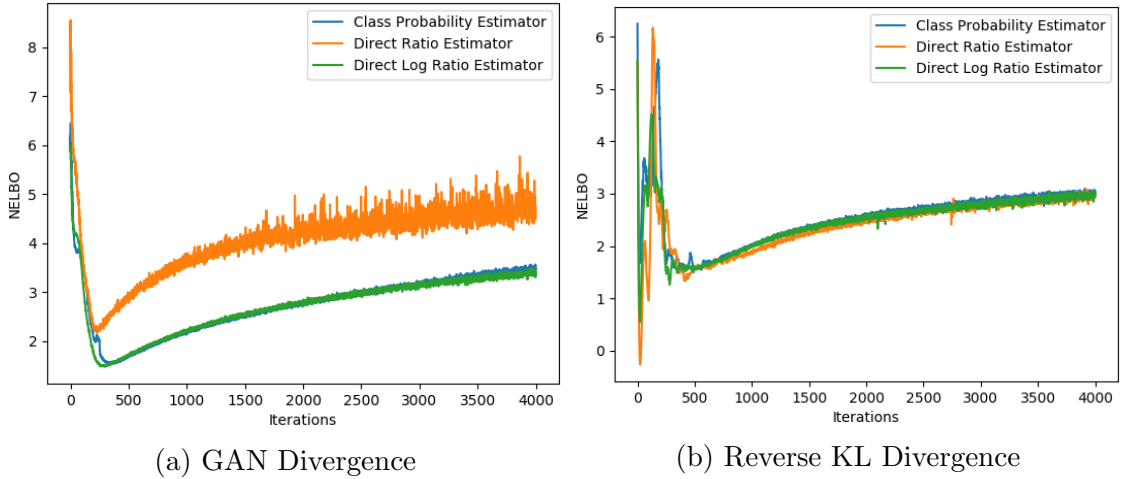


Figure 7.7: The joint-contrastive estimated $NELBO$ plots above generally have similar trends to the corresponding estimator plots. Here we note that the final $NELBO$ value of the reverse KL divergence experiments is lower than that of the GAN divergence. However, this may be due to its initial fluctuations delaying the start of the increasing $NELBO$ trend by approximately 250 iterations.

CHAPTER 8

Autoencoder Experiment - (MNIST Dataset)

In this chapter we compare the different f -divergence bounds and estimator parametrisations in the density ratio estimation involved with the autoencoder formulation. Specifically, we use the MNIST dataset: a popular dataset used in machine learning algorithms. Again, we undertrain the estimators to determine which parametrisation performs the best. The primary goals of this experiment are to confirm the conclusions presented in Chapter 7, and to possibly gain further insights by applying the algorithms to a different experimental setting. Due to limited experimental time, we only test the prior-contrastive algorithms. We repeat the experiment with two different latent spaces, one with 2 dimensions and one with 10 dimensions, to determine if the dimensionality of the densities in the density ratio $\frac{q_\phi(z|x)}{p(z)}$ has any effect on the results.

8.1 Experiment Outline

The MNIST (Modified National Institute of Standards and Technology) dataset is widely used for testing machine learning algorithms related to image analysis. It contains 60,000 labelled training images and 10,000 testing images of handwritten digits, each greyscale and of 28x28 pixel size. A sample of the images can be seen in Figure 8.1. Our algorithms do not require the images to be labelled so we combine the two image sets and ignore the labelling.

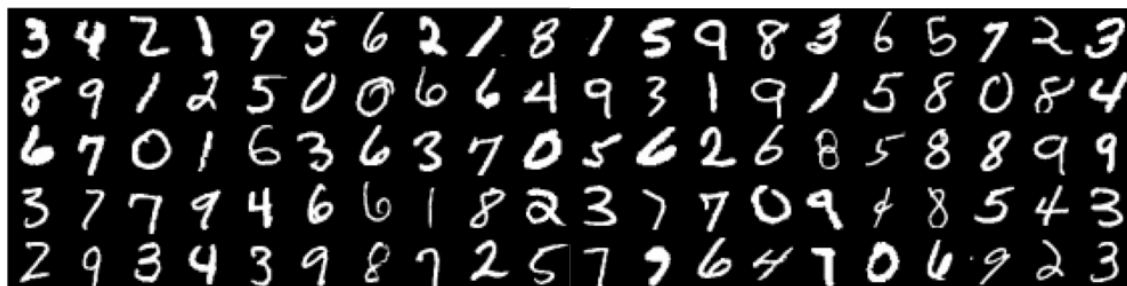


Figure 8.1: Samples from the MNIST Dataset

In this problem, we aim to generate new MNIST images indistinguishable from those in the original dataset. To do so, we use the “Adversarial Variational Bayes” variation of the autoencoder as described in Subsection 3.8.1. Recall that the associated optimisation problem is:

$$\min_{\phi, \theta} \mathbb{E}_{q^*(x)} \left[-\mathbb{E}_{q_\phi(z|x)} [\log p_\theta(x|z)] + KL(q_\phi(z|x) || p(z)) \right].$$

We therefore have three neural networks:

- An encoder network $\mathcal{G}_\phi(\varepsilon; x)$ that outputs samples from the variational posterior $q_\phi(z|x)$, effectively creating a latent representation of a data sample x .

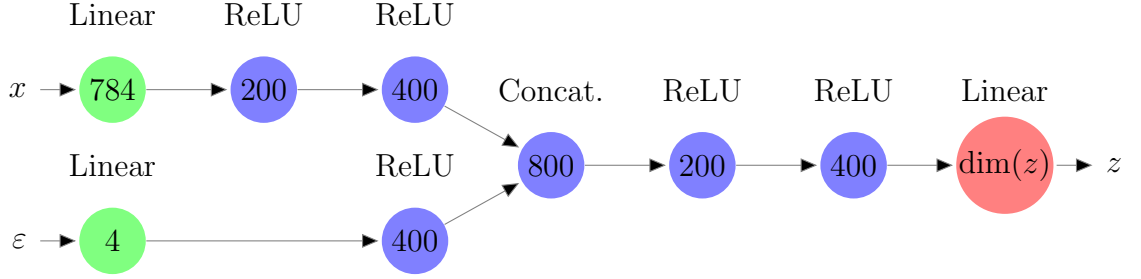


Figure 8.2: This figure illustrates the structure of the generator network $\mathcal{G}(x, \varepsilon)$ used in the MNIST data generation experiment. The notation used in the figure is the same as in Figures 5.2 and 5.3, and overall the network structure is very similar except significantly more nodes are used, suiting the higher dimensionality of the data. The dimensionality of latent variable z is either 2 or 10 depending on the experimental setting. We have arbitrarily chosen the number of random noise inputs ε to be 4.

- A decoder network representing the likelihood distribution $p_\theta(x|z)$ that reconstructs a data sample x from a latent variable input z .

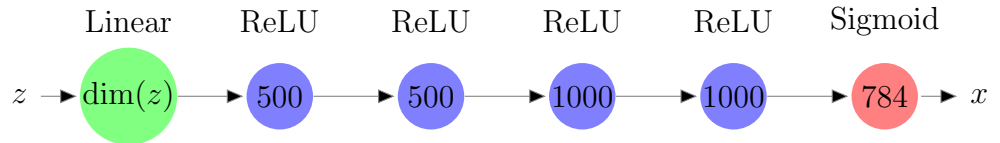


Figure 8.3: This is a diagram of the decoder network used in the MNIST data generation experiment. A sigmoid output layer is used to map the network output to $(0, 1)$, suiting the grayscale nature of the data. The amount of effective hidden layers is the same as in the encoder network, but there are significantly more nodes in each layer. This is because the objective of the program is to output relatively high dimensional image data. Although this problem involves image analysis, due to the relatively small image size we refrain from using convolutional layers. This is consistent with other similar MNIST experiments [Nowozin et al., 2016; Uehara et al., 2016].

- A density ratio estimator network ($D_\alpha(z, x)$, $r_\alpha(z, x)$ or $T_\alpha(z, x)$) used to evaluate the intractable $KL(q_\phi(z|x)||p(z))$ term in the optimisation problem.

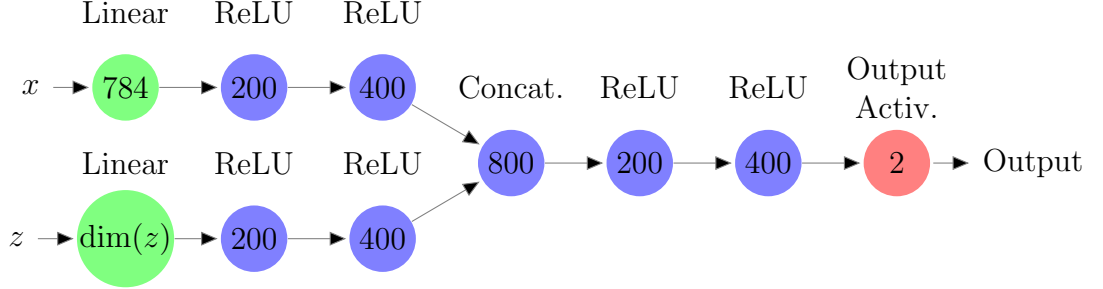


Figure 8.4: This figure depicts the estimator network for the MNIST data generation experiment. Depending on the estimator parametrisation, the output activation function is either sigmoid for the class probability estimator $D_\alpha(z, x) \simeq \frac{q_\phi(z|x)}{q_\phi(z|x)+p(z)}$, exponential for the direct ratio estimator $r_\alpha(z, x) \simeq \frac{q_\phi(z|x)}{p(z)}$ or linear for the direct log ratio estimator $T_\alpha(z, x) \simeq \log \frac{q_\phi(z|x)}{p(z)}$.

The program alternates between several iterations of estimator training and a simultaneous training step of the encoder and decoder weights.

Unlike the exact “Adversarial Variational Bayes” specification in Subsection 3.8.1, we do not add random noise to the decoder, therefore resulting in a deterministic output. To express the likelihood term $\mathbb{E}_{q_\phi(z|x)}[\log p_\theta(x|z)]$ in the optimisation problem, we use the likelihood function of a Bernoulli distribution, with probability equal to the output of the decoder. This likelihood representation is common in literature, and is used for several reasons [Nowozin et al., 2016; Tiao et al., 2018; Uehara et al., 2016]:

- Image blurriness is reduced as there is no random noise in the pixel values.
- We use the reconstruction error $\|x - \tilde{x}\|^2$ to evaluate convergence, so a noisy sample reconstruction can make it difficult to compare the algorithms.
- In this experiment, we are primarily interested in the accuracy of the density ratio estimation between the variational posterior and the prior: this is independent of the decoder parametrisation.

We avoid using kernel density estimation to evaluate convergence as it is inaccurate in high dimensions.

The network structure and parameters have been configured to be similar to the MNIST experiment performed in “f-GAN: Training Generative Neural Samplers using Variational Divergence Minimization” by Nowozin et al. [2016]: a large batch size of 2048 is used and for each network, a training rate of 0.0004 is used in the low

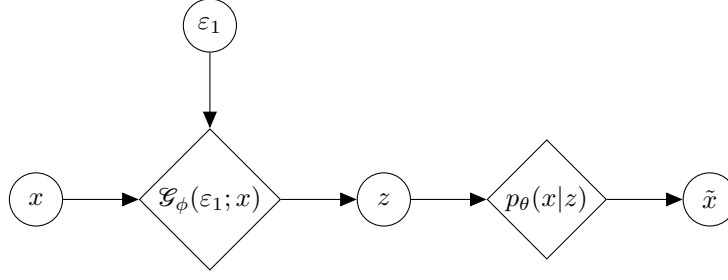


Figure 8.5: This diagram depicts the “Adversarial Variational Bayes” formulation of the variational autoencoder used in the MNIST data generation experiment. Note that there is no random noise added to the decoder.

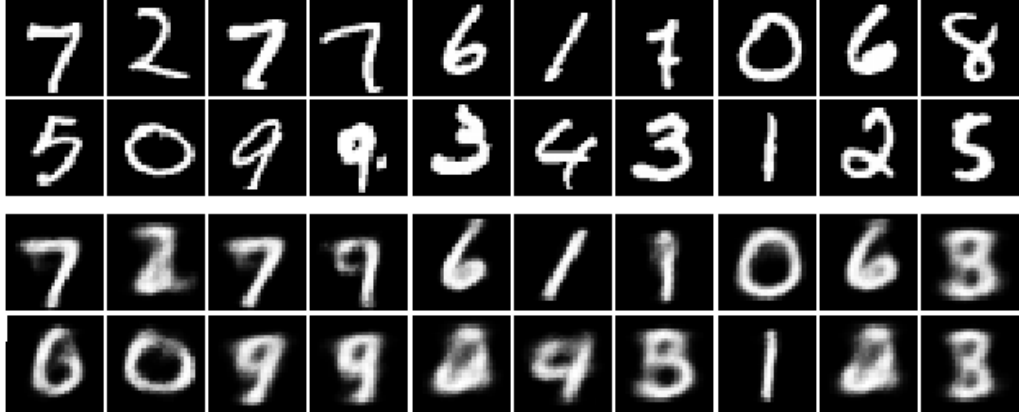
dimensional configuration, whilst the high dimensional setting uses a training rate of 0.0001. Again, the estimator is pre-trained for 5000 iterations, afterwards the program alternates between 20 iterations of estimator optimization and 1 iteration of posterior training, for 4000 total posterior iterations. Like in the “Sprinkler” experiments, the estimator loss and estimated *NELBO* at each posterior iteration was saved, and every 10 posterior iterations, 500 MNIST samples were passed through the autoencoder and the average reconstruction error $\|x - \tilde{x}\|^2$ was saved.

8.2 Low Dimensional Experiment Results

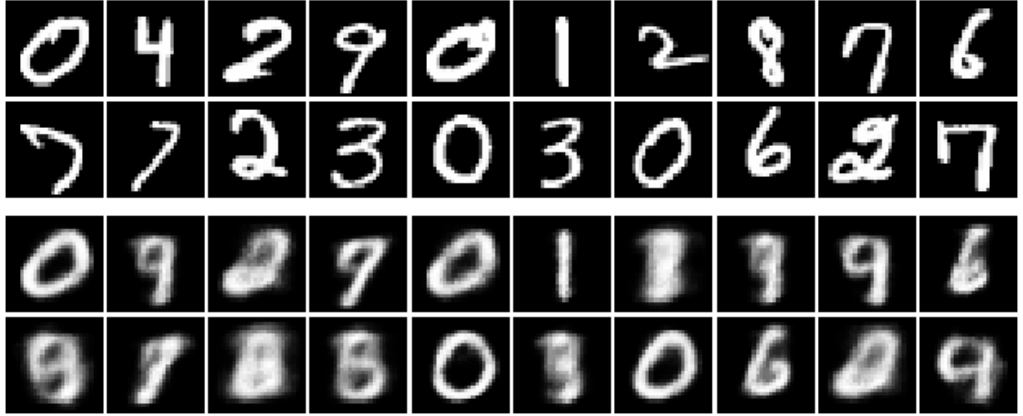
Table 8.1 below tabulates the mean and standard deviation of the autoencoder’s final reconstruction error between the 30 experiment repetitions. The majority of the distinctions are insignificant, likely because the estimators experience a relatively higher level of training in comparison to the experiment in Chapter 7. Additionally, the presence of the likelihood term in the *NELBO* loss function reduces the importance of accurate density ratio estimation.

| Algorithm | Mean Reconstruction Error | Standard Deviation |
|----------------------------------|---------------------------|--------------------|
| PC Reverse KL - $D_\alpha(z, x)$ | 0.08662 | 0.00154 |
| PC Reverse KL - $r_\alpha(z, x)$ | 0.08710 | 0.00214 |
| PC Reverse KL - $T_\alpha(z, x)$ | 0.08730 | 0.00157 |
| PC GAN - $D_\alpha(z, x)$ | 0.08673 | 0.00129 |
| PC GAN - $r_\alpha(z, x)$ | 0.08716 | 0.00151 |
| PC GAN - $T_\alpha(z, x)$ | 0.10683 | 0.00199 |

Table 8.1: The low-dimensional MNIST autoencoder experiment results are tabulated above. The only notable observation is that the direct log ratio estimator trained with a GAN divergence leads to significantly higher reconstruction error. There is also a consistent but relatively insignificant trend in the estimator parametrisations: again the class probability estimator correlates with the lowest reconstruction errors, followed by the direct ratio estimator and the direct log ratio estimator. Additionally, the reverse KL divergence correlates to superior posterior convergence.

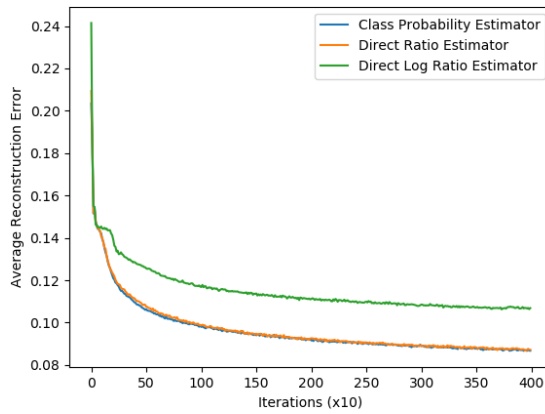


(a) Reconstruction Error of 0.08673

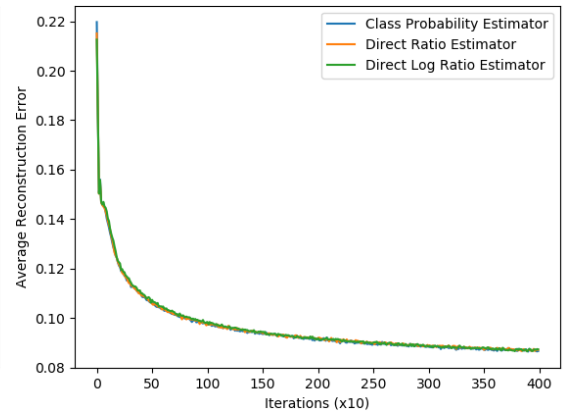


(b) Reconstruction Error of 0.10533

Figure 8.6: These figures exemplify data reconstruction corresponding to different reconstruction errors. The first two rows of each sub-figure depict example data input x , and the last two rows show the reconstructed output \tilde{x} .



(a) GAN Divergence



(b) Reverse KL Divergence

Figure 8.7: As shown in the above average reconstruction error plots, the direct log ratio estimator in sub-figure (a) consistently has a higher reconstruction error.

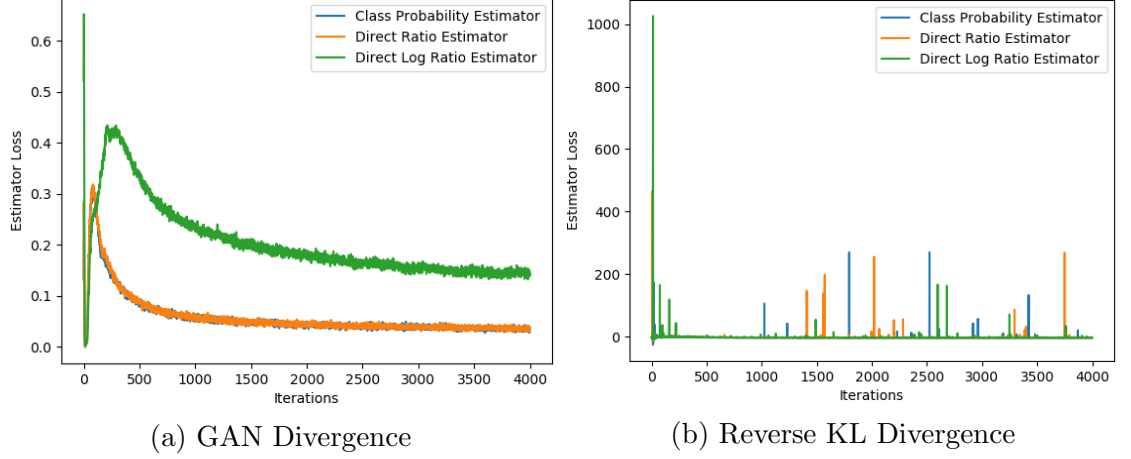


Figure 8.8: Noting the scale of the estimator loss plot in sub-figure (b), it is evident that the reverse KL divergence leads to unstable estimator training. Unlike the estimators plotted in Figure 7.3 (b), these estimators don’t appear to stabilise after a certain period. Sub-figure (a) shows that the direct log ratio estimator loss is consistently higher than the other two estimators, correlating with its poorer reconstruction.

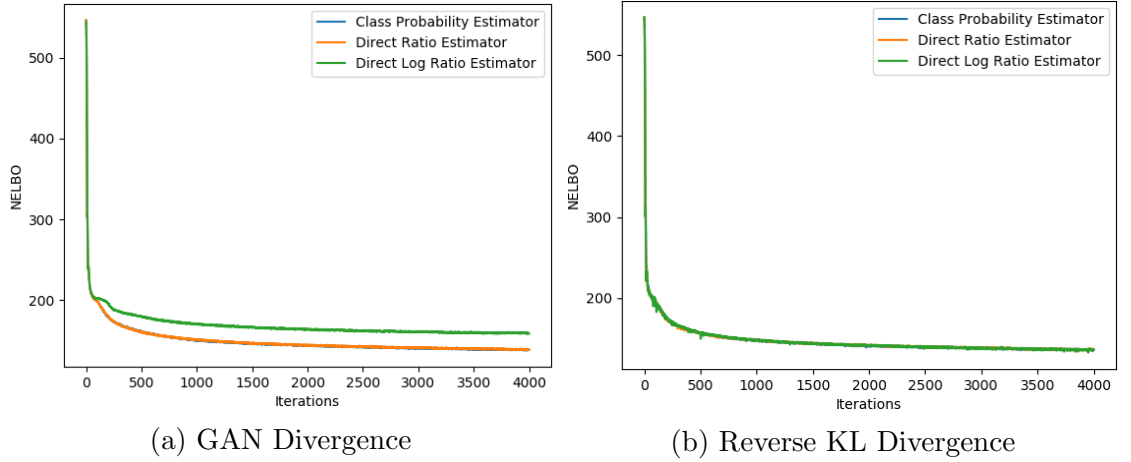


Figure 8.9: Despite the apparent instability of the estimators trained with the reverse KL divergence, the *NELBO* plot in sub-figure (b) is relatively consistent, leading to a smooth convergence as plotted in Figure 8.7 (b). The high direct log ratio estimator loss associated with the GAN divergence corresponds to a relatively large *NELBO* as depicted in sub-figure (a).

8.3 High Dimensional Experiment Results

When the dimensionality of the latent space was increased to 10, the direct ratio and direct log ratio estimator loss functions involved quantities greater than the largest representable 64-bit floating point number, overflowing to `Inf` and outputting `NaN` for the remainder of the program runtime. This is because the density ratio $\frac{q_\phi(z|x)}{p(z)}$ increases with the dimensionality of the latent space, eventually reaching a value that is too large to be represented by a 64-bit float. The direct ratio estimator

$r_\alpha(z, x) \simeq \frac{q_\phi(z|x)}{p(z)}$ therefore fails in this scenario. Now recall that the direct log ratio estimator loss function involves taking the exponential of the estimator output. For example, the loss function formulated by the reverse KL divergence is

$$-\mathbb{E}_{q^*(x)\pi(\varepsilon)}[T_\alpha(\mathcal{Z}(\varepsilon; x), x)] + \mathbb{E}_{p(z)q^*(x)}[\exp(T_\alpha(z, x))].$$

So despite $T_\alpha(z, x)$ outputting the log of the density ratio, the exact density ratio is expressed in the loss function when the exponential is taken, causing the program to fail. On the other hand, the class probability estimator does not experience this problem as its output is bound in $(0, 1)$.

Lemma 8.3.1. *In the prior-contrastive setting, the class probability estimator network output before passing through the sigmoid activation function $g(x) = \frac{1}{1+e^{-x}}$ is the estimated log density ratio $\log \frac{q_\phi(z|x)}{p(z)}$. A similar result holds in the joint-contrastive setting.*

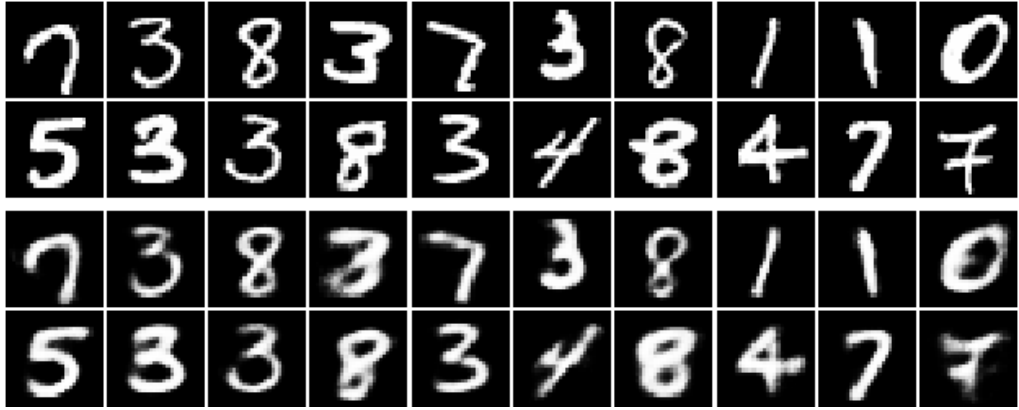
Proof. Proof of this lemma can be found in Appendix A.5. □

Remark 8.3.2. *The calculations with the class probability estimator involve values that lie within a larger bound of floating point representations than the values concerned with the direct ratio and direct log ratio estimators.*

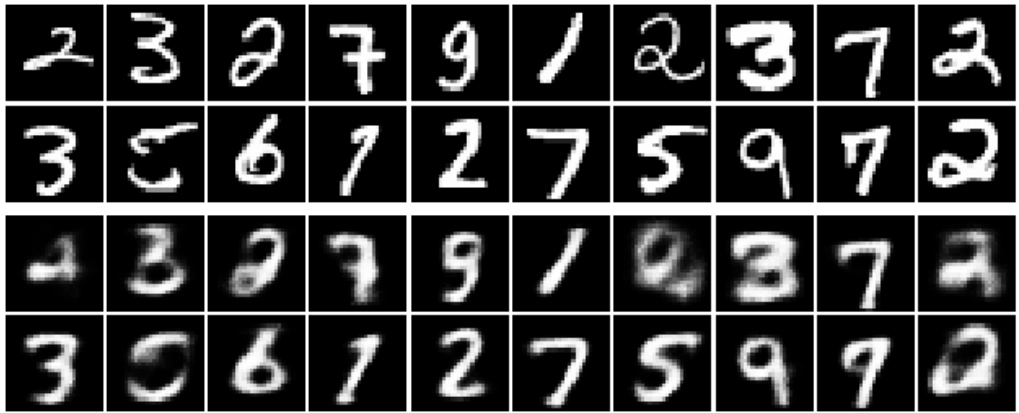
We can therefore conclude that the class probability estimator is superior in the sense that it is the only feasible parametrization. It remains to compare the f -divergence used to formulate the estimator loss function. The reconstruction errors are tabulated in Table 8.2 below.

| Algorithm | Mean Reconstruction Error | Standard Deviation |
|----------------------------------|---------------------------|--------------------|
| PC Reverse KL - $D_\alpha(z, x)$ | 0.06470 | 0.01949 |
| PC GAN - $D_\alpha(z, x)$ | 0.04440 | 0.00174 |

Table 8.2: In the high dimensional MNIST autoencoder experiment results, it is evident that the GAN divergence correlates with significantly lower reconstruction error mean and standard deviation, contradicting the superiority of the reverse KL divergence shown in previous experiments. An analysis of the plots in Figures 8.11-8.13 may explain this occurrence.



(a) Reconstruction Error of 0.04494



(b) Reconstruction Error of 0.064834

Figure 8.10: Similar to Figure 8.6, these figures exemplify data reconstruction corresponding to different reconstruction errors.

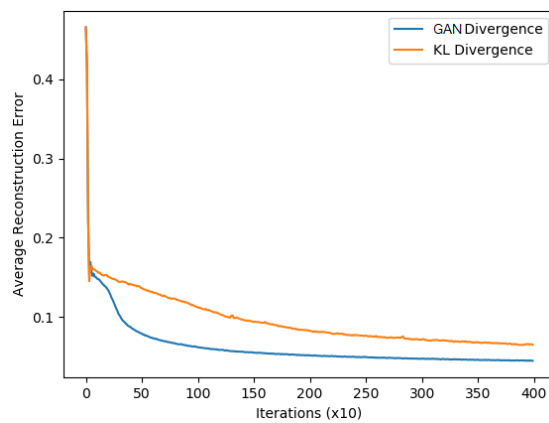


Figure 8.11: This plot shows that the reconstruction error associated with the reverse KL divergence is consistently higher for the majority of the program runtime.

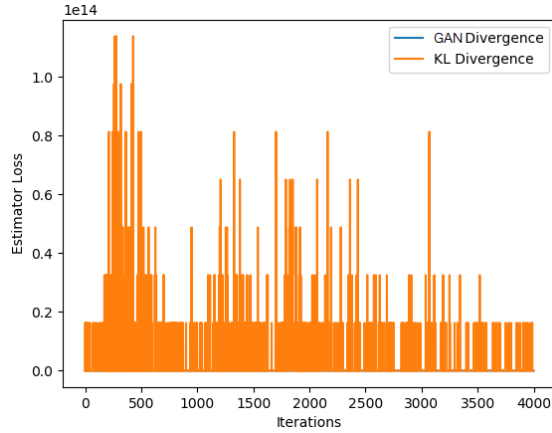


Figure 8.12: The estimator loss corresponding to the reverse KL divergence appears to be extremely unstable for the entire program runtime, spiking to values exceeding 10^{14} . On the other hand, the GAN divergence estimator loss appears to be relatively stable.

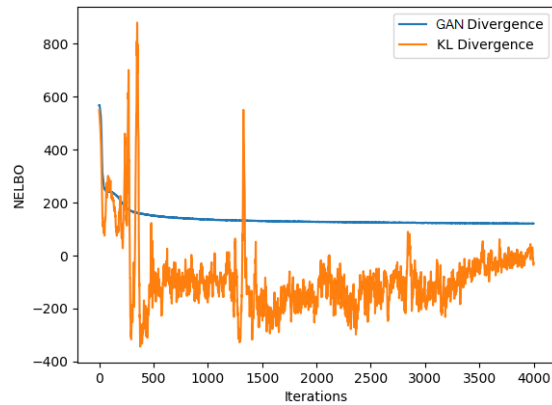


Figure 8.13: The instability of the reverse KL divergence estimator loss propagates to its *NELBO* estimation, which appears to fluctuate wildly. This correlates to the superiority of the GAN divergence in this particular experiment. Recalling the results in Chapter 7, estimators formulated by the reverse KL divergence experience initial instability, but have more accurate density ratio estimation when stable. It is possible that the estimator in this experiment has not stabilised, leading to poorer network convergence. This may be due to the increased complexity of the MNIST dataset distribution, as opposed to the simplicity of the previous “Sprinkler” problem.

CHAPTER 9

Conclusion and Further Research

In this thesis, we have compared various density ratio estimator loss functions in both prior-contrastive and joint-contrastive contexts for a simple Bayesian posterior inference problem, and in the prior-contrastive context for an autoencoder trained on the MNIST dataset. In Chapter 5, we generalised the estimator loss function specification to the choice of f -divergence and estimator parametrisation. Chapters 6 and 7 showed that the different estimator parametrisations have similar accuracies when optimally trained, but when under-trained, higher posterior convergence is correlated with faster estimator convergence, exhibited by the class probability estimator. These chapters also demonstrated that estimators trained with the reverse KL divergence may be initially unstable, particularly when undertrained, but demonstrate high density ratio estimation accuracy when stable. On the other hand, estimators trained with the GAN divergence are relatively stable but lead to lower posterior convergence. These results were verified in the MNIST autoencoder experiment discussed in Chapter 8, which additionally cemented the class probability estimator as the superior estimator parametrisation, as the values associated with the direct ratio and direct log ratio estimators were too large to be efficiently stored in a digital representation.

9.1 Further Research

In this thesis, we have only compared the use of the reverse KL divergence and the GAN divergence in formulating the estimator loss function. “f-GAN: Training Generative Neural Samplers using Variational Divergence Minimisation” by Nowozin et al. [2016] compares several different f -divergences such as the Pearson divergence and the forward KL divergence, but only assesses the posterior convergence. An analysis on the estimator losses and estimated *NELBOs* over the program runtime may reveal insights on the tradeoff between estimator stability and accuracy. Nowozin’s paper also uses different estimator parametrisations for

each f -divergence; comparing the f -divergences with the same class probability estimator parametrisation may lead to more reliable results.

There are alternative estimator parametrisations to test. For example, to alleviate the issues associated with an excessively high density ratio, “Generative Adversarial Nets from a Density Ratio Estimation Perspective” by Uehara et al. [2016] proposes that the direct density ratio estimator be parametrised as $r_\alpha(u) \simeq \frac{q(u)}{\beta q(u) + (1-\beta)p(u)}$ where $\beta > 0$ is small.

In our experiments, we have excluded the joint-contrastive autoencoder formulation, as described in “Adversarially Learned Inference” by Dumoulin et al. [2016] due to lack of computational time, but comparing the estimators in this context may present new insights.

There are alternate methods of estimating the intractable KL divergence term in the *NELBO* that do not involve Theorem 4.2.1. “Divergence Estimation for Multidimensional Densities via k -Nearest-Neighbor Distances” by Wang et al. [2009] describes a non-parametric method of estimating the KL divergence between two high dimensional densities. Rather than estimate the density ratio directly, a denoiser estimates the gradient of the log density, which can be used to minimise the KL divergence term in the *NELBO* [Vincent et al., 2008]. These methods can be used to formulate new variational inference algorithms, and their performances can be compared with the algorithms discussed in this thesis.

Posterior convergence in our autoencoder experiment can be assessed more effectively by using Annealed Importance Sampling (AIS) to estimate the negative of the marginal distribution $-p(x)$, which can be compared with the estimated *NELBO* which attains its minimum at that value. This process is detailed in “On the Quantitative Analysis of Decoder-Based Generative Models” by Wu et al. [2016].

References

- Beck, A. (2014). *Introduction to Nonlinear Optimization: Theory, Algorithms, and Applications with MATLAB*. Society for Industrial and Applied Mathematics, Philadelphia, PA, USA.
- Bengio, Y. (2012). *Practical Recommendations for Gradient-Based Training of Deep Architectures*, pages 437–478. Springer Berlin Heidelberg, Berlin, Heidelberg.
- Bishop, C. M. (1995). *Neural Networks for Pattern Recognition*. Oxford University Press, Inc., New York, NY, USA.
- Bishop, C. M. (2006). *Pattern Recognition and Machine Learning (Information Science and Statistics)*. Springer-Verlag, Berlin, Heidelberg.
- Blei, D. M., Kucukelbir, A., and McAuliffe, J. D. (2017). Variational inference: A review for statisticians. *Journal of the American Statistical Association*, 112(518):859–877.
- Boyd, S. and Vandenberghe, L. (2004). *Convex Optimization*. Cambridge University Press.
- Cheng, B. and Titterton, D. M. (1994). Neural networks: A review from a statistical perspective. *Statist. Sci.*, 9(1):2–30.
- Cybenko, G. (1989). Approximation by superpositions of a sigmoidal function. *Mathematics of Control, Signals and Systems*, 2(4):303–314.
- Doersch, C. (2016). Tutorial on Variational Autoencoders. *ArXiv e-prints*.
- Dumoulin, V., Belghazi, I., Poole, B., Mastropietro, O., Lamb, A., Arjovsky, M., and Courville, A. (2016). Adversarially Learned Inference. *ArXiv e-prints*.
- E. Rumelhart, D., E. Hinton, G., and J. Williams, R. (1986). Learning representations by back propagating errors. 323:533–536.
- Floudas, C. A. (2005). *Deterministic Global Optimization: Theory, Methods and (NONCONVEX OPTIMIZATION AND ITS APPLICATIONS Volume 37) (Nonconvex Optimization and Its Applications)*. Springer-Verlag, Berlin, Heidelberg.

- Fuglede, B. and Topsøe, F. (2004). Jensen-shannon divergence and hilbert space embedding. In *International Symposium on Information Theory, 2004. ISIT 2004. Proceedings.*, pages 31–.
- Gelman, A., Carlin, J. B., Stern, H. S., and Rubin, D. B. (2004). *Bayesian Data Analysis*. Chapman and Hall/CRC, 2nd ed. edition.
- Glorot, X. and Bengio, Y. (2010). Understanding the difficulty of training deep feed-forward neural networks. In *Proceedings of the thirteenth international conference on artificial intelligence and statistics*, pages 249–256.
- Glorot, X., Bordes, A., and Bengio, Y. (2011). Deep sparse rectifier neural networks. In Gordon, G., Dunson, D., and Dudík, M., editors, *Proceedings of the Fourteenth International Conference on Artificial Intelligence and Statistics*, volume 15 of *Proceedings of Machine Learning Research*, pages 315–323, Fort Lauderdale, FL, USA. PMLR.
- Goodfellow, I., Bengio, Y., and Courville, A. (2016). *Deep Learning*. MIT Press.
- Goodfellow, I., Pouget-Abadie, J., Mirza, M., Xu, B., Warde-Farley, D., Ozair, S., Courville, A., and Bengio, Y. (2014). Generative Adversarial Networks. 3.
- Goodman, L. A. (1960). On the exact variance of products. *Journal of the American Statistical Association*, 55(292):708–713.
- Haykin, S. (1998). *Neural Networks: A Comprehensive Foundation*. Prentice Hall PTR, Upper Saddle River, NJ, USA, 2nd edition.
- Hornik, K. (1991). Approximation capabilities of multilayer feedforward networks. *Neural Networks*, 4(2):251 – 257.
- Huszár, F. (2017). Variational Inference using Implicit Distributions. *ArXiv e-prints*.
- Kingma, D. P. and Ba, J. (2014). Adam: A method for stochastic optimization. *CoRR*, abs/1412.6980.
- Kingma, D. P. and Welling, M. (2013). Auto-Encoding Variational Bayes. *ArXiv e-prints*.
- Kolen, J. F. and Kremer, S. C. (2001). *Gradient Flow in Recurrent Nets: The Difficulty of Learning LongTerm Dependencies*. IEEE.
- Kullback, S. (1959). *Information Theory and Statistics*. Wiley, New York.
- LeCun, Y. A., Bottou, L., Orr, G. B., and Müller, K.-R. (2012). *Efficient BackProp*, pages 9–48. Springer Berlin Heidelberg, Berlin, Heidelberg.

- Li, M., Zhang, T., Chen, Y., and Smola, A. J. (2014). Efficient mini-batch training for stochastic optimization. In *Proceedings of the 20th ACM SIGKDD International Conference on Knowledge Discovery and Data Mining*, KDD '14, pages 661–670, New York, NY, USA. ACM.
- Mescheder, L. M., Nowozin, S., and Geiger, A. (2017). Adversarial Variational Bayes: Unifying Variational Autoencoders and Generative Adversarial Networks. *CoRR*, abs/1701.04722.
- Mohamed, S. and Lakshminarayanan, B. (2016). Learning in Implicit Generative Models. *ArXiv e-prints*.
- Nguyen, X., Wainwright, M. J., and Jordan, M. I. (2010). Estimating Divergence Functionals and the Likelihood Ratio by Convex Risk Minimization. *IEEE Trans. Inf. Theor.*, 56(11):5847–5861.
- Nowozin, S., Cseke, B., and Tomioka, R. (2016). f-gan: Training generative neural samplers using variational divergence minimization.
- P. Wellman, M. and Henrion, M. (1993). Explaining ‘explaining away’. 15:287–292.
- Ruder, S. (2016). An overview of gradient descent optimization algorithms. *CoRR*, abs/1609.04747.
- Simard, P. Y., Steinkraus, D., and Platt, J. C. (2003). Best practices for convolutional neural networks applied to visual document analysis. In *ICDAR*.
- Snyman, J. (2005). *Practical Mathematical Optimization*.
- Sugiyama, M., Suzuki, T., and Kanamori, T. (2012). *Density Ratio Estimation in Machine Learning*. Cambridge University Press.
- Tiao, L. C., Bonilla, E. V., and Ramos, F. (2018). Cycle-Consistent Adversarial Learning as Approximate Bayesian Inference. *ArXiv e-prints*.
- Tran, D., Ranganath, R., and Blei, D. M. (2017). Hierarchical Implicit Models and Likelihood-Free Variational Inference. *ArXiv e-prints*.
- Uehara, M., Sato, I., Suzuki, M., Nakayama, K., and Matsuo, Y. (2016). Generative Adversarial Nets from a Density Ratio Estimation Perspective. *ArXiv e-prints*.
- Vincent, P., Larochelle, H., Bengio, Y., and Manzagol, P.-A. (2008). Extracting and composing robust features with denoising autoencoders. In *Proceedings of the 25th International Conference on Machine Learning*, ICML '08, pages 1096–1103, New York, NY, USA. ACM.
- Wang, Q., Kulkarni, S. R., and Verdú, S. (2009). Divergence estimation for multi-dimensional densities via k-nearest-neighbor distances. *IEEE Trans. Inf. Theor.*, 55(5):2392–2405.

- Wu, H. (2009). Global stability analysis of a general class of discontinuous neural networks with linear growth activation functions. 179:3432–3441.
- Wu, Y., Burda, Y., Salakhutdinov, R., and Grosse, R. B. (2016). On the quantitative analysis of decoder-based generative models. *CoRR*, abs/1611.04273.
- Zanin Zambom, A. and Dias, R. (2012). A Review of Kernel Density Estimation with Applications to Econometrics. *ArXiv e-prints*.
- Zhang, C., Bütepage, J., Kjellström, H., and Mandt, S. (2017). Advances in variational inference. *CoRR*, abs/1711.05597.
- Zilles, K. (1992). Neuronal plasticity as an adaptive property of the central nervous system. *Annals of Anatomy - Anatomischer Anzeiger*, 174(5):383 – 391.

APPENDIX A

Proofs

A.1 Proof of Proposition 2.6.2

First we show that

$$\frac{d}{d\alpha} f(\mathbf{x}^{(n)} + \alpha \mathbf{s}^{(n)}) = \nabla f(\mathbf{x}^{(n)} + \alpha \mathbf{s}^{(n)})^\top \mathbf{s}^{(n)},$$

where $\mathbf{x}^{(n)} = [x_1^{(n)}, \dots, x_k^{(n)}]^\top$ and $\mathbf{s}^{(n)} = [s_1^{(n)}, \dots, s_k^{(n)}]^\top$.

Let

$$x_i^{(n)}(\alpha) = x_i^{(n)} + \alpha s_i^{(n)}, \quad i = 1, \dots, n,$$

so that $\mathbf{x}^{(n)} + \alpha \mathbf{s}^{(n)} = [x_1^{(n)}(\alpha), \dots, x_k^{(n)}(\alpha)]^\top$. We have

$$\begin{aligned} \frac{d}{d\alpha} f(\mathbf{x}^{(n)} + \alpha \mathbf{s}^{(n)}) &= \frac{d}{d\alpha} f(x_1^{(n)}, \dots, x_k^{(n)}(\alpha)) \\ &= \sum_{i=1}^k \frac{\partial f(\mathbf{x})}{\partial x_i} \Big|_{\mathbf{x}=\mathbf{x}^{(n)}+\alpha \mathbf{s}^{(n)}} \frac{d(x_i^{(n)}(\alpha))}{d\alpha} \\ &= \sum_{i=1}^k \frac{\partial f(\mathbf{x})}{\partial x_i} \Big|_{\mathbf{x}=\mathbf{x}^{(n)}+\alpha \mathbf{s}^{(n)}} s_i^{(n)} \\ &= \nabla f(\mathbf{x}^{(n)} + \alpha \mathbf{s}^{(n)})^\top \mathbf{s}^{(n)} \end{aligned}$$

Setting $\alpha = 0$ and using Definition 2.7.1,

$$\frac{d}{d\alpha} f(\mathbf{x}^{(n)} + \alpha \mathbf{s}^{(n)}) \Big|_{\alpha=0} = \nabla f(\mathbf{x}^{(n)})^\top \mathbf{s}^{(n)} < 0.$$

Therefore for sufficiently small $\alpha > 0$,

$$f(x^{(n)} + \alpha s^{(n)}) < f(x^{(n)}).$$

A.2 Proof of Lemma 3.7.1

Denoting the identity matrix as I and the covariance matrix of $q_\phi(\mathbf{z}|\mathbf{x})$ as Σ , we state the probability density functions of the two densities:

$$q_\phi(\mathbf{z}|\mathbf{x}) = \frac{1}{(2\pi)^{M/2} \det(\Sigma)^{1/2}} \exp \left(-\frac{1}{2}(\mathbf{z} - \boldsymbol{\mu})^\top \Sigma^{-1}(\mathbf{z} - \boldsymbol{\mu}) \right),$$

$$p(\mathbf{z}) = \frac{1}{(2\pi)^{M/2}} \exp \left(-\frac{1}{2}\mathbf{z}^\top I \mathbf{z} \right).$$

From Definition 3.2.2, we have:

$$\begin{aligned} KL(q_\phi(\mathbf{z}|\mathbf{x})||p(\mathbf{z})) &= \mathbb{E}_{q_\phi(\mathbf{z}|\mathbf{x})}[\log q_\phi(\mathbf{z}|\mathbf{x}) - \log p(\mathbf{z})] \\ &= -\frac{1}{2} \log(\det \Sigma) + \frac{1}{2} \mathbb{E}_{q_\phi(\mathbf{z}|\mathbf{x})} [-(\mathbf{z} - \boldsymbol{\mu})^\top \Sigma^{-1}(\mathbf{z} - \boldsymbol{\mu}) + \mathbf{z}^\top I \mathbf{z}] \\ &= -\frac{1}{2} \log(\det \Sigma) + \frac{1}{2} \mathbb{E}_{q_\phi(\mathbf{z}|\mathbf{x})} [-\text{tr}(\Sigma^{-1}\Sigma) + \text{tr}(I\mathbf{z}\mathbf{z}^\top)] \\ &= -\frac{1}{2} \log(\det \Sigma) - \frac{M}{2} + \frac{1}{2} \text{tr}(I + (\Sigma + \mu\mu^\top)) \\ &= \frac{1}{2} \sum_{i=1}^M (\sigma_i^2 + \mu_i^2 - \log(\sigma_i^2) - 1). \end{aligned}$$

A.3 Proof of Lemma 4.1.1

First we write the discriminator loss function in integral form:

$$\min_{\alpha} L_D = - \int q(u) \log D_{\alpha}(u) du - \int p(u) \log(1 - D_{\alpha}(u)) du.$$

Now we take the functional derivative of the expression and equate it to 0:

$$\begin{aligned} \frac{\partial L_D}{\partial D_{\alpha}(u)} &= 0 \\ -\frac{q(u)}{D_{\alpha}(u)} + \frac{p(u)}{1 - D_{\alpha}(u)} &= 0 \\ D_{\alpha}(u)(q(u) + p(u)) &= q(u) \\ D_{\alpha}(u) &= \frac{q(u)}{q(u) + p(u)}. \end{aligned}$$

Observing that $q(u)$ and $p(u)$ are densities, this expression is a minimum as

$$\frac{\partial^2 L_D}{\partial D_{\alpha}^2(u)} = \frac{q(u)}{D_{\alpha}^2(u)} + \frac{p(u)}{(1 - D_{\alpha}(u))^2}$$

$$> 0.$$

It can be shown that the conditions to take the first and second functional derivative using the Euler-Legendre equation are met.

A.4 Proof of Lemma 4.2.2

First we write the ratio loss function in integral form:

$$\min_{\alpha} L_r = - \int q(u) \log r_{\alpha}(u) du + \int p(u) r_{\alpha}(u) du.$$

Now we take the functional derivative of the expression and equate it to 0:

$$\begin{aligned} \frac{\partial L_r}{\partial r_{\alpha}(u)} &= 0 \\ -\frac{q(u)}{r_{\alpha}(u)} + p(u) &= 0 \\ r_{\alpha}(u) &= \frac{q(u)}{p(u)}. \end{aligned}$$

Observing that $q(u)$ is a density, this expression is a minimum as:

$$\begin{aligned} \frac{\partial^2 L_r}{\partial r_{\alpha}^2(u)} &= \frac{q(u)}{r_{\alpha}^2(u)} \\ &> 0. \end{aligned}$$

A.5 Proof of Lemma 8.3.1

Letting x be the neural network output before being mapped to $(0, 1)$, we have:

$$\begin{aligned} \frac{1}{1 + e^{-x}} &\simeq \frac{q_{\phi}(z|x)}{p(z) + q_{\phi}(z|x)} \\ e^{-x} + 1 &\simeq \frac{p(z) + q_{\phi}(z|x)}{q_{\phi}(z|x)} \\ e^{-x} &\simeq \frac{p(z)}{q_{\phi}(z|x)} \\ x &\simeq \log \frac{q_{\phi}(z|x)}{p(z)}. \end{aligned}$$

APPENDIX B

Algorithms

B.1 Back-Propagation Algorithm

Data: Training Data $\{(\mathbf{x}^{(1)}, \mathbf{y}^{(1)}), \dots, (\mathbf{x}^{(N)}, \mathbf{y}^{(N)})\}$

Result: Cost Function Partial Derivatives $\frac{\partial}{\partial \Theta_{m,n}^{(j)}} L(\Theta)$

begin

 Initialize weights Θ using Xavier Initialisation;

 Set $\Delta_{m,n}^{(j)} = 0 \quad \forall j, m, n$;

for $I = 1$ **to** N **do**

 Set $\mathbf{a}^{(1)} = \mathbf{x}^{(I)}$;

for $j = 2$ **to** J **do**

 Set $\mathbf{a}^{(j)} = \Theta^{(j-1)\top} \mathbf{a}^{(j-1)}$;

end

 Set $\boldsymbol{\delta}^{(J)} = \mathbf{a}^{(J)} - \mathbf{y}^{(I)}$;

for $j = J - 1$ **to** 2 **do**

 Set $\boldsymbol{\delta}^{(j)} = ((\Theta^{(j)})^\top \boldsymbol{\delta}^{(j+1)}) \cdot g'(\Theta^{(j)\top} \mathbf{a}^{(j)})$;

end

for $j = 1$ **to** $J - 1$ **do**

 Set $\Delta^{(j)} = \Delta^{(j)} + \boldsymbol{\delta}^{(j+1)} (\mathbf{a}^{(j)})^\top$;

end

end

for all j, m, n **do**

 Set $\frac{\partial}{\partial \Theta_{m,n}^{(j)}} L(\Theta) = \frac{1}{N} \Delta_{m,n}^{(j)}$;

end

end

Algorithm 5: Back-Propagation Algorithm

B.2 Coordinate Ascent Variational Inference Algorithm

Data: Dataset \mathbf{x} and Bayesian Model $p(\mathbf{x}, \mathbf{z})$

Result: Variational density $q(\mathbf{z}) = \prod_{i=1}^M q_i(z_i)$

begin

 Initialize random variational factors $q_j(z_j)$;

while $ELBO(q)$ has not converged **do**

for $j = 1$ **to** m **do**

 Set $q_j(z_j) \propto \exp(\mathbb{E}_{\mathbf{z}_{-j}}[\log p(z_j | \mathbf{z}_{-j}, \mathbf{x})])$;

end

 Calculate $ELBO(q) = \mathbb{E}_{q(\mathbf{z})}[\log p(\mathbf{z}, \mathbf{x})] - \mathbb{E}_{q(\mathbf{z})}[\log q(\mathbf{z})]$;

end

 Return $q(\mathbf{z})$;

end

Algorithm 6: Coordinate Ascent Variational Inference (CAVI)

B.3 Algorithms for “Sprinkler” Experiment

Data: Dataset distribution $q^*(x) = \{0, 5, 8, 12, 20\}$,

(Implicit) Prior distribution $p(z) \sim \mathcal{N}(0, 2I_{2 \times 2})$,

Likelihood distribution $p(x|z) \sim \text{Exp}(3 + \max(0, z_1)^3 + \max(0, z_2)^3)$,

Noise distribution $\pi(\varepsilon) \sim \mathcal{N}(0, I_{3 \times 3})$

Result: Optimized posterior generator $\mathcal{G}_\phi(\varepsilon; x)$

```

for  $j = 1$  to 5000 do
    Sample  $\{\varepsilon^{(i,j)}\}_{i=1}^{1000} \sim \pi(\varepsilon)$ ;
    Sample  $\{0, 5, 8, 12, 50\}_{i=1}^{200} = \{x^{(i,j)}\}_{i=1}^{1000} \sim q^*(x)$ ;
    Sample  $\{z_p^{(i,j)}\}_{i=1}^{1000} \sim p(z)$ ;
    foreach  $\varepsilon^{(i,j)}, x^{(i,j)}$  do
        | Sample  $z_q^{(i,j)} = \mathcal{G}(\varepsilon^{(i,j)}; x_q^{(i,j)})$ ;
    end
    update Estimator weights  $\alpha$ 
end

for  $j = 1$  to 10000 do
    for  $k = 1$  to 100 do
        Sample  $\{\varepsilon^{(i,k)}\}_{i=1}^{1000} \sim \pi(\varepsilon)$ ;
        Sample  $\{0, 5, 8, 12, 50\}_{i=1}^{200} = \{x^{(i,k)}\}_{i=1}^{1000} \sim q^*(x)$ ;
        Sample  $\{z_p^{(i,k)}\}_{i=1}^{1000} \sim p(z)$ ;
        foreach  $\varepsilon^{(i,k)}, x^{(i,k)}$  do
            | Sample  $z_q^{(i,k)} = \mathcal{G}(\varepsilon^{(i,k)}; x_q^{(i,k)})$ ;
        end
        update Estimator weights  $\alpha$ 
    end
    Sample  $\{\varepsilon^{(i)}\}_{i=1}^{1000} \sim \pi(\varepsilon)$ ;
    Sample  $\{0, 5, 8, 12, 50\}_{i=1}^{200} = \{x^{(i)}\}_{i=1}^{1000} \sim q^*(x)$ ;
    update Variational posterior weights  $\phi$ 
end

```

Algorithm 7: Sprinkler Prior-Contrastive Algorithm

Data: Dataset distribution $q^*(x) = \{0, 5, 8, 12, 20\}$,

(Implicit) Prior distribution $p(z) \sim \mathcal{N}(0, 2I_{2 \times 2})$,

(Implicit) Likelihood distribution

$p(x|z) \sim EXP(3 + \max(0, z_1)^3 + \max(0, z_2)^3)$,

Noise distribution $\pi(\varepsilon) \sim \mathcal{N}(0, I_{3 \times 3})$

Result: Optimized posterior generator $\mathcal{G}_\phi(\varepsilon; x)$

```
for  $j = 1$  to 5000 do
    Sample  $\{\varepsilon^{(i,j)}\}_{i=1}^{1000} \sim \pi(\varepsilon)$ ;
    Sample  $\{0, 5, 8, 12, 20\}_{i=1}^{200} = \{x_q^{(i,j)}\}_{i=1}^{1000} \sim q^*(x)$ ;
    Sample  $\{z_p^{(i,j)}\}_{i=1}^{1000} \sim p(z)$ ;
    foreach  $\varepsilon^{(i,j)}, x^{(i,j)}$  do
        Sample  $z_q^{(i,j)} = \mathcal{G}(\varepsilon^{(i,j)}; x_q^{(i,j)})$ ;
    end
    foreach  $z_p^{(i,j)}$  do
        Sample  $x_p^{(i,j)} \sim p(x|z)$ ;
    end
    update Estimator weights  $\alpha$ 
end
for  $j = 1$  to 40000 do
    for  $k = 1$  to 100 do
        Sample  $\{\varepsilon^{(i,k)}\}_{i=1}^{1000} \sim \pi(\varepsilon)$ ;
        Sample  $\{0, 5, 8, 12, 20\}_{i=1}^{200} = \{x_q^{(i,k)}\}_{i=1}^{1000} \sim q^*(x)$ ;
        Sample  $\{z_p^{(i,k)}\}_{i=1}^{1000} \sim p(z)$ ;
        foreach  $\varepsilon^{(i,k)}, x^{(i,k)}$  do
            Sample  $z_q^{(i,k)} = \mathcal{G}(\varepsilon^{(i,k)}; x_q^{(i,k)})$ ;
        end
        foreach  $z_p^{(i,k)}$  do
            Sample  $x_p^{(i,k)} \sim p(x|z)$ ;
        end
        update Estimator weights  $\alpha$ 
    end
    Sample  $\{\varepsilon^{(i)}\}_{i=1}^{1000} \sim \pi(\varepsilon)$ ;
    Sample  $\{0, 5, 8, 12, 20\}_{i=1}^{200} = \{x_q^{(i)}\}_{i=1}^{1000} \sim q^*(x)$ ;
    update Variational posterior weights  $\phi$ 
end
```

Algorithm 8: Sprinkler Joint-Contrastive Algorithm

APPENDIX C

Coordinate Ascent Variational Inference Derivation

Firstly, we express $ELBO(q)$ as an integral:

$$\begin{aligned}
ELBO(q) &= \mathbb{E}_{q(\mathbf{z})}[\log p(\mathbf{x}|\mathbf{z})] - KL(q(\mathbf{z})||p(\mathbf{z})) \\
&= \mathbb{E}_{q(\mathbf{z})}[\log p(\mathbf{x}|\mathbf{z}) + \log p(\mathbf{z}) - \log q(\mathbf{z})] \\
&= \mathbb{E}_{q(\mathbf{z})}[\log p(\mathbf{x}, \mathbf{z}) - \log q(\mathbf{z})] \\
&= \int_{\mathbb{R}^M} q(\mathbf{z})(\log p(\mathbf{x}, \mathbf{z}) - \log q(\mathbf{z}))d\mathbf{z}.
\end{aligned}$$

Substituting $q(\mathbf{z}) = \prod_{i=1}^M q_i(z_i)$ and factoring out $q_j(z_j)$ yields:

$$\begin{aligned}
ELBO(q) &= \int_{\mathbb{R}^M} \left[\prod_{i=1}^M q_i(z_i) \right] \left(\log p(\mathbf{x}, \mathbf{z}) - \sum_{i=1}^M \log q_i(z_i) \right) d\mathbf{z} \\
&= \int_{\mathbb{R}} q_j(z_j) \left(\int_{\mathbb{R}^{M-1}} \log p(\mathbf{x}, \mathbf{z}) \prod_{i \neq j} q_i(z_i) d\mathbf{z}_{-j} \right) dz_j \\
&\quad - \int_{\mathbb{R}} q_j(z_j) \left(\int_{\mathbb{R}^{M-1}} \left[\prod_{i \neq j} q_i(z_i) \right] \sum_{i=1}^M \log q_i(z_i) d\mathbf{z}_{-j} \right) dz_j \\
&= \int_{\mathbb{R}} q_j(z_j) \mathbb{E}_{\mathbf{z}_{-j}}[\log p(\mathbf{x}, \mathbf{z})] dz_j \\
&\quad - \int_{\mathbb{R}} q_j(z_j) \log q_j(z_j) \left(\int_{\mathbb{R}^{M-1}} \prod_{i \neq j} q_i(z_i) d\mathbf{z}_{-j} \right) dz_j \\
&\quad - \int_{\mathbb{R}} q_j(z_j) \left(\int_{\mathbb{R}^{M-1}} \left[\prod_{i \neq j} q_i(z_i) \right] \sum_{i \neq j} \log q_i(z_i) d\mathbf{z}_{-j} \right) dz_j \\
&= \int_{\mathbb{R}} q_j(z_j) \mathbb{E}_{\mathbf{z}_{-j}}[\log p(\mathbf{x}, \mathbf{z})] dz_j - \int_{\mathbb{R}} q_j(z_j) \log q_j(z_j) dz_j \\
&\quad - \int_{\mathbb{R}^{M-1}} \left[\prod_{i \neq j} \log q_i(z_i) \right] \sum_{i \neq j} \log q_i(z_i) d\mathbf{z}_{-j} \tag{C.0.1}
\end{aligned}$$

$$= \int_{\mathbb{R}} q_j(z_j) (\mathbb{E}_{\mathbf{z}_{-j}}[\log p(\mathbf{x}, \mathbf{z})] - \log q_j(z_j)) dz_j + C. \tag{C.0.2}$$

where C is a constant.

The term in Expression (C.0.1) is constant with respect to $q_j(z_j)$. We want to maximize $ELBO(q)$, so we formulate the Lagrangian equation with the constraint that $q_i(z_i)$ are probability density functions:

$$ELBO(q) - \sum_{i=1}^M \lambda_i \int_{\mathbb{R}} q_i(z_i) dz_i = 0,$$

or using Expression (C.0.2),

$$\int_{\mathbb{R}} q_j(z_j) (\mathbb{E}_{\mathbf{z}_{-j}} [\log p(\mathbf{x}, \mathbf{z})] - \log q_j(z_j)) dz_j - \sum_{i=1}^M \lambda_i \int_{\mathbb{R}} q_i(z_i) dz_i + C = 0. \quad (\text{C.0.3})$$

Using the Euler-Legendre equation, we then take the functional derivative of Equation (C.0.3) with respect to $q_j(z_j)$ [Bishop, 2006]:

$$\begin{aligned} \frac{\partial ELBO(q)}{\partial q_j(z_j)} &= \frac{\partial}{\partial q_j(z_j)} [q_j(z_j) (\mathbb{E}_{\mathbf{z}_{-j}} [\log p(\mathbf{x}, \mathbf{z})] - \log q_j(z_j)) - \lambda_j q_j(z_j)] \\ &= \mathbb{E}_{\mathbf{z}_{-j}} [\log p(\mathbf{x}, \mathbf{z})] - \log q_j(z_j) - 1 - \lambda_j. \end{aligned} \quad (\text{C.0.4})$$

Equating Expression (C.0.4) to 0 and observing that $1 + \lambda_j$ is constant with respect to z , we have:

$$\begin{aligned} \log q_j^*(z_j) &= \mathbb{E}_{\mathbf{z}_{-j}} [\log p(\mathbf{x}, \mathbf{z})] - C \\ q_j^*(z_j) &= \frac{\exp(\mathbb{E}_{\mathbf{z}_{-j}} [\log p(\mathbf{x}, \mathbf{z})])}{\exp(C)} \\ &= \frac{\exp(\mathbb{E}_{\mathbf{z}_{-j}} [\log p(\mathbf{x}, \mathbf{z})])}{\int \exp(\mathbb{E}_{\mathbf{z}_{-j}} [\log p(\mathbf{x}, \mathbf{z})]) dz_j}. \end{aligned} \quad (\text{C.0.5})$$

The normalization constant on the denominator of Expression (C.0.5) is derived by observing $q_j^*(z_j)$ as a density. Finally, we derive a simpler expression of $q_j^*(z_j)$ by observing that terms independent of z_j can be treated as a constant:

$$\begin{aligned} q_j^*(z_j) &\propto \exp(\mathbb{E}_{\mathbf{z}_{-j}} [\log p(\mathbf{x}, \mathbf{z})]) \\ &\propto \exp(\mathbb{E}_{\mathbf{z}_{-j}} [\log p(z_j | \mathbf{z}_{-j}, \mathbf{x})]). \end{aligned} \quad (\text{C.0.6})$$

APPENDIX D

Mean Field Variational Inference Example

To illustrate the mean-field variational inference approach, we closely follow the “Bayesian mixture of Gaussians” example from “Variational Inference: A Review for Statisticians” by Blei et al. [2017].

Consider the hierarchical model

$$\begin{aligned}\mu_k &\sim N(0, \sigma^2), & k &= 1, \dots, K, \\ c_i &\sim \text{Categorical}\left(1; \frac{1}{K}, \dots, \frac{1}{K}\right), & i &= 1, \dots, n, \\ x_i | c_i, \boldsymbol{\mu} &\sim N(c_i^\top \boldsymbol{\mu}, 1), & i &= 1, \dots, n,\end{aligned}$$

where $\boldsymbol{\mu} = (\mu_1, \dots, \mu_K)^\top$.

This is a Bayesian mixture of univariate Gaussian random variables with unit variance. In this model, we draw K identical copies of the variable μ_k from a prior Gaussian distribution $N(0, \sigma^2)$ (σ^2 is a fixed hyperparameter), forming the vector $\boldsymbol{\mu}$. We then generate an indicator vector c_i of length K from a prior categorical distribution. This vector has zeros for every element except for one element, where it is 1. Each element has equal probability $1/K$ of being the non-zero element. The transpose of this c_i is then multiplied by $\boldsymbol{\mu}$. This is a practical implementation to choose one of the $\boldsymbol{\mu}_k$ at random. We then draw x_i from the resulting $N(c_i^\top \boldsymbol{\mu}, 1)$. Defining $\mathbf{c} = (c_1, \dots, c_n)^\top$, our latent variables are $\mathbf{z} = \{\mathbf{c}, \boldsymbol{\mu}\}$. Assuming n samples, our joint density is

$$p(\boldsymbol{\mu}, \mathbf{c}, \mathbf{x}) = p(\boldsymbol{\mu}) \prod_{i=1}^n p(c_i) p(x_i | c_i, \boldsymbol{\mu}). \quad (\text{D.0.1})$$

To evaluate the posterior distribution over the latent variables $p(\boldsymbol{\mu}, \mathbf{c} | \mathbf{x})$, we apply variational inference, approximating it with a variational distribution $q(\boldsymbol{\mu}, \mathbf{c})$. We

will assume this distribution follows the mean-field variational family:

$$q(\boldsymbol{\mu}, \mathbf{c}) = \prod_{k=1}^K q(\mu_k; m_k, s_k^2) \prod_{i=1}^n q(c_i; \boldsymbol{\phi}_i).$$

In this distribution, we have K Gaussian factors with mean m_k and variance s_k^2 , and n categorical factors with index probabilities defined by the vector $\boldsymbol{\phi}_i$, such that

$$\begin{aligned} \mu_k &\sim N(m_k, s_k^2), & k &= 1, \dots, K, \\ c_i &\sim \text{Categorical}(\boldsymbol{\phi}_i), & i &= 1, \dots, n. \end{aligned}$$

Using this and Equation (C.0.1), we can derive the evidence lower bound as a function of the variational parameters $\mathbf{m} = (m_1, \dots, m_K)^\top$, $\mathbf{s}^2 = (s_1^2, \dots, s_K^2)^\top$ and $\boldsymbol{\phi} = [\boldsymbol{\phi}_1, \dots, \boldsymbol{\phi}_n]^\top$:

$$\begin{aligned} ELBO(\mathbf{m}, \mathbf{s}^2, \boldsymbol{\phi}) &= \mathbb{E}_{p(\mathbf{z}, \mathbf{x})}[\log p(\mathbf{z}, \mathbf{x})] - \mathbb{E}_{q(\mathbf{z})}[\log q(\mathbf{z})] \\ &= \mathbb{E}_{p(\boldsymbol{\mu}, \mathbf{c}, \mathbf{x})}[\log p(\boldsymbol{\mu}, \mathbf{c}, \mathbf{x})] - \mathbb{E}_{q(\boldsymbol{\mu}, \mathbf{c})}[\log q(\boldsymbol{\mu}, \mathbf{c})] \\ &= \sum_{k=1}^K \mathbb{E}_{p(\mu_k)}[\log p(\mu_k); m_k, s_k^2] \\ &\quad + \sum_{i=1}^n (\mathbb{E}_{p(c_i)}[\log p(c_i); \boldsymbol{\phi}_i] + \mathbb{E}_{p(x_i|c_i, \boldsymbol{\mu})}[\log p(x_i|c_i, \boldsymbol{\mu}); \boldsymbol{\phi}_i, \mathbf{m}, \mathbf{s}^2]) \\ &\quad - \sum_{k=1}^K \mathbb{E}_{q(\mu_k; m_k, s_k^2)}[\log q(\mu_k; m_k, s_k^2)] - \sum_{i=1}^n \mathbb{E}_{q(c_i; \boldsymbol{\phi}_i)}[\log q(c_i; \boldsymbol{\phi}_i)]. \end{aligned}$$

From the CAVI algorithm in Equation (3.5.7), which we restate to be

$$q_j^*(z_j) \propto \exp(\mathbb{E}_{\mathbf{z}_{-j}}[\log p(\mathbf{x}, \mathbf{z})]),$$

we derive the optimal categorical factor by only considering terms from the true distribution $p(\cdot)$ dependent on c_i :

$$q^*(c_i; \boldsymbol{\phi}_i) \propto \exp(\log p(c_i) + \mathbb{E}_{p(x_i|c_i, \boldsymbol{\mu})}[\log p(x_i|c_i, \boldsymbol{\mu}); \mathbf{m}, \mathbf{s}^2]). \quad (\text{D.0.2})$$

Now since $\mathbf{c}_i = (c_{i1}, \dots, c_{iK})^\top$ is an indicator vector, we have:

$$p(x_i | \mathbf{c}_i, \boldsymbol{\mu}) = \prod_{k=1}^K p(x_i | \mu_k)^{c_{ik}}.$$

We can now evaluate the second term of Equation (C.0.2):

$$\begin{aligned}
\mathbb{E}_{p(x_i|c_i, \boldsymbol{\mu})} ([\log p(x_i|c_i, \boldsymbol{\mu}); \mathbf{m}, \mathbf{s}^2]) &= \sum_{k=1}^K c_{ik} \mathbb{E}_{p(x_i|\mu_k)} [\log p(x_i|\mu_k); m_k, s_k^2] \\
&= \sum_{k=1}^K c_{ik} \mathbb{E}_{x_i} [-(x_i - \mu_k)^2/2; m_k, s_k^2] + C \\
&= \sum_{k=1}^K c_{ik} \left(\mathbb{E}_{\mu_k} [\mu_k; m_k, s_k^2] x_i - \mathbb{E}_{\mu_k^2} [\mu_k^2; m_k, s_k^2]/2 \right) \\
&\quad + C.
\end{aligned}$$

In each line, terms constant with respect to c_{ik} have been absorbed into the constant C . Our optimal categorical factor becomes

$$q^*(c_i; \boldsymbol{\phi}_i) \propto \exp \left(\log p(c_i) + \sum_{k=1}^K c_{ik} \left(\mathbb{E}_{\mu_k} [\mu_k; m_k, s_k^2] x_i - \mathbb{E}_{\mu_k^2} [\mu_k^2; m_k, s_k^2]/2 \right) \right).$$

By proportionality, we then have the variational update

$$\phi_{ik} \propto \exp \left(\mathbb{E}_{\mu_k} [\mu_k; m_k, s_k^2] x_i - \mathbb{E}_{\mu_k^2} [\mu_k^2; m_k, s_k^2]/2 \right).$$

Now we find the variational density of the k th mixture component, again using Equation (3.5.7) with the ELBO and ignoring terms independent of $p(\cdot)$ and μ_k :

$$q(\mu_k; m_k, s_k^2) \propto \exp \left(\log p(\mu_k) + \sum_{i=1}^n \mathbb{E}_{p(x_i|c_i, \boldsymbol{\mu})} [\log p(x_i|c_i, \boldsymbol{\mu}); \boldsymbol{\phi}_i, \mathbf{m}_{-k}, \mathbf{s}_{-k}^2] \right).$$

The log of this density is

$$\begin{aligned}
\log q(\mu_k) &= \log p(\mu_k) + \sum_{i=1}^n \mathbb{E}_{p(x_i|c_i, \boldsymbol{\mu})} [\log p(x_i|c_i, \boldsymbol{\mu}); \boldsymbol{\phi}_i, \mathbf{m}_{-k}, \mathbf{s}_{-k}^2] + C \\
&= \log p(\mu_k) + \sum_{i=1}^n \mathbb{E}_{c_{ik}, p(x_i|\mu_k)} [c_{ik} \log p(x_i|\mu_k); \boldsymbol{\phi}_i] + C \\
&= -\frac{\mu_k^2}{2\sigma^2} + \sum_{i=1}^n \mathbb{E}_{c_{ik}} [c_{ik}; \boldsymbol{\phi}_i] \log p(x_i|\mu_k) + C \\
&= -\frac{\mu_k^2}{2\sigma^2} + \sum_{i=1}^n \phi_{ik} \frac{-(x_i - \mu_k)^2}{2} + C \\
&= -\frac{\mu_k^2}{2\sigma^2} + \sum_{i=1}^n \left(\phi_{ik} x_i \mu_k - \frac{\phi_{ik} \mu_k^2}{2} \right) + C
\end{aligned}$$

$$\begin{aligned}
&= \mu_k \left(\sum_{i=1}^n \phi_{ik} x_i \right) - \mu_k^2 \left(\frac{1}{2\sigma^2} + \frac{\sum_{i=1}^n \phi_{ik}}{2} \right) + C \\
&= -\frac{1}{2} \left(\frac{1}{\sigma^2} + \sum_{i=1}^n \phi_{ik} \right) \left(\mu_k^2 - \frac{2 \sum_{i=1}^n \phi_{ik} x_i}{1/\sigma^2 + \sum_{i=1}^n \phi_{ik}} \mu_k \right) + C.
\end{aligned}$$

The density is therefore

$$q(\mu_k) \propto \sqrt{\frac{1/\sigma^2 + \sum_{i=1}^n \phi_{ik}}{2\pi}} \exp \left(-\frac{1}{2} \left(\frac{1}{\sigma^2} + \sum_{i=1}^n \phi_{ik} \right) \left(\mu_k - \frac{\sum_{i=1}^n \phi_{ik} x_i}{1/\sigma^2 + \sum_{i=1}^n \phi_{ik}} \right)^2 \right).$$

It can be seen that $q(\mu_k)$ is a Gaussian distribution, so our variational updates for m_k and s_k^2 are its mean and variance:

$$m_k = \frac{\sum_{i=1}^n \phi_{ik} x_i}{1/\sigma^2 + \sum_{i=1}^n \phi_{ik}}, \quad s_k^2 = \frac{1}{1/\sigma^2 + \sum_{i=1}^n \phi_{ik}}.$$

We can now formulate the CAVI algorithm (Algorithm 9), which simply iterates the cluster assignment probabilities ϕ_{ik} and the variational density parameters m_k and s_k^2 until the ELBO converges.

Data: Data \mathbf{x} , Number of Gaussian components K , Hyperparameter value σ^2

Result: Optimal variational factors $q(\mu_k; m_k, s_k^2)$ and $q(c_i; \phi_i)$

begin

Randomly initialize parameters \mathbf{m}, \mathbf{s}^2 and ϕ ;

while *ELBO has not converged* **do**

for $i = 1$ **to** n **do**

Set $\phi_{ik} \propto \exp \left(\mathbb{E}_{\mu_k} [\mu_k; m_k, s_k^2] x_i - \mathbb{E}_{\mu_k^2} [\mu_k^2; m_k, s_k^2] / 2 \right)$;

end

for $k = 1$ **to** K **do**

Set $m_k = \frac{\sum_i \phi_{ik} x_i}{1/\sigma^2 + \sum_i \phi_{ik}}$;

Set $s_k^2 = \frac{1}{1/\sigma^2 + \sum_i \phi_{ik}}$;

end

Compute $ELBO(\mathbf{m}, \mathbf{s}^2, \phi)$;

end

Return $q(\mathbf{m}, \mathbf{s}^2, \phi)$;

end

Algorithm 9: CAVI Algorithm for Bayesian mixture of Gaussians

APPENDIX E

Kernel Density Estimation

Kernel density estimation is a non-parametric method used to estimate the probability density function of a distribution, using only samples [Zanin Zambom and Dias, 2012]. It can therefore be used to estimate implicit distributions. For simplicity we only explain the univariate form of the kernel density estimator.

Let $\{x^{(i)}\}_{i=1}^n$ be an i.i.d. sample from a distribution with unknown probability density function f . Its kernel density estimator is defined as

$$\hat{f}_h(x) = \frac{1}{nh} \sum_{i=1}^n K\left(\frac{x - x^{(i)}}{h}\right).$$

K is the kernel, a symmetric non-negative weighting function that integrates to 1. Examples of kernel functions are:

- Epanechnikov: $K(u) = \frac{3}{4}(1 - u^2), |u| \leq 1$,
- Uniform: $K(u) = \frac{1}{2}, |u| \leq 1$,
- Gaussian: $K(u) = \frac{1}{\sqrt{2\pi}} \exp\left(-\frac{1}{2}u^2\right)$.

Typically, the Gaussian kernel is used due to its statistical properties.

The bandwidth $h > 0$ acts as a smoothing parameter, determining the width of the kernel. If h is too small, \hat{f} will be ‘undersmoothed’ as too much weight is placed on the areas nearest the data-points, leading to a spiky estimate with high variance. On the other hand, if h is too large, \hat{f} will be ‘oversmoothed’ with too little weight on areas nearest to the data-points, resulting in a relatively flat estimate with high bias. It is therefore ideal to choose h such that the mean integrated square error $MISE(h) = \mathbb{E} \left[\int (\hat{f}_h(x) - f(x))^2 dx \right]$ is minimized. For a Gaussian kernel, this is approximately $h = 1.06\hat{\sigma}n^{-1/5}$ where $\hat{\sigma}$ is the sample standard deviation.

The kernel density estimator works by placing a kernel on each data point and summing up the kernels to produce a smooth curve. Each point on the curve is essentially a weighted average of nearby data points. Regions of the curve with many data points will therefore have a high estimated probability density.

APPENDIX F

Prior-Contrastive Optimal Estimator Experiment Plots

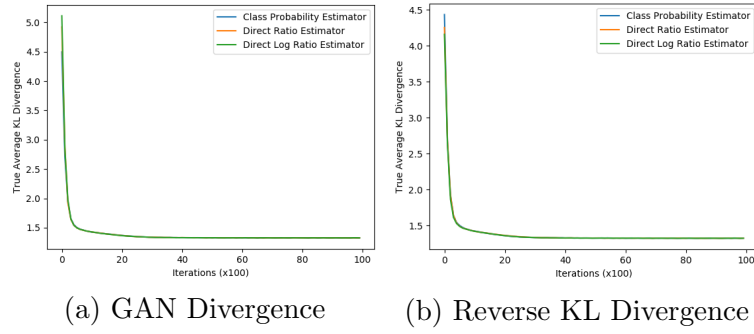


Figure F.1: Prior-Contrastive Average KL Divergence

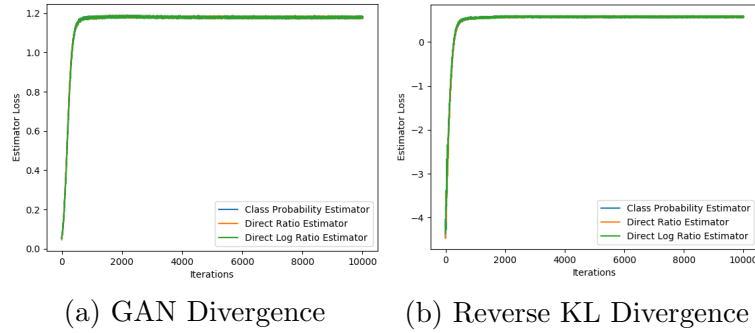


Figure F.2: Prior-Contrastive Estimator Loss

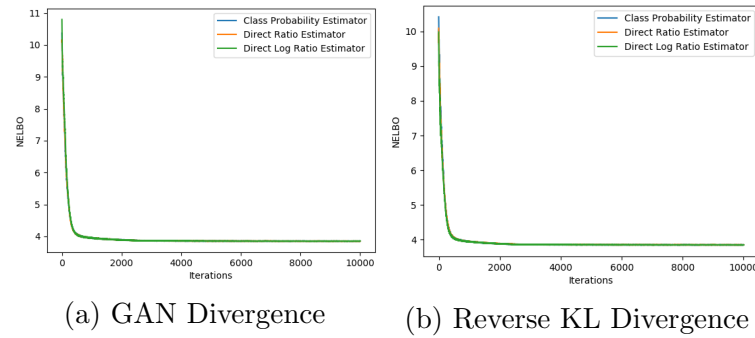


Figure F.3: Prior-Contrastive *NELBO*

APPENDIX G

Second Functional Derivatives of Direct Log Ratio Estimator Losses

Reverse KL Divergence Bound

Direct Log Ratio Estimator:

$$\begin{aligned} f_{RKL}(u) &:= -\mathbb{E}_{q(u)}[T(u)] + \mathbb{E}_{p(u)}[e^{T(u)}] \\ &= -\int q(u)T(u)du + \int p(u)e^{T(u)}du \\ \frac{df_{RKL}(u)}{dT(u)} &= -q(u) + p(u)e^{T(u)} \\ \frac{d^2 f_{RKL}(u)}{dT^2(u)} &= p(u)e^{T(u)}. \end{aligned}$$

GAN Divergence Bound

Direct Log Ratio Estimator:

$$\begin{aligned} f_{GAN}(u) &:= -\mathbb{E}_{q(u)}[T(u) - \log(e^{T(u)} + 1)] + \mathbb{E}_{p(u)}[\log(e^{T(u)} + 1)] \\ &= \int q(u)[\log(e^{T(u)} + 1) - T(u)]du + \int p(u)[\log(e^{T(u)} + 1)]du \\ \frac{df_{GAN}(u)}{dT(u)} &= -q(u) + \frac{(q(u) + p(u))e^{T(u)}}{e^{T(u)} + 1} \\ \frac{d^2 f_{GAN}(u)}{dT^2(u)} &= \frac{(q(u) + p(u))\exp(T(u))}{e^{T(u)} + 1} - \frac{(q(u) + p(u))e^{2T(u)}}{(e^{T(u)} + 1)^2} \\ &= \frac{(q(u) + p(u))(e^{2T(u)} + e^{T(u)}) - (q(u) + p(u))e^{2T(u)}}{(e^{T(u)} + 1)^2} \\ &= \frac{(q(u) + p(u))e^{T(u)}}{(e^{T(u)} + 1)^2}. \end{aligned}$$